Université d'Ottawa • University of Ottawa

Université d'Ottawa · University of Ottawa

FACULTÉ DES ÉTUDES SUPÉRIEURES ET POSTDOCTORALES

FACULTY OF GRADUATE AND POSTDOCTORAL STUDIES

Xinming LI

AUTEUR DE LA THÈSE - AUTHOR OF THESIS

M. A. Sc. (Mechanical Engineering)

GRADE - DEGREE

Department of Mechanical Engineering

FACULTÉ, ÉCOLE, DÉPARTEMENT - FACULTY, SCHOOL, DEPARTMENT

TITRE DE LA THÈSE - TITLE OF THE THESIS

Piezoelectric-based Structural Health Monitoring of Flexible Beam Connection Damage

D. Necsulescu

DIRECTEUR DE LA THÈSE - THESIS SUPERVISOR

CO-DIRECTEUR DE LA THÈSE - THESIS CO-SUPERVISOR

EXAMINATEURS DE LA THÈSE - THESIS EXAMINERS

M. Liang

J. Sasiadek

J.-M. De Koninck, Ph.D.

LE DOYEN DE LA FACULTÉ DES ÉTUDES SUPÉRIEURES ET POSTDOCTORALES

SIGNATURE

DEAN OF THE FACULTY OF GRADUATE AND POSTDOCTORAL STUDIES

Piezoelectric-Based Structural Health Monitoring of Flexible Beam Connection Damage

A thesis submitted to the
University of Ottawa
in partial fulfillment of the requirements
for the degree of

Master of Applied Science
in
Mechanical Engineering

By
Li, Xinming

Ottawa-Carleton Institute for Mechanical and Aerospace Engineering
University of Ottawa
Ottawa, Ontario, Canada

Your file Votre référence
ISBN: 0-612-90107-6
Our file Notre référence
ISBN: 0-612-90107-6

Abstract

Structural health monitoring is an emerging technology addressing major concerns in the operation of in-service structures, i.e. the reliability of the structures and the cost associated with maintaining reliability. In this thesis, the motivation of structural health monitoring has been discussed within the framework of non-destructive evaluation. To be a common failure mode, connection damage or lap joint damage is chosen as damage signature in a structure, consisting of a flexible aluminum beam jointed on a frame by bolts. To simulate connection damage, the stress relaxing on the bolt is achieved by the action of bolt looseness quantified by rotation angle. The dynamic response of flexible beam system is monitored with a piezoelectric transducer. To produce exciting signal, an electro-mechanical system processes the voltage signal. Response interpretation is carried out on PC or on an embedded DSP chip in real time. The two analysis methods, frequency response method and wavelet analysis method, were explored to identify early "changes" of beam connection so as to reach the goal of structural health monitoring.

Acknowledgement

There are some people I would like to recognize for their help and support with my research. Without them, I would not have been able to accomplish my thesis research with such good results. I would like to thank my supervisor Dr. Dan S. Necsulescu in his trust for my abilities and whatever advices and resources provided to me for accomplishing my goals.

Next, I would like to thank the members of my defense committee, Dr. M. Liang and Dr. J. Sasiadek, for examining my thesis.

I would also like to acknowledge everyone who provided technical support for my experiments. Thanks to Ms. Xiaojia Hu, the Master student of Prof. David Redekop, for her help in finite element analysis of beam connection on ADINA. A special thanks goes to Goran Basic for his help on my experiment. Thanks to technical support of Motorola, William Jiang and Dr. Xiangjun Rong, for their patience on modification of my DSP program.

Lastly, I need to thank my lovely wife for her continuous support and encouragement.

Table of Contents

List of Figures

List of Tables

Nomenclature

A	cross-sectional area of the beam
c	viscous damping coefficient
C_p	2-norm of the P-th derivative of $Gaus(x,n)$ is equal to 1
C_ψ	constant dependent on the type of mother wavelet used
$CWT(\tau,s)$	calculated wavelet coefficients
D	damage index
E	Young' s elastic modulus
f_1	the lower frequency of the range of interest
f_2	the upper frequency of the range of interest
$f(t)$	general time-varying force
$f(x,t)$	distributed force along beam
F	complex amplitude of external force
Δf	frequency spacing
$H(\omega_f)$, $\alpha(\omega_f)$	frequency response funtion
I	cross-sectional area moment of inertia of the beam
k	spring constant
l	length of beam
m	mass of system
N	blocksize
$RMSD$	Root-mean-square deviation
s	the scale parameter
Δt	time spacing

$w(x,t)$	transverse deflection
$x(t)$	time domain signal
X	complex amplitude of motion
$X(f)$	frequency distribution of signal
y_i^D	The amplitude of frequency response of loose connection
y_i^H	The amplitude of frequency response of initial tight connection
β	wave number of the beam
ρ	material density
ω	frequency in radians per second
ω_0	natural frequency of system
ω_f	frequency of oscillation of external sinusoidal force
ζ	viscous damping ratio
τ	the translation parameter
ψ^*	mother wavelet
$\hat{\psi}(k)$	Fourier Transform of $\psi(x)$

Chapter 1

Introduction

Structural health monitoring (SHM) is a solution of damage detection that has recently become a research area of interest for aerospace, civil and mechanical engineering. This technique is defined by Chang F-K in his literature review as a 'technology to develop autonomous systems for the continuous monitoring, inspection, and damage detection of structures with minimum labor involvement' [1]. Structural health monitoring system, which monitors its own integral structure while in operation or throughout its lifetimes, is highly desirable by users, maintenance crews, as well as manufacturers.

To categorize the structural health monitoring process, five stages could be summarized as: (1) identification of damage presence in a structure, (2) localization of damage, (3) identification of the damage type, (4) quantification of damage severity, and (5) prediction of the remaining service life of the structure [2]. The essential consideration of SHM is to understand the status of "health", and in particular to perceive "changes" of structure from time to time. These "changes" could be crack, delamination development or fastener looseness, deformation or broken, which were caused by corrosion, fatigue or external impact. Bridge health monitoring is a field at which lots of SHM researchers were devoted. Finding solutions to prevent accidents related to bridge or building

attracted civil engineers interest. Also, marine industry has the requirements of SHM to monitor the deformation of vessel body by pressure, especially on submarines.

Aerospace engineering could have the significant payoffs from SHM. In an aging structure, like the structure of an aircraft, spacecraft, etc, structural "changes" mean defects development, which can result in failure of structure or sometimes catastrophe. At present it is anticipated that aging aircrafts in fleet of military and civil will keep increasing in number. To maintain cost-effectively a large number of aircrafts that are near or beyond designed lifetime is a growing challenge. Currently, 27% of an average aircraft' s life cycle cost is spent on inspection and repair [3], and in this is not included the opportunity cost associated with the time the aircraft is grounded for scheduled maintenance.

Conventional non-destructive evaluation (NDE) inspections are employed at periodic maintenance checks. The execution of inspections generally requires the system to be temporarily taken out of operation. Since a "change" in structural health may become serious and affect structural performance in some degree between regular inspections, the repair cost increases due to unexpected remedial actions while an early stage of damage repair would reduce entire lifecycle maintenance cost and prolong structure lifetime. SHM will play more important role in the future because the integrity of the structures must be monitored during operation to prevent failure. This system monitors the condition of a structure during its operation to diagnose any faults as they occur and can provide the advantages of lighter, faster, cheaper, safer, longer lasting and more reliable structures.

Comparing SHM and NDE from technical viewpoint could identify also other differences. The traditional NDE techniques tend to use direct measurements to determine the physical condition of the structures and no historical data is needed. The accuracy of the diagnosis strongly depends upon the resolution of the measurements, which rely heavily on the equipment. However, the SHM techniques would use the change in the measurements at the same location at two different times to identify the condition of the structures. Hence, historical data is crucial for the technique.

The present research of SHM combines smart materials, smart structures, signal processing and software within one system. The accuracy of SHM strongly depends upon the sensitivity of sensors and interpretation of damage. Many kinds of sensors or transducers have been tested for SHM such as strain gauges, shape memory alloys and optical fibers, which detect damage through a variety of techniques–some more effectively than others. Piezoelectric sensors and actuators have become of particular interest in this thesis due to their versatility, conformability, low power consumption and high bandwidth. Several of these sensors and detection methods will be described in detail in chapter 2.

Failure mode discussed in this thesis emphasis on connection failure or lap joint failure. The joint types could be classified as welded, bonded, riveted and bolted, while the signature of defects usually comes from crack, debonding, deformation or even cutoff of fastener and fastener looseness. Some effective methods of detection have been cited to particular lap joint damage, including accelerometers for bridge columns connection crack, embedded optical fibers for strain distribution and some NDE methods like radiography, ultrasonic and Eddy

current. However, there is no such information covering dynamic response monitor of bolt looseness. R. D. Abreu and K. V. Iong, former Master students of Prof. D. Necsulescu have dedicated before 2000 in the research of amplitude method by transient signal [4,5]. Also a paper published by M-F Dandine, D. Necsulescu presents wavelet analysis for failure detection in a flexible structure [6]. In this thesis, other interpreting methods, frequency response and wavelet analysis, are introduced to identify the "changes" and damage level.

Chapter 2

Background

This chapter presents a survey of damage detection methods for bolted or riveted lap joint assembly. Lap joint assembly gains acceptance and demand in large complex structures of civil, mechanical engineering, transportation and or aerospace industry. In the event of fatigue or severe loading condition, these joints can loosen or fail leading to a potential hazard while these structures are still in service. In many of these systems, such as bridge or aircraft, a reliable damage detection approach is pursued by the public, customers and military for reasons of safety and cost saving. To achieve structural safety, the solution of damage tolerant design approach is very important. Due to the close relation of structural health monitoring and non-destructive evaluation, some non-destructive evaluation techniques are compared on the basis of their strengths and weaknesses for in-service testing of lap joint assembly. This chapter concludes with a discussion of the implementation of a structural health monitoring system.

2.1 Durability and damage tolerance designation

Fatigue design or safe-life design was actively pursued in aircraft engineering following the British Comet accidents in 1954. Fatigue life was defined as estimation by combining a service stress description with basic fatigue properties obtained from laboratory experiments. The safe-life approach is based

on the number of loading cycles before crack initiation [6]. The aim of fatigue or safe-life deign is to make the time required for the initiation of cracks longer than the operational life of the structure. However, it is virtually impossible to ensure a crack free operational life for most structures. Even though the safety factor lasts over four life times, an individual aircraft with an initial flaw could not survive even one life in service. This point is recognized after the crash of a U.S. Air Force F-111 in 1969, which flied only 105 flight hours against 8000 flight hours safe-life design [7].

In the early 1970's, durability and damage tolerance were introduced to assure structural health of aerospace vehicles - the durability assures continuous operation while the damage tolerance assures safety of flight for a specified design life [8]. The primary concept of damage tolerance assumes that flaws exist in structures due to material or environmental degradation under operational loads during material processing, manufacturing and during service usage. It gives a quantitative basis in the form of the size of damage like flaw as opposite to damage initiation to enhance reliability prediction methodology. In damage tolerance design, concern has shifted from the damage initiation to the damage propagation.

Many discussions about damage tolerance method can be found in Proceedings of FAA/NASA international symposium on advanced structural integrity methods for airframe durability and damage tolerance in 1994 [9]. deKoning A. U. *et al* [9] presented an analysis of bolt/nut assemble on damage tolerance in their publication. The authors set up this assemble from fracture mechanics viewpoint and indicated that its complexity affected by material,

manufacturing, mounting processes, stiffness, surface conditions and geometry of the parts, makes fastener and joints to be one of the most challenging problems. By analysis, the authors also think that a fastener is a link in a multi load path design and load distribution and stress intensity factors can be available through advanced 3D finite element analysis. It can be seen from their analysis and experiments that stress intensity factors are related to effective length of the bolt shank on the load transfer, which has positive ratio to clamping force. Using the results of stress intensity factor, defect locations and shapes, and bending load assumptions for fasteners in bolted joints can be defined. Hence, the damage propagation and the thresholds can be specified accordingly. There are other contributions regarding damage tolerance by different structures or components, like composite sandwich structures from FAA [11,12], Critical helicopter components are presented in papers [13,14].

Since the FAA adopted damage tolerance concept from 1970's, much attention has been focused on the reliability of nondestructive inspections of structures [15] so that at least two opportunities to detect damage were available before it grows to its critical size [7].

2.2 Non-Destructive Evaluation (NDE) Methodology

In both military and commercial aircraft operations, detecting and characterizing defects at very early stage is an increasing need. The lap joint damage is the result of fasteners loosening or breaking, corrosion, stress cracking or fatigue, etc. Several common NDE methods have already been developed for actual inspection work. The following sections provide brief descriptions of

various non-destructive approaches that have been developed for the detection of damage in lap joint connections.

2.2.1 Ultrasonic methods

Ultrasonic methods are widely used for inspecting aircraft structures for defects that reflect the ultrasonic pulse [16]. These tests are usually conducted with a coupled water-jet probe moving along the surface of the structure, sending ultrasound waves through the water stream into the surface. The reflected waves due to existing flaw would be analyzed based on their amplitude and time-of-arrival. The reason of water or other gels couplant use is high attenuation of ultrasonic wave when propagating through atmosphere. Perhaps this is the main limitation given that the speed of scanning the surface of aircraft is significantly reduced by couplant requirement. Besides the size and cost of the equipment, the depth of pulse penetration is seriously dependent on media. Any air in the ultrasound path will totally prevent propagation any deeper into the structure. The results could be confusing in the case of tests of lap joints with or without jointing compound.

2.2.2 Eddy current methods

The use of eddy currents is another valuable impedance-based technique for metallic structures. This approach functions by detecting changes in electromagnetic impedance due to corrosion in lap joint because the corrosion products have a greater volume than the original uncorroded metal and the layers are forced apart. Eddy currents offer advantages of speed, ease of use and

multiple-layer penetration compared with ultrasonics [16]. However, these methods require large amounts of power and the data produced is among the most complicated to interpret due to the structural effects. These can be considered main disadvantages of eddy currents use.

2.2.3 X-radiography methods

X-radiographic techniques rely on recording the difference in X-rays attenuation rates through the structure [17]. These methods can be implemented digitally in real-time, or by taking static radiographs, whereas areas of different permeability or density are differentiated by the magnitude of X-ray exposure to the media on the opposite side of the lap-jointing surface after a predetermined excitation time. This is important for identifying defects to evaluate X-radiography using samples with real corrosion products. Although these techniques are relatively inexpensive and simple to implement and interpret, they require large and costly equipment that is difficult to use on large structures without removing them from the aircraft or vehicle. The most important limitation to using X-radiography in-situ application, however, is that all of these methods require access to both sides of the surface for emitter and receiver, which is often not practical for actual structures.

2.2.4 Strain gauge methods

Strain gauge methods are currently perhaps the most common way to monitor damage on in-service vehicle. A voltage applied across a strain gauge depends upon the change of resistance due to deformation, which is related to

stain [18]. These sensors are relatively small, light and inexpensive making them easy to implement while the data collected are readily interpreted. They are capable of monitoring local time-variation strain due to crack, corrosion, fastener looseness, etc. The limitation of this technique is the sensitivity that is achieved covering only small area of surface. For this purpose, the sensor should be bonded close to designated places that are vulnerable to damages. Otherwise, numerous sensors have to be scattered to monitor the entire structure yielding, however, a complex system with many wires.

2.2.5 Optical fiber methods

Embedded optical fibers are used in order to cover a larger area on a structure for strain measurement, which can be multiplexed to record measurements over large regions [19,20]. In using this method of detection, pulses of polarized laser light are transmitted along an optical fiber and gratings are placed in various locations to reflect a portion of the light at a certain wavelength. By recording the time of flight of the beam, the length of that segment of fiber can be easily deduced; if a strain has been applied to that segment of fiber, the time of flight would change. Besides inaccurate measurement by shear-lag effect due to the cladding, coating and adhesion layers surrounding the optical core, its major shortcoming result with respect to repair when optical fibers have to be integrated into the material in places according to the major stress and strain.

2.2.6 Vibration-based methods

Vibration-based damage detection technique, also called modal testing, is based on the dynamic response of the structure. Active structural vibration can be produced by predetermined exciting action coming from impactor, external shaker or embedded actuators. The time domain history of dynamic structural response is then recorded by accelerometers or embedded strain gauges for amplitude and resonant frequencies analysis. Changes in normal modes can be correlated with loss of stiffness in the structure, and usually analytical models or response history is helpful to determine the severity degree. These methods are implemented easily within the existing infrastructure of a vehicle at a low cost; however, the procedure of inspection produces a large amount of data for analysis and high noise level can affect accuracy. Further discussion about vibration-based methods will be presented in Chapter 3.

2.3 Structural Health Monitoring (SHM)

In-operation inspection or operational health monitoring is much more challenging than ground inspection or stationary inspection, and conventional NDE methods may not be suitable for SHM. The essential character of SHM is integrity of in-service structures. Given the variety of structural damage, several SHM have been established in laboratory, and some have been used on products ranging from industrial machinery to spacecraft.

2.3.1 Motivations of SHM

Structural health monitoring is an emerging technology addressing major concerns in the operation of in-service structures, i.e. the reliability of the

structures and the cost associated with maintaining reliability [21]. Among various aspects, life-safety ranks as the essential consideration of design and ongoing maintenance in transportation systems and vehicles (spacecraft, aircraft, helicopters, ground vehicles, etc.), civil structures (bridges, highways, power plants, tunnels, etc.), and other expensive products (satellites, launch systems, etc.). The goal of SHM systems is to improve reliability and safety while reducing maintenance costs.

Conventional NDE performs structural damage inspection according to maintenance manuals derived from the results of loading, fatigue or corrosion test. However, the real operational environment has typically random variability in time and vary from case to case. Especially, the incidental load increase or the impact could significantly reduce the structural safety-life. Nevertheless, the time intervals of inspection from manuals are not updated or revised unless a catastrophe or unexpected failure occurs.

Another challenge to conventional NDE comes from both military and commercial aircrafts, which are near or beyond their lifetime. Based on statistics, in US and Europe, the number of aging aircraft (older than 15 years) has increased continuously from 4600 in 1997 to 4730 by 1999, and meanwhile by 1999, from 1900 to 2130 aircrafts were older than 25 years [22]. These aging aircraft combined with those enduring severe in-service conditions require intensified inspection, which means shorter and shorter inspection intervals to maintain the reliability. This results in a time-consuming, labor-intensive, and very expensive operation as higher maintenance service frequency leads to higher maintenance costs.

Multi-element damage is the simultaneous manifestation of small cracks, where the crack size is so small that is hard to detect by conventional inspection and lead to Aloha incident in 1988 [21]. Since then, an effective SHM was eagerly expected by manufacturers and customers because a reliable procedure for early damage detection could reduce the design uncertainties, increase designer confidence, and result in lower reserve factors, smaller weight, and reduced initial cost [23].

2.3.2 Essential issues of SHM

Sensing technology In an effective SHM, sensors play a very important role in damage detection. Beside adequate sensitivity to damage, their cost, reliability, capability of integrated to structures or embedded in structures is very important. At present, some sensors are available in the market but many others are still in development such as fiber optics, dielectric measurement sensors, piezoelectric materials, strain gages, MEMS sensors and will be used for applications for SHM purposes. Although a variety of sensors are available for SHM, the distribution and optimal number should be considered carefully for obtaining accurate signals.

Diagnostic signal generation The dynamic response of the system comes from passive excitation and active excitation. Passive sensing is in response to external thermal, mechanical, or chemical loads while active sensing corresponds to built-in actuators or transducers integrated with structures. Passive sensing methods, like rotor-shaft or gearbox, need to receive signals from unknown excitations while active sensing methodology use easy to

recognize signals but additional actuators are indispensable. In this thesis research for connection damage detection, the piezoelectric transducer is used for global detection under active exciting and sensing.

Damage interpretation methodology The damage interpretation plays a major role in the health monitoring system [24]. No matter what signal is obtained, the result might be useless if no right data processing method is adopted. In this thesis, vibration based frequency response and wavelet analysis will be used to process the vibration signal for identifying connection damage.

2.3.3 Application of SHM

Although there are no mature standards and codes available to specify the technology of SHM, some SHM systems have been developed to be applied in practice on various structures such as buildings and bridges.

One of the important SHM applications is for aircrafts and spacecrafts for both military and civil use. NASA has tested a Health and Usage Monitoring System (HUMS) during 1996 Summer Olympic Games in Atlanta [25]. In that called HeliSTAR project, a Bell Model 412 helicopter with a HUMS and data recorder was operated for the purpose of performing component fatigue life testing. A potential benefit obtained from HUMS is the retirement extension of parts if the actual usage severity is milder than the basis for certification. Furthermore, the economic impact of incorporating a HUMS on a Model 412 shows significant cost savings. New military fighter-crafts, such as the Eurofighter, the Joint Strike Fighter and the F-22, all incorporate Health Usage Monitoring Systems (HUMS), which record peak stress, strain and acceleration experienced

in key components of the vehicle [26]. Caron *et al* presented a paper about SHM on F-18, in which they were able to show that the operational life of the F-18 of the Canadian Air Force could be extended by 12 years due to the monitoring of operational loads, thus leading to savings of 400 million Canadian dollars [27]. There are several publications about SHM applied on bulkhead of F/A-18, F-16 fighter and other aircrafts [28-30].

Above SHM applications are limited to monitoring and damage analysis to be carried out offline. Cowan, R. S. *et al* provided an example of real-time and on-line methods for mechanical seal wear and rolling-element bearing failure detection, in which piezoelectric transducers are placed to monitor lubricating film collapse [31].

Chapter 3

Analytical Models for Vibration-Based Damage Detection

In static analysis of a bolt joint, a bolt or group of bolts provide a clamping force between two or more members in tensile or shear joints. The bolts or fasteners are supposed to clamp the joint members together with enough force to prevent them from separating or slipping. The key issue regarding fastener life and integrity depends upon how much clamping force is imparted to the joint. However, due to high shock and vibration dynamics effects, as for example those on the aircraft wing, the damage of the connection could happen in one or more modes listed below [32]:

-fastener self-loosen, shake apart, or break.

-fasteners break due to corrosion, stress cracking or fatigue.

-separation of members supporting tensile loads which can lead to rapid fatigue failure of fasteners.

-slipping in a joint which can change the way a structure absorbs a load.

-leakage of lubricant or fluids in a joint that can lead to accelerated corrosion.

For vibration-based connection damage detection, it is necessary to simulate or specify these damages in research. Since the lap joint is needed at the edges of components, it naturally defines by boundary conditions.

3.1 Boundary conditions

Boundary conditions are a decisive factor in determining the dynamic response of vibration on a structure. In real cases, a lap joint is needed when two or more various shape of plates have to be connected with rows of fasteners fixed along other parts, like fuselage, vehicle body, vessel shell, etc. The force of fasteners tightness determines the connection status of tight or loose, even though the basic failures around fastener holes have the same result of connection looseness [33]. The installation of fasteners and looseness degree on edges of a plate can be expressed in the boundary condition of this plate. Any change on fasteners state leads to alteration of vibration parameters on this plate. That is the basic premise of vibration-based damage monitoring on plate lap joint fasteners.

This thesis research focuses on some effective methods of investigation of the dynamic response to discover the structural change due to fastener looseness. Next is presented a simple structure in which an aluminum beam was positioned with one end fixed on a frame and another end fastened on another frame by a bolt (Figure 3.1). The experiment covered the boundary conditions changes from tight bolt to full loose bolt. For this purpose, the bolt is turned with some angular displacement and the vibration data are analyzed accordingly.

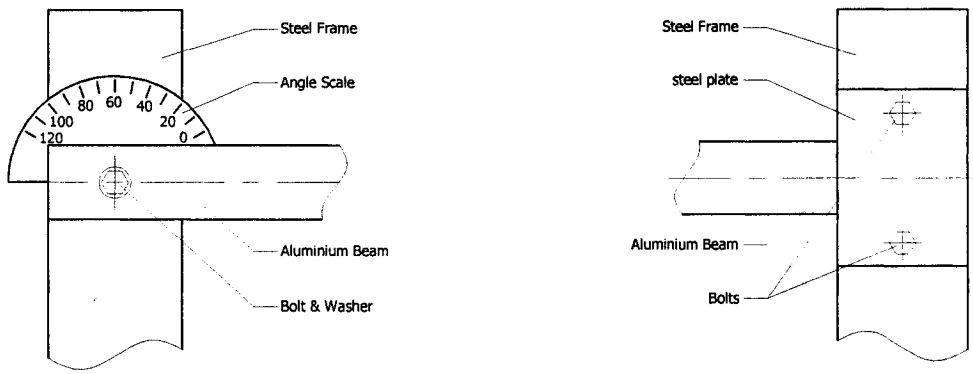

Figure 3.1 Demonstration of boundary conditions of an aluminum beam

The geometrical and material specification of the beam can be found in Figure 3.2 and Table 3.1.

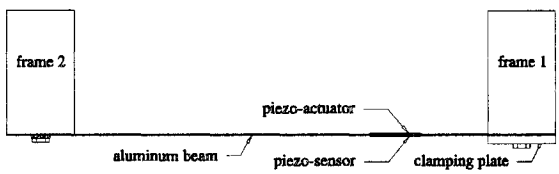

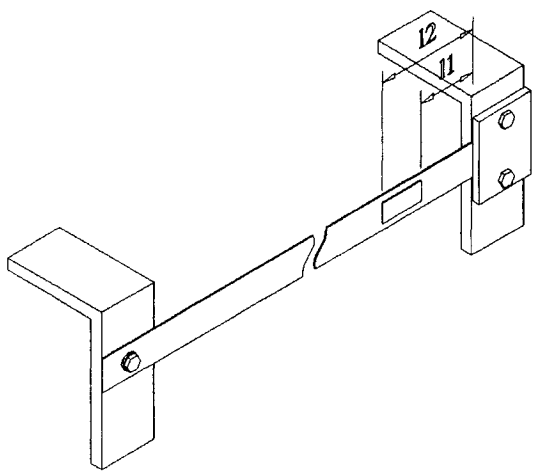

In Figure 3.2, l1, l2 indicate the location of piezo-ceramic sensor at 0.05m and 0.087m. A piezo-ceramic Approximately same size is used as actuator and is installed at same distance on the back of the beam.

Figure 3.2 Beam installation sketch

Table 3.1 Specifications of the aluminum beam

Geometrical Dimension [m]		Physical Properties	
Length l	0.890	Density ρ	2700 kg/m^2
Width	0.028	Elastic modulus E	71.4 GPa
Thickness	0.0012	Poisson ratio	0.33

3.2 Analytical model

To better understand how boundary conditions are correlated to beam vibration parameters, an elementary theory about bending of thin beams will be presented using finite element method (FEM). FEM was created for this case using ADINA, which could accurately predict the natural frequencies even for complicated boundary conditions, as well as plot their mode shapes for verifying and optimize the modes to fit the residual of piezoelectric sensor.

3.2.1 Thin beam theory

For lateral vibration of an uniform thin beam, when rotary inertia and shear deformation are neglected, Euler-Bernolli beam equation is [34-36]

$$EI\frac{\partial^4 w}{\partial x^4}(x,t)+\rho A\frac{\partial^2 w}{\partial t^2}(x,t)=f(x,t) \tag{3.1}$$

where

E -- Young' s elastic modulus [N/m^2]

I -- cross-sectional area moment of inertia of the beam [m^4]

ρ -- material density [kg/m^3]

A -- cross-sectional area [m^2]

$f(x,t)$ -- distributed force along beam [N/m]

Since the equation of motion involves a second order derivative with respect to time and a fourth order derivative with respective to x, to find a unique solution for $w(x,t)$, four boundary conditions are needed and two initial conditions are needed. These boundary conditions can be defined by four values, including displacement, slope, moment and shear force, at both ends. The natural frequencies of the beam lateral vibration can be obtained as

$$\omega = (\beta l)^2 \sqrt{\frac{EI}{\rho A l^4}} \tag{3.2}$$

where l is the length of the beam. Some extreme boundary conditions, like clamped, free, support, etc. can easily define four boundary conditions. A series of values for βl can be obtained for limiting boundary conditions, and the details can be found in (Necsulescu and DeAbreu 1998) [34]. The analysis of thin beam theory gives the relation between boundary conditions and vibration parameters. For complex boundary conditions, like bolt tightness or looseness, this traditional method does not give a easy solution.

3.2.2 Finite element method

A 2-D finite element analysis was performed with ADINA to determine the frequency response of aluminum beam [36]. Four-node qudrilaterial shell elements were used (6851 in total) to model the 890 x 28 x 1.2 mm beam [38-42]. To determine an optimized edge length, which is related to element numbers divided on beam, the case of tight bolt and of clamped end boundary conditions

were modeled. A parametric study for Mode 12 (literal vibration Mode 9) was convinced out for various values of the edge length of one element and the results are listed in Table 3.2.

Table 3.2 Frequency of Mode 12 vs. number of element

Edge Length	6mm	5mm	4mm	3mm	2mm	1.5mm
The Number of Elements	1829	2752	3882	6851	16773	29416
Natural Freq. [Hz]	391.846	390.639	389.663	388.890	388.347	388.126

The trend of convergence with the number of elements is shown in Figure 3.3.

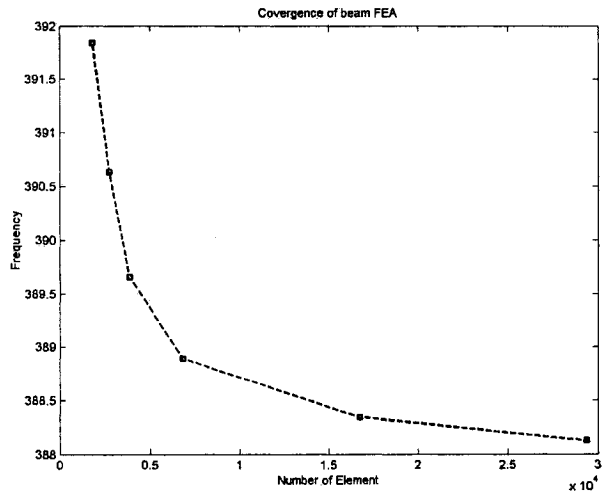

Figure 3.3 The variation of natural frequency with the number of elements in beam FEA

The whole beam cannot divided into a very large number of elements given the limits of the computer. Considering both the calculating capability of available computers and the accuracy of simulation, the 3 mm edge length for every element was chosen to solve for the normal modes of the beam, given that a change in natural frequencies of less than 0.1% by result from decreasing further the element edge by 1 mm at the edge length less than 3 mm.

To simulate a clamped boundary condition at right end, 153 elements in the area (50x 28 mm) on the left end were all constrained in all of their degrees of freedom, while, at left end, 68 elements in a concentric ring (outside diameter 14 mm, inside diameter 7mm), which was the area covered by the washer, were constrained in all of their degrees of freedom to simulate bolt tightness. Figure 3.4 shows the detail.

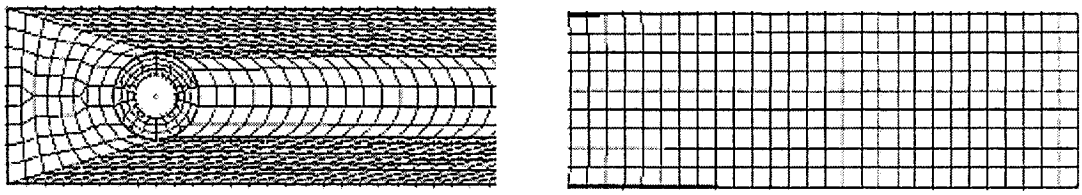

Figure 3.4 Boundary condition in detail for FEM

Isotropic aluminum shell was defined with thickness 1.2mm. Natural frequencies of beam were calculated up to Mode 13 (lateral vibration Mode 10) and listed in Table 3.3. Mode shapes are shown in Figure 3.5.

Table 3.3 Natural frequencies of tight bolt beam by FEM

	Mode 1	Mode 2	Mode 3	Mode 4	Mode 5	Mode 6
F [Hz]	9.722	26.80	52.55	86.90	129.9	167.0
Mode 7	Mode 8	Mode 9	Mode 10	Mode 11	Mode 12	Mode 13
181.5	225.4	241.9	311.0	334.4	388.9	475.6

It is more difficult, however, to simulate every stages of bolt looseness, and consequently the solution is to reduce numbers of constraint element in the area of washer covered. This solution can result from assuming that constrained elements between the beam and the washer surfaces suffer an adjustment to

match the torque increase or decrease on bolt and consequently, when more torque is applied, more elements are affected. In this thesis, an analysis of totally free bolt on the left end was simulated with vertical centerline of concentric ring, constrained like two short pins along this line, and the natural frequencies up to mode 13 were calculated and shown in Table 3.4. Mode shapes can be seen in Figure 3.6. The results shown in Fig 3.5 and 3.6 are used later for the analysis of detectable modes.

Table 3.4 Natural frequencies of loose bolt beam by FEM

	Mode 1	Mode 2	Mode 3	Mode 4	Mode 5	Mode 6
F [Hz]	6.585	21.34	44.51	76.10	116.1	164.5
Mode 7	Mode 8	Mode 9	Mode 10	Mode 11	Mode 12	Mode 13
165.6	220.0	221.3	286.4	331.6	359.7	441.1

These natural frequencies by FEM are close to experimental results and a detailed comparison will be given in Chapter 4.

Detectable Mode Analysis Besides the calculation of natural frequencies with FEM, the relationship between sensor residue and vibration mode remains still to be found in order to obtain an indication regarding the exciting frequency.

Although the sensing ability of piezo-ceramic depends on the strain applied on a piezo-sensor, the PZT strain has inevitable relation with the curvature of mode shape of lateral vibration. By checking mode shape of lateral vibration of beam, the largest strain should locate on the area of crest or trough of mode shape, where the curvature is smallest. So, the most detectable mode

under mode 14 can be deduced accordingly. For piezo-sensor located 100 mm away from the end, one mode from mode 9, mode10, mode12 and mode 13 (mode 7, mode 8, mode 9, mode10 in lateral only) could be the most detectable mode because the sensor positions on the crests of these mode shapes by the results on ADINA, and the voltage signal must be the strongest due to the highest strain when that mode shape appears. Comparing the results of experiment, mode 12(mode 9 in transverse) proved to have the strongest effect.

Mode 1

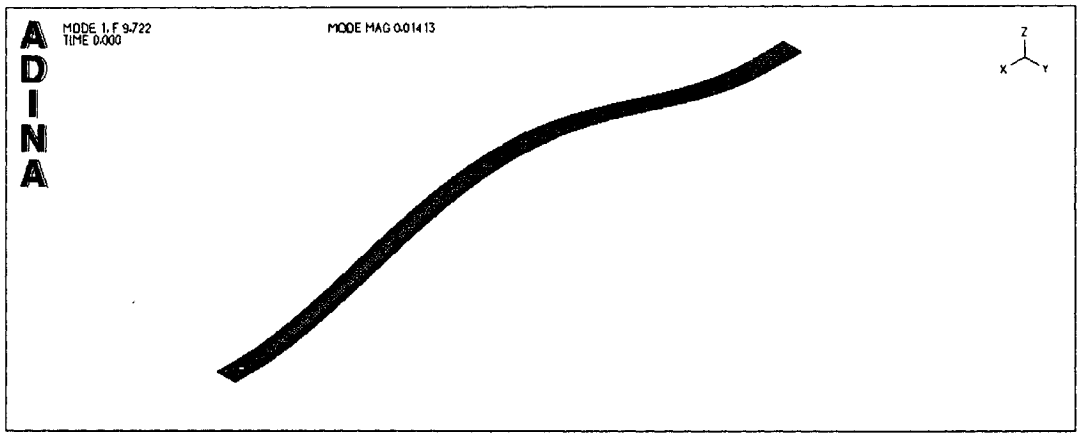

Mode 2

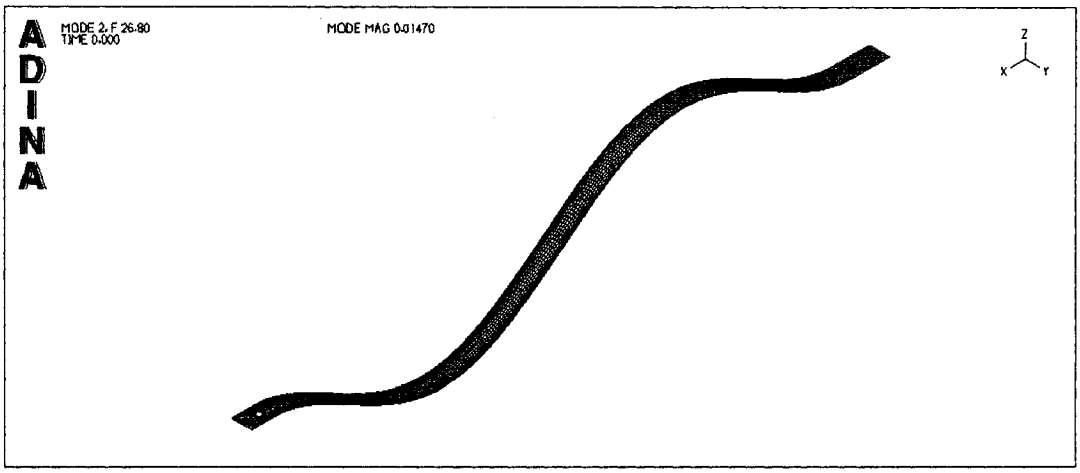

Mode 3

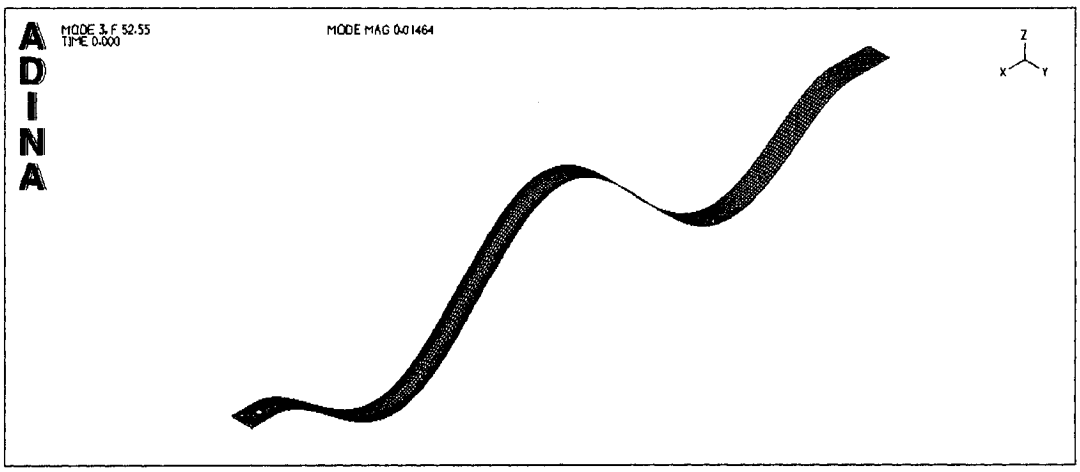

Figure 3.5 Mode shapes of tight bolt by FEM

Continued Sketch 1

Mode 4

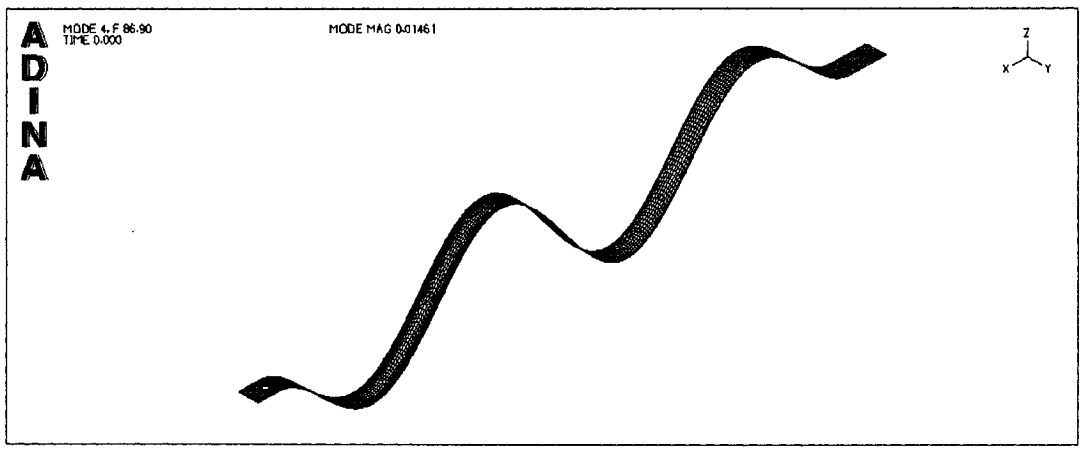

Mode 5

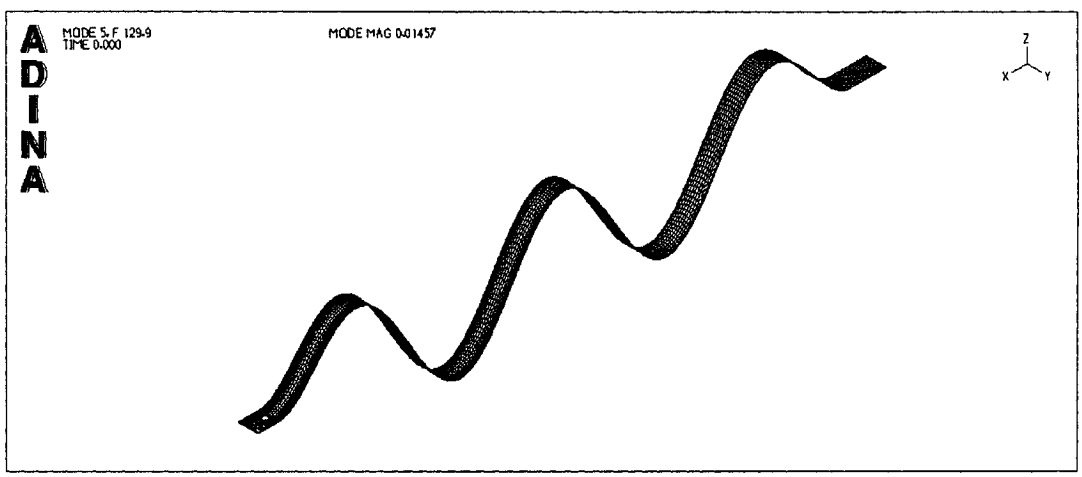

Mode 6

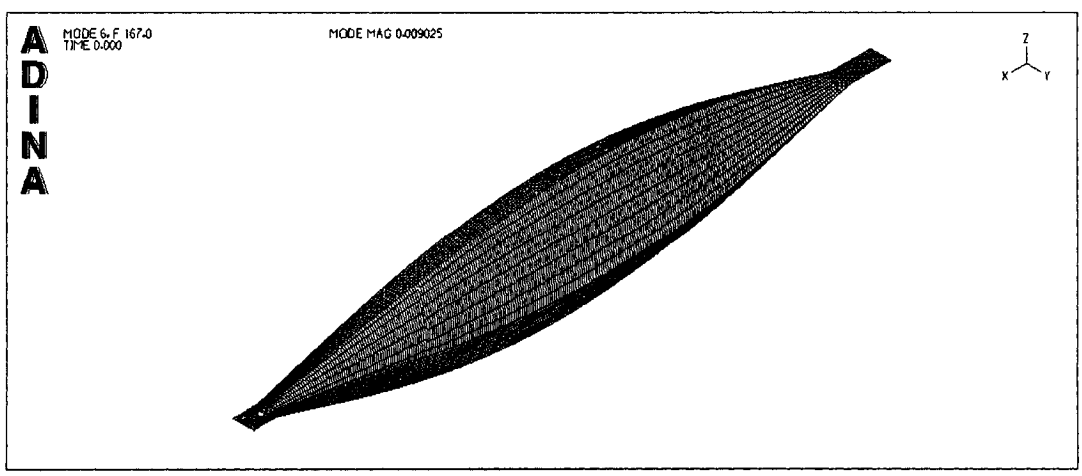

Continued Sketch 1

Mode 7

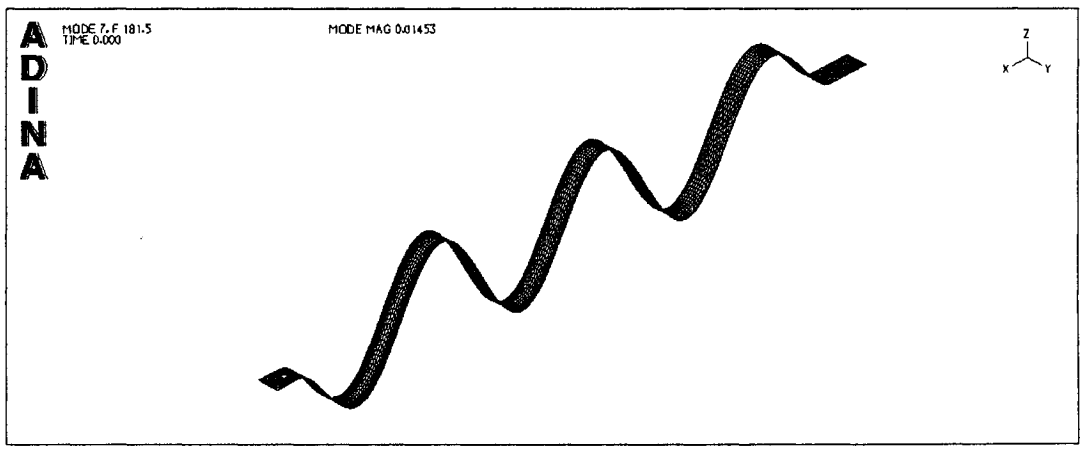

Mode 8

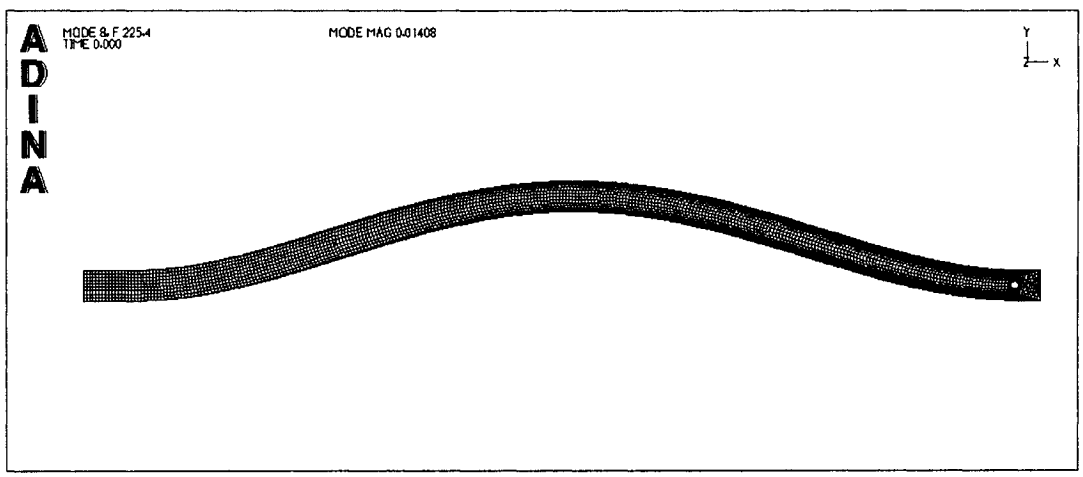

Mode 9

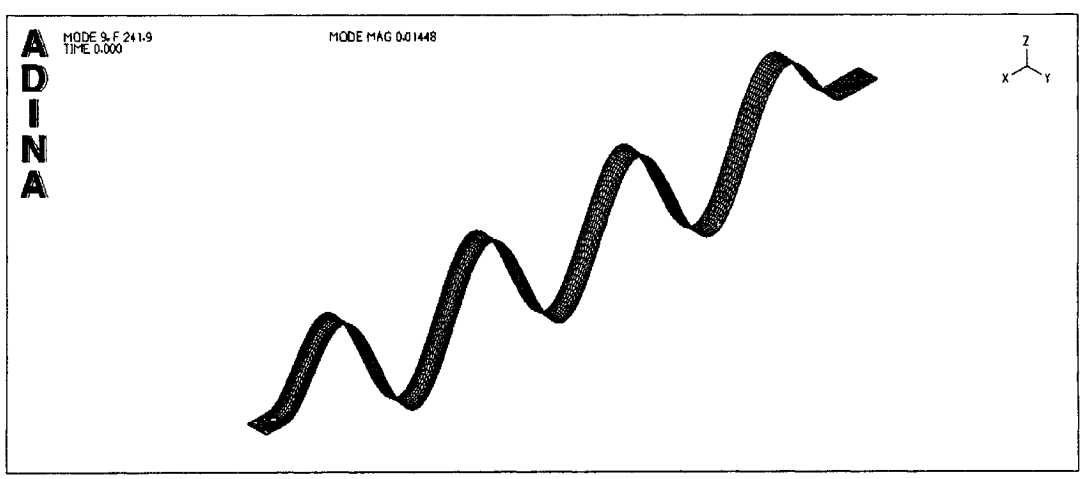

Continued Sketch 1

Mode 10

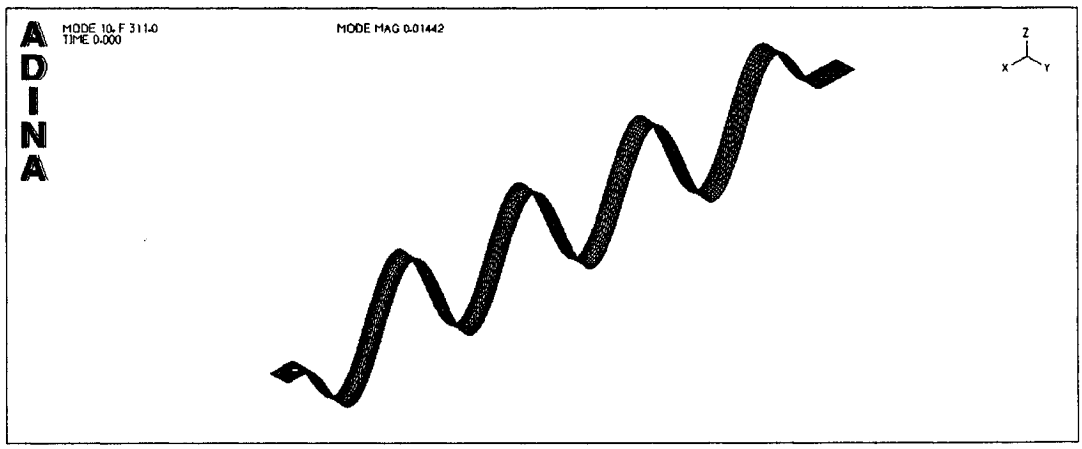

Mode 11

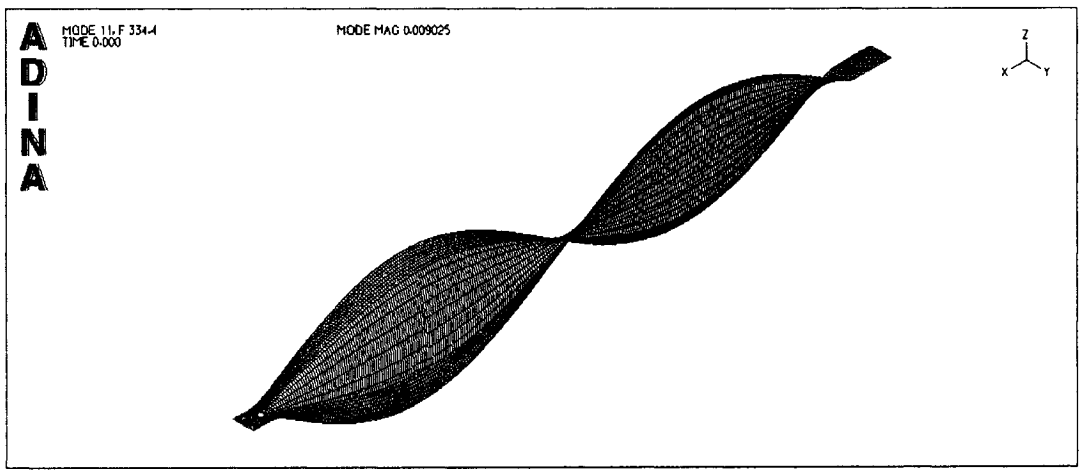

Mode 12

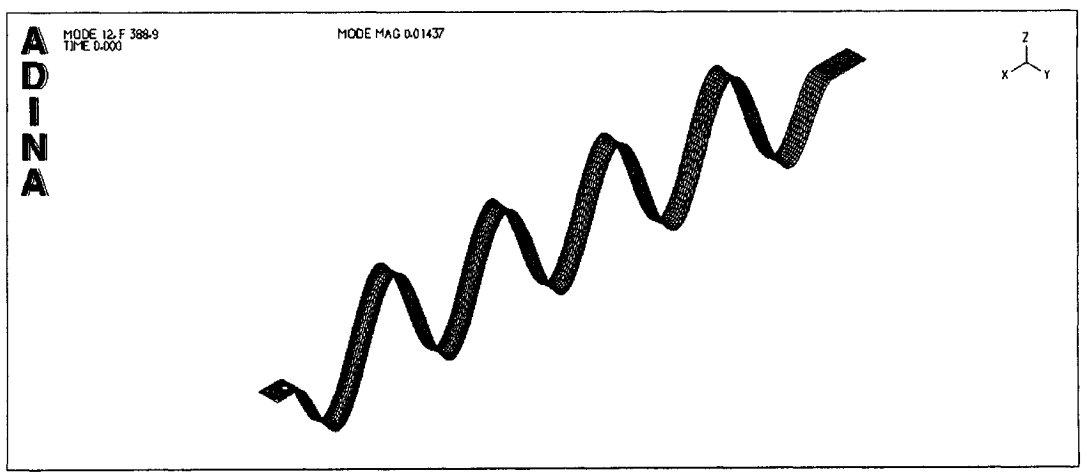

Continued Sketch 1

Mode 13

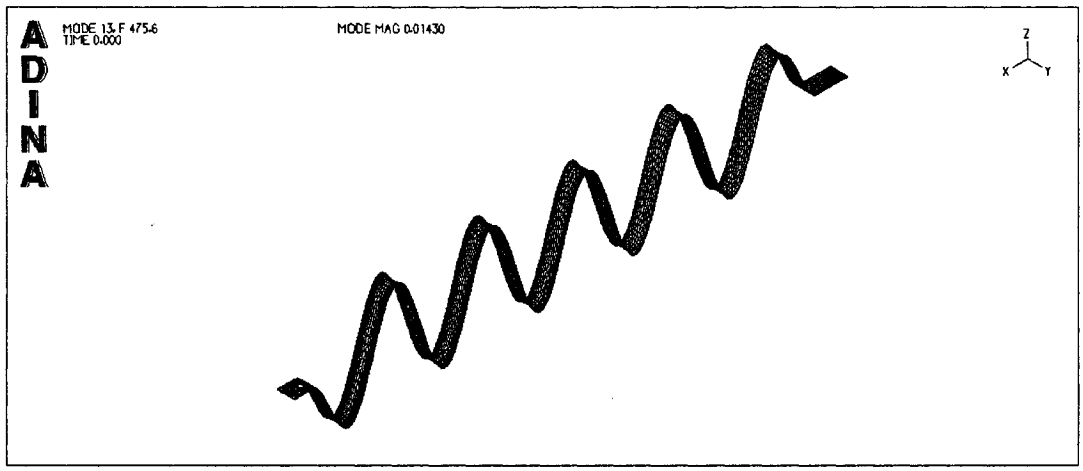

Mode 1

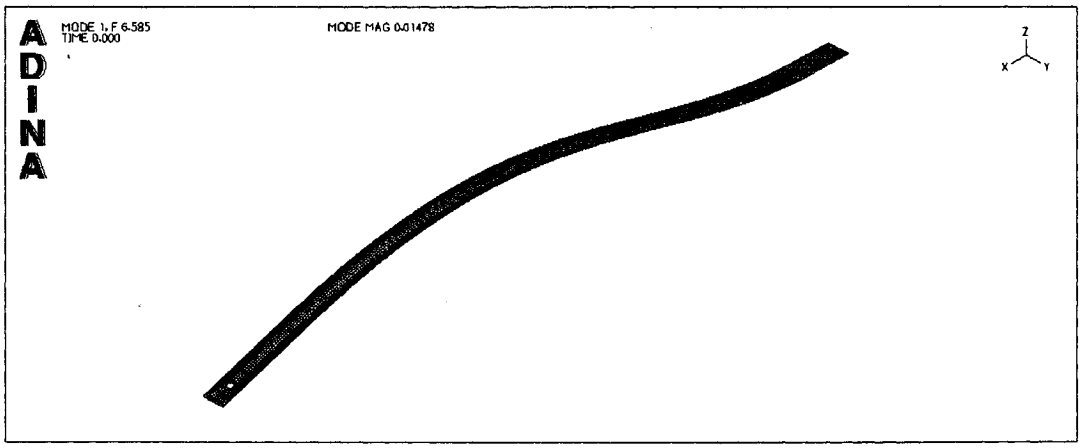

Mode 2

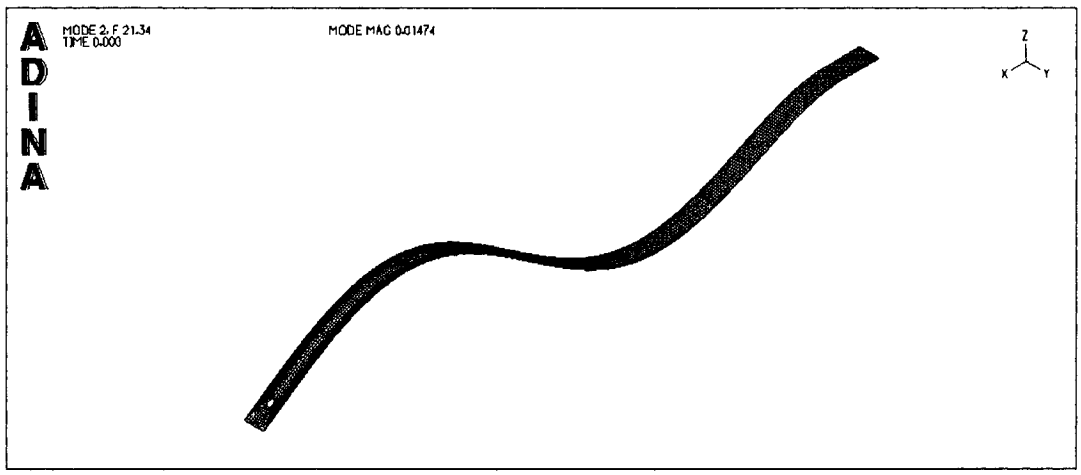

Mode 3

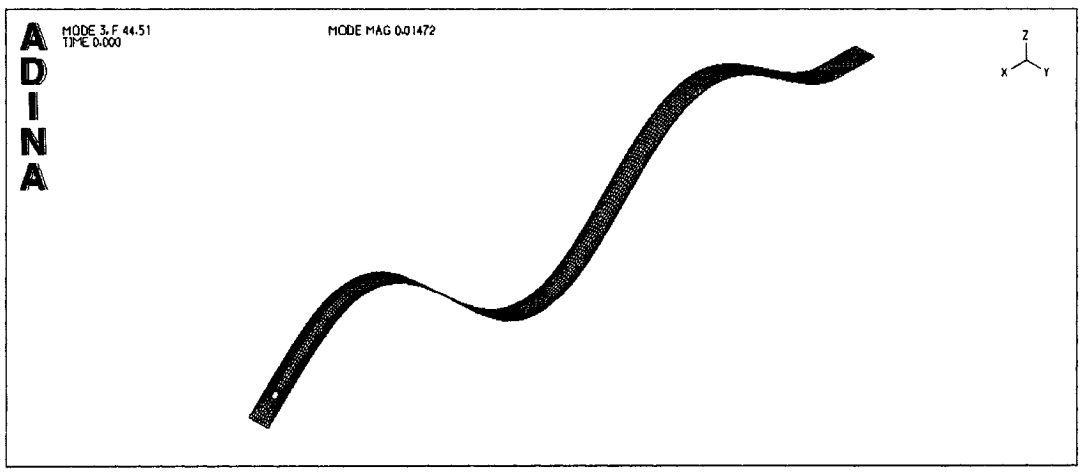

Figure 3.6 Mode shapes of totally loose bolt by FEM

Continued Sketch 1

Mode 4

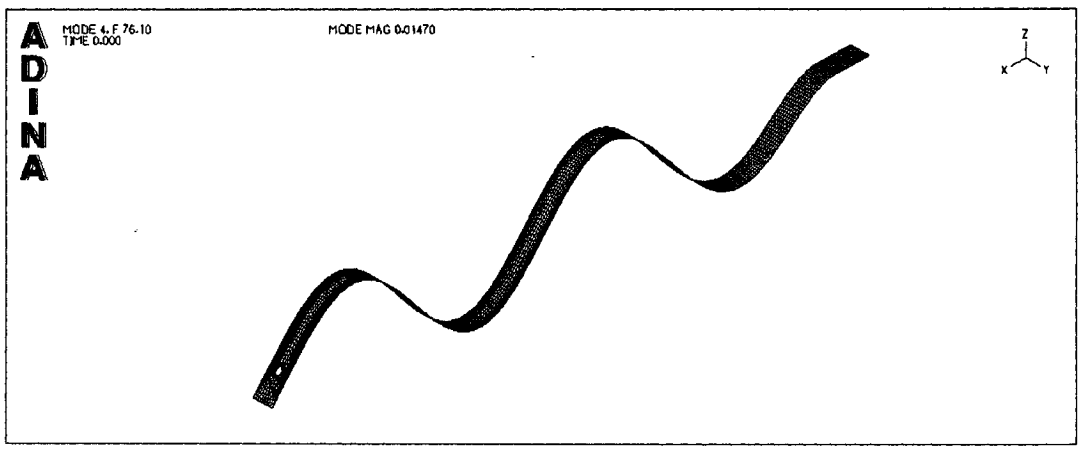

Mode 5

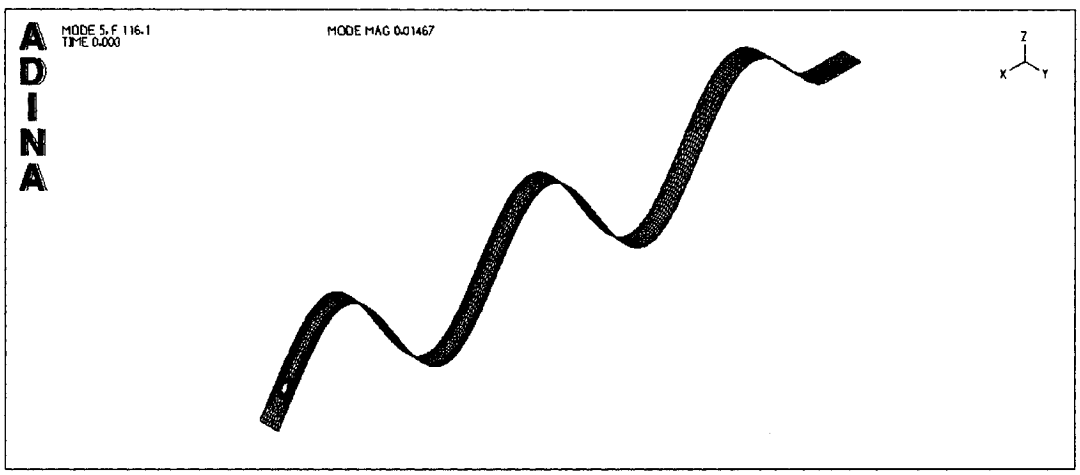

Mode 6

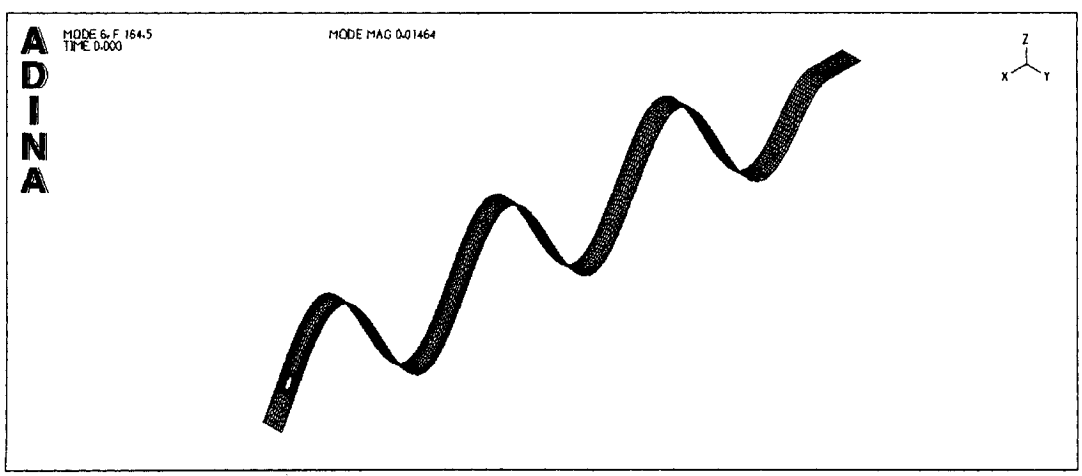

Continued Sketch 1

Mode 7

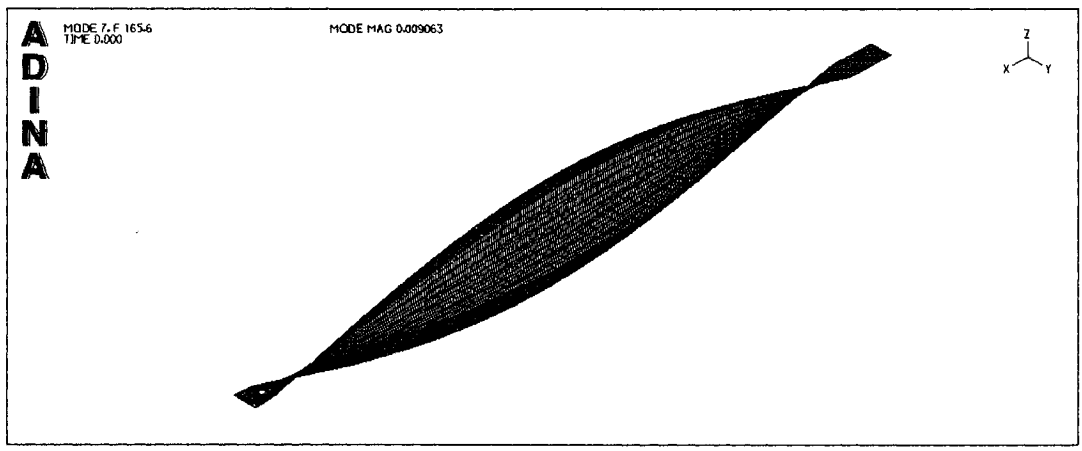

Mode 8

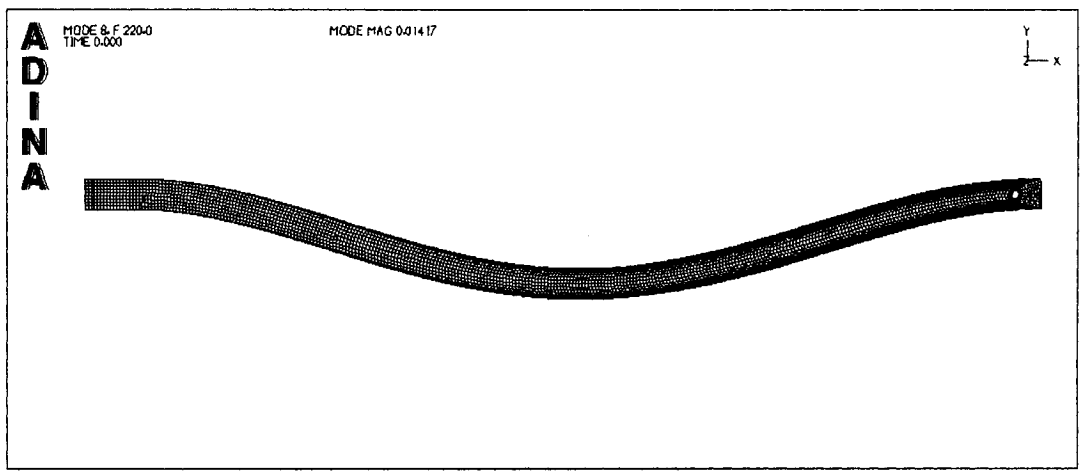

Mode 9

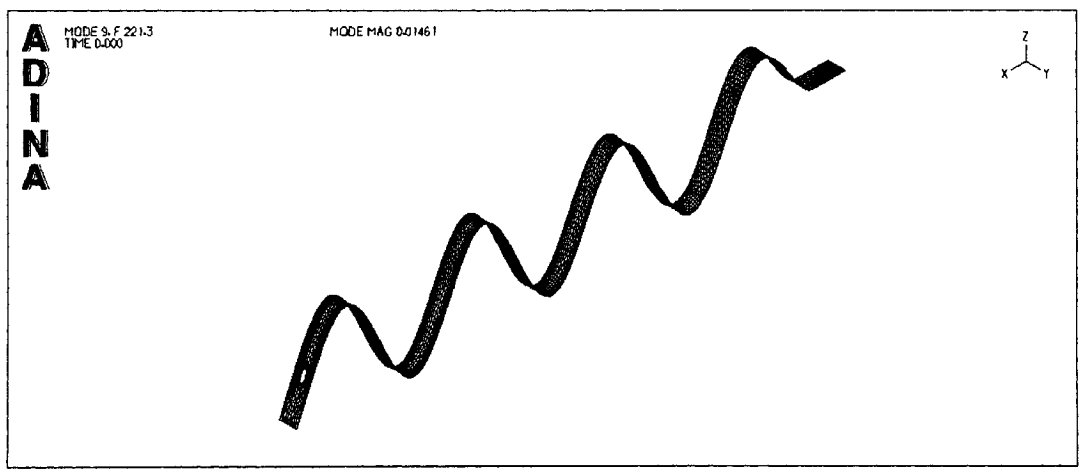

Continued Sketch 1

Mode 10

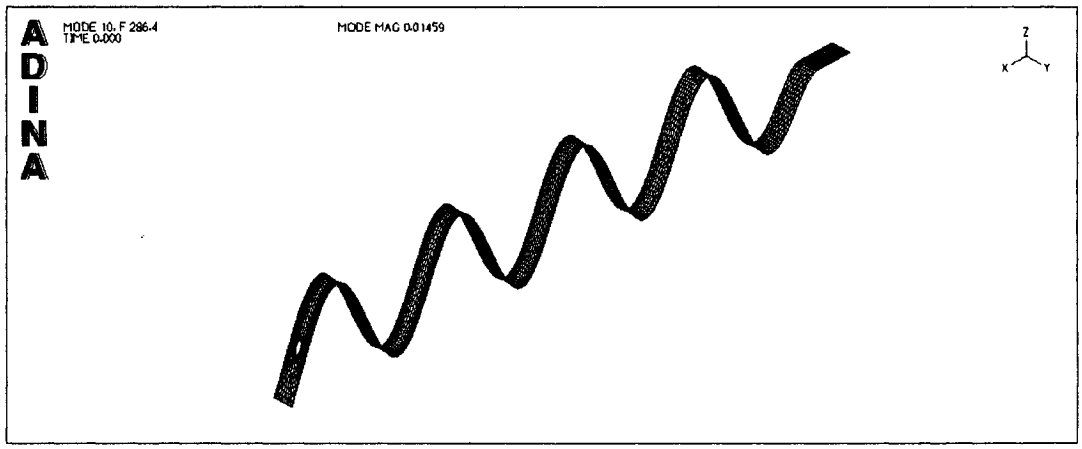

Mode 11

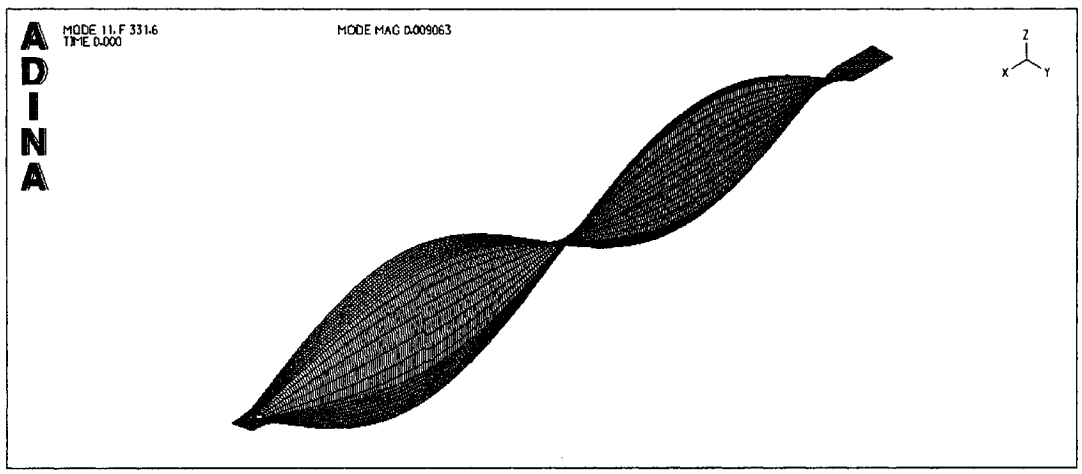

Mode 12

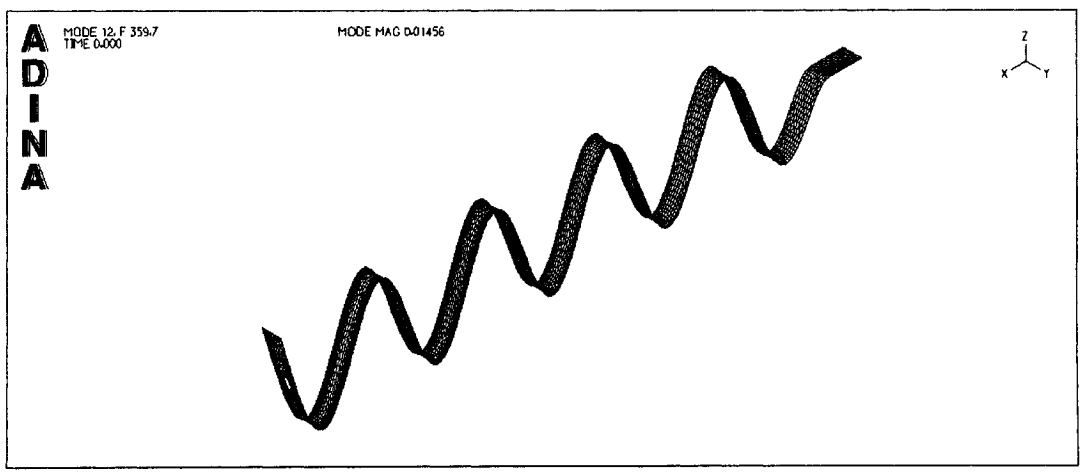

Continued Sketch 1

Mode 13

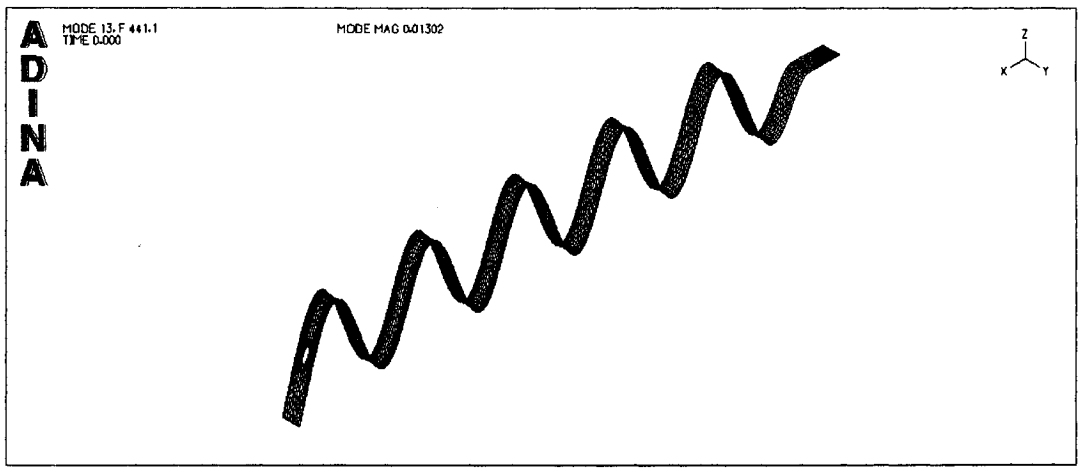

Chapter 4

Experimental Study

This thesis involves three series of SHM experiments defined by the approach used: frequency response approach, real time damage detection exploration and wavelet analysis method. Similar detection systems were used to perform these experiments for all levels of connection damage, defined by circular angle of bolt loosing rotation. The design of exciting signals depends upon signal processing methods because specified types of vibration responses are needed for different transform analysis respectively.

4.1 Experimental Setups

In Chapter 3, the structure of beam connection combined with piezoelectric patch actuator and sensor are described in conjunction with the purpose of this research. The physical characteristics of piezoelectric actuator and strain sensor can be found in [43]. A spring washer was added between the bolt and the plain washer so that loosening rotation could be counted longer until totally free. Figure 4.1 shows the devices involved in connection damage detection experiment. The three routes of the experiments are shown in Figure 4.2 and the function of devices is summarized in the following section.

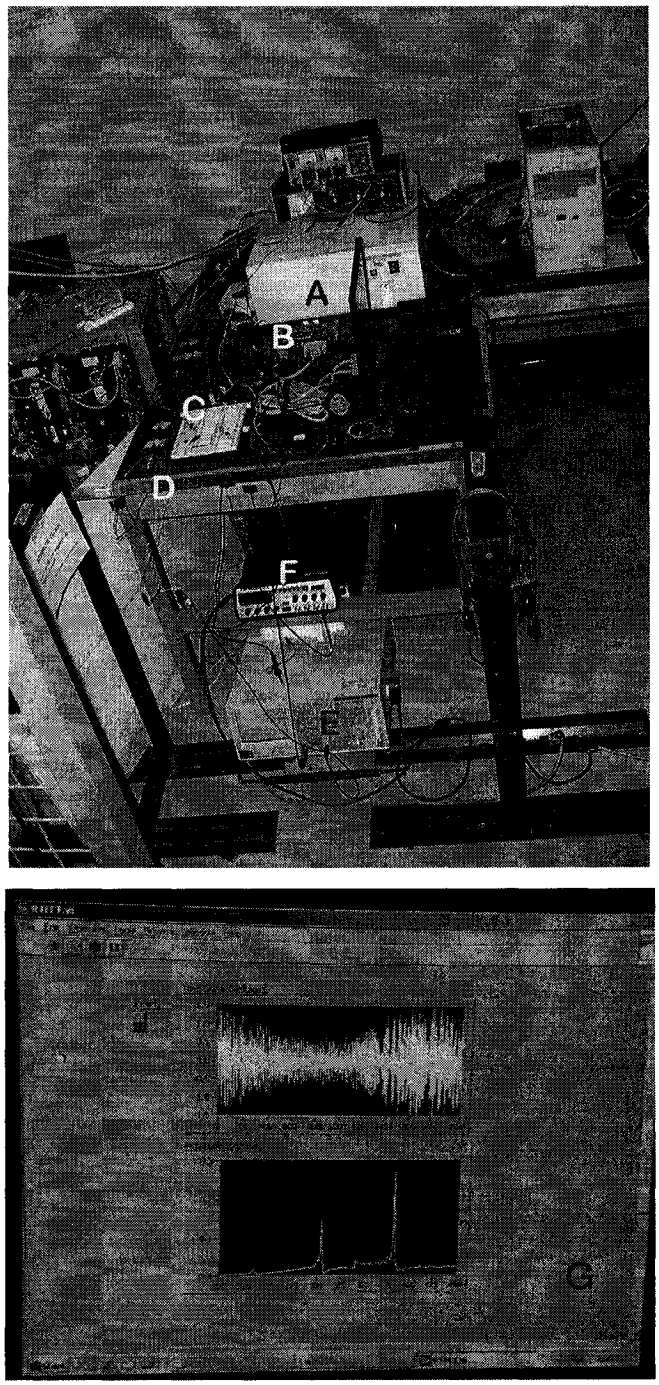

Figure 4.1 Setup of experiment

A - dSPACE (an expended hardware system for digital signal processing)

B - DSP56F807 Evaluation Board

C - Analog signal processing circuits

D - Aluminum beam with two piezoelectric patches

E - BK Precision oscilloscope 2522

F - BK Precision signal generator 3022

G - LabVIEW front panel (LabVIEW system interface)

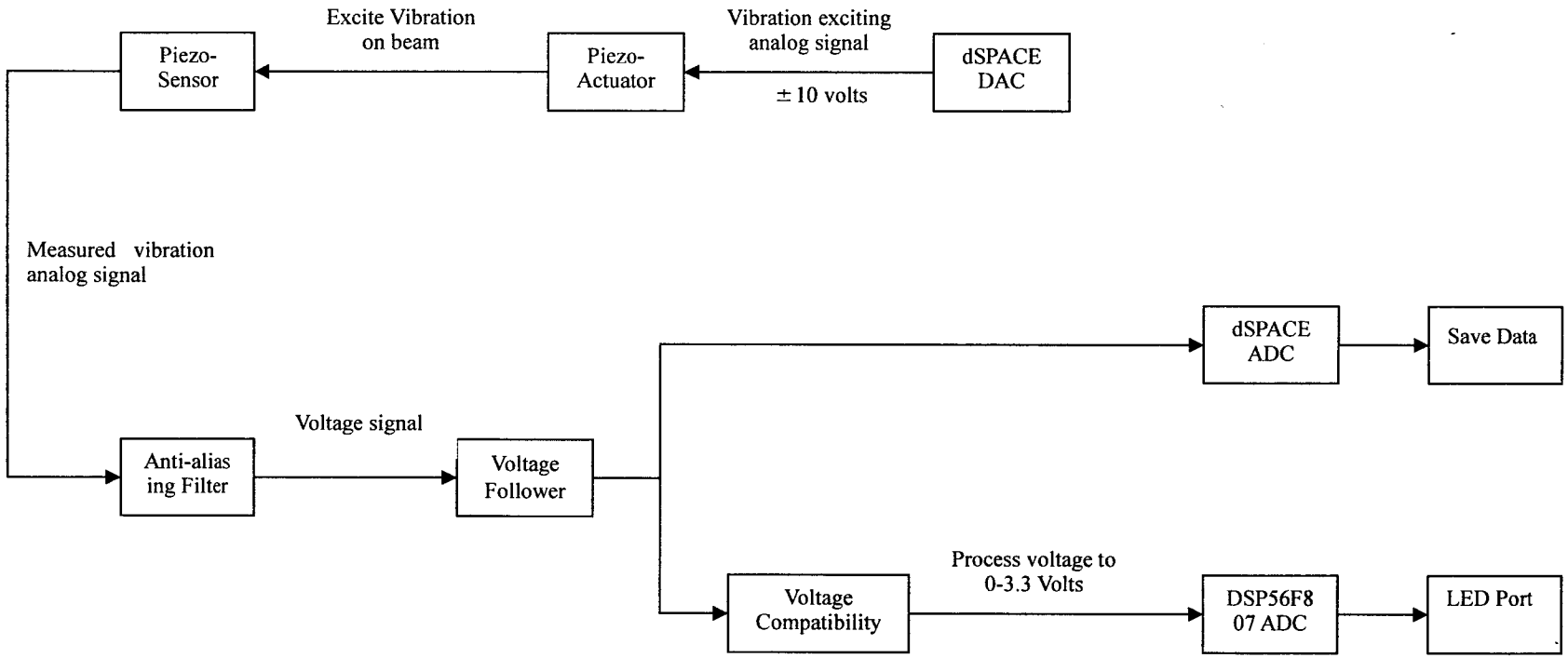

Figure 4.2 Connection damage testing signal routine

4.1.1 Frequency response approach

In Figure 4.3 is shown the experimental set up using C program PC-compiled for dSPACE for generating multi-cycle chirp signals and then outputting analog chirp exciting signal with amplitude ± 10 volts through D/A port on DS2101 board to piezoelectric actuator to produce actual beam vibrations. The chirp signal is a type of sine wave signal with frequency higher and higher during its time duration. There is also an impulsive type of input or fast sine sweep that can have excitation over a wide range of frequencies. The piezoelectric sensor, on the backside of beam, transmits electrical signals dependent of beam motion to the analog Signal Processing unit. Figure 4.2 shows this Signal Processing section composed of an anti-aliasing low-pass filter and a voltage follower. From this purpose, the data are transmitted back to dSPACE through ADC located on DS2001 board [42]. Afterwards, the digital data were saved on the memory of dSPACE system and eventually transferred into PC for off-time analysis.

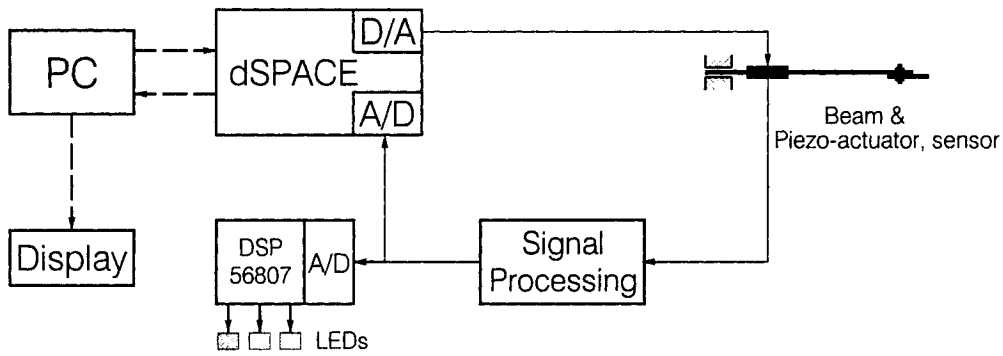

Figure 4.3 dSPACE detection system

4.1.2 Real time damage detection

The excitation signal, response signals and resulting data processed in real time are the same as in the case of frequency response approach but, for

acquiring data, a Motorola DSP56F807 evaluation board was used instead of dSPACE. Between voltage follower and DSP56F807, an ADC compatible circuit was needed for achieving voltage compatibility.

The goal of real-time SHM is to determine the health condition during actual the operation, in order to address a major safety concern to pilots in flying vehicles. The fundamental requirements for these systems are low cost, lightweight, space saving, embedded form and low power consumption. For this thesis, a 16 bit fractional computational Motorola DSP56807 embedded chip [44-46] is used to process time domain signal to frequency domain in real time, because its hybrid design provides both advantages of a micro-controller and a DSP. It is small, cheap and fully embedded and can be used for various applications, for example, communication, real-time control, detection, etc.

4.1.3 Wavelet analysis method

The transient multi-cycle sinusoidal excitation command signals were generated by dSPACE for driving the piezo-actuator. The response signals from beam vibration were first transmitted to an anti-aliasing low-pass filter. The data were collected by ADC on DS2001 board and saved in dSPACE.

At the beginning of experiments, a BK Precision signal generator (Model No. 3022) served to evaluate frequency response and characteristics of analog circuits while a BK oscilloscope (Model No. 2522) was used to check the amplitude and frequency of response signal prior to actual test as well as for amplitude monitoring during the experiments, especially for the case when the signal voltage is transmitted to DSP56F807.

4.2 Excitation signal

The modal-based structural connection damage detection depends upon the inherent structural response from external disturbance. Hence, the excitation signal plays an important role to bring out the characteristic of the structure. The choice of input to be used to excite the system, in order to determine the frequency or vibration response, depends upon the characteristics of the system, upon the characteristics of the modal parameter estimation, and upon the expected utilization of the data [47].

4.2.1 Classification of excitation signals

Random excitation methods Signals of this form can only be defined by their statistical properties over some time period. Some typical random excitations include pure random, pseudo random, periodic random, burst random and their combinations. In general, the frequency content of the random signal contains energy at all frequencies and depending on the need, the signal may be filtered to include only information in a frequency band of interest. These methods are usually used to measure linear systems with a shaker acting on the structure for providing adequate vibration energy. For the embedded PZT wafer SHM system, the signal-to-noise ratio could be high because the motion induced by PZT actuator is relatively small.

Deterministic excitation methods Signals of this form can be represented in an explicit mathematical form. Typical forms include impact (impulse), step relaxation, slow sweep sine and periodic chirp. The most common

inputs in the periodic deterministic signal designation are sinusoidal in nature while the most common inputs in the non-periodic deterministic designation are transient in form. The impact excitation could be produced by the mechanical action from a shaker or from a piezoelectric wafer subject to impulse limit cycles of sinusoidal voltage inputs. For extracting frequency information in a specific range, however, the sweep signal or chirp signal is interesting to be used because these signals can be devised to cover any range of frequency and can be easily implemented algorithmically in digital signal processors. In this thesis, well-designed periodic chirp signals were used for the goal of obtaining specific range of output frequency as well as for minimizing the ratio of signal-to-noise. The vibration-based wavelet transform analysis, however, requires transient signal to process and consequently limit cycles of sinusoidal signal were used for wavelet methods.

4.2.2 Chirp signal for beam frequency response

In this thesis research, a chirp signal is designed for frequency response approach.

The advantage of chirp signal in frequency response can be summarized as follows:

1. Chirp signals can sweep a given range of frequencies, so that they can be used to excite beam vibrations in some specific range of frequencies. This means that we can get the response of beam vibration covering several natural frequencies. The chirp signal can especially be used to detect the structural damage including boundary condition changes

because any structural damage would lead to frequency drift in a given range. The chirp signal can be designed to cover a range of frequencies so as to provide information regarding the damage.

2. Closely spaced natural frequencies for the chirp signal is used to drive the piezoelectric patch for beam damage detection.
3. The approach using chirp vibration is a global indicator of damage when comparing to methods that use single frequency tone bursts and wave reflection to detect damage.

4.2.3 Selection of chirp signal

A function of a sinusoid signal can be expressed as $\sin(2\pi * f * t)$, where t is time and f is the frequency of the signal. The product of (f*t) is linear if f is a constant and the frequency of signal is fixed. For frequency of a chirp signal changing higher and higher with time going, for example when f(t) = b + c*t, we obtain a parabolic function $(f(t)*t) = b*t + c*t^2$. The prototype of a chirp signal function is $\sin(2\pi (a + b*t + c* t^2))$ and contains a constant $a \neq 0$.

Figure 4.4 shows some curves of stable frequencies, 50t (50Hz), 100t (100Hz), 200t (200Hz), 300t (300Hz), 400t (400Hz), 500t (500Hz), 600t (600Hz), and two chirp signals at $(f*t) = 120*t+180*t^2$ and $40+180*t+200*t^2$ for frequencies of 120+360*t and 180+400*t respectively. These signals are generated in 1-second cycle. We can see that $\frac{d}{dt}(120*t+180*t^2)$ = 120+360*t starts from 120 Hz, intersects with some stable frequency lines and stops at 480 Hz, while 180+400*t spans at a higher range of frequencies from 180 to 580 Hz with time,

getting faster and faster.

The simulation of FEM in Chapter 3 indicated that the strongest response obtained by PZT patch sensor should be occurred in mode 9, mode10, mode 12 or mode 13, where the natural frequencies under bolt tightness boundary conditions is from 241.9 to 475.6 Hz. For a cycle of the chirp excitation of 1 second, the signal function $\sin(2\pi(40+180*t+200*t^2))$ covers in this case the whole range of frequencies. Figure 4.5 shows the time domain of the chirp signal, and the power density distribution in the range of frequencies.

The figure of power density distribution versus frequency verifies the chirp signal concentration in 180 to 580 Hz range. This chirp signal will be used to excite beam for determining resonant frequency drift due to bolt connection damage.

4.3 Modal data acquisition and signal processing

Acquisition of vibration signal data that will be used in the estimation of a modal model involves many important technical concerns. The primary concern is the digital signal processing part regarding the conversion of analog signals into a corresponding sequence of digital values that accurately describe the time varying characteristics of the system inputs and responses. Once the data is available in digital form, the most common approach is to transform the data from the time domain to the frequency domain by use of a FFT algorithm [48]. Since this algorithm involves discrete data over a limited time period, there are

significant potential limitations with this approach that must be well understood.

4.3.1 Signal Processing

In order to determine modal parameters, the response data from piezo-sensor must be processed and put into a form that is compatible with the frequency response processing methods. The signal processing in this modal testing involves both analog and digital signal processing is applied for anti-aliasing, noise or leakage reduction, and ADC compatibility.

The important utilization of analog signal processing in this thesis experiment is in the field of anti-aliasing filter because it is indispensable to obtain an accurate spectrum of response by sequential FFT on a digital signal processor. Since the aliasing error is brought in by digital signal processing itself, it cannot be solved by digital methods [49]. Hence, an anti-aliasing filter was designed using a general impedance converter (GIC) filter [50], which is an active low-pass filter with cutoff frequency at 600 Hz and minimum 40 dB at 1000 Hz suitable for the case of a chirp signal excitation in 180 to 580 Hz range. Figure 4.6 shows the circuit and 4.7 shows the ADC compatible circuit required by DSP56F807 ADC port. Figure 4.8 shows the frequency versus magnitude diagram after anti-aliasing filter

Digital signal processing methods involved in these experiments were utilized to reduce leakage and noise through both PC and embedded DSP chip, where MATLAB toolboxes were used to analyze data offline on a PC and online for real-time operation for the DSP56807 chip. For leakage reduction, the measured time-domain signal data series were convoluted with a series

traditional effective weighting factors from the Hanning Window function, then the weighting signal were transformed to frequency domain by FFT. To lower the effect of external noise, however, different methods should be used based on identification of noises such as zero-mean electrical transducer noise and bias noise. The methods of coping with these two noises are described as linear average method and digital filter usage respectively. The simplest linear average method reduces zero mean noise through finding the mean value of several cycles of response signal. Digital high-pass filter was devised to reduce the DC bias due to analog signal processing [51,52], which is of Chebyshev type with parameters of 15 Hz stop and 40 Hz pass frequency (Figure 4.9).

4.3.2 Analog to digital conversion

The goal of the analog to digital conversion (ADC) process is to obtain the conversion while maintaining sufficient accuracy in terms of frequency, magnitude and phase. The error of ADC could be explained by Shannon' s Sampling Theorem stating that at least two samples per period should be obtained for any frequency below the Nyquist frequency [43], which is 2 times of meaningful maximum frequency of signal. For frequency response experiments, the natural frequency of interest is below 600 Hz, according to FEM simulation presented in Chapter 3. To avoid aliasing error, the ADC sampling rate on dSPACE was selected 8192 Hz, corresponding to the sampling rate of DAC, since lower sampling frequency brings in noise due to the impulse. For wavelet analysis experiments, the sampling rate is 19100 Hz so as to provide 50 samples in each cycle for reducing excitation noise.

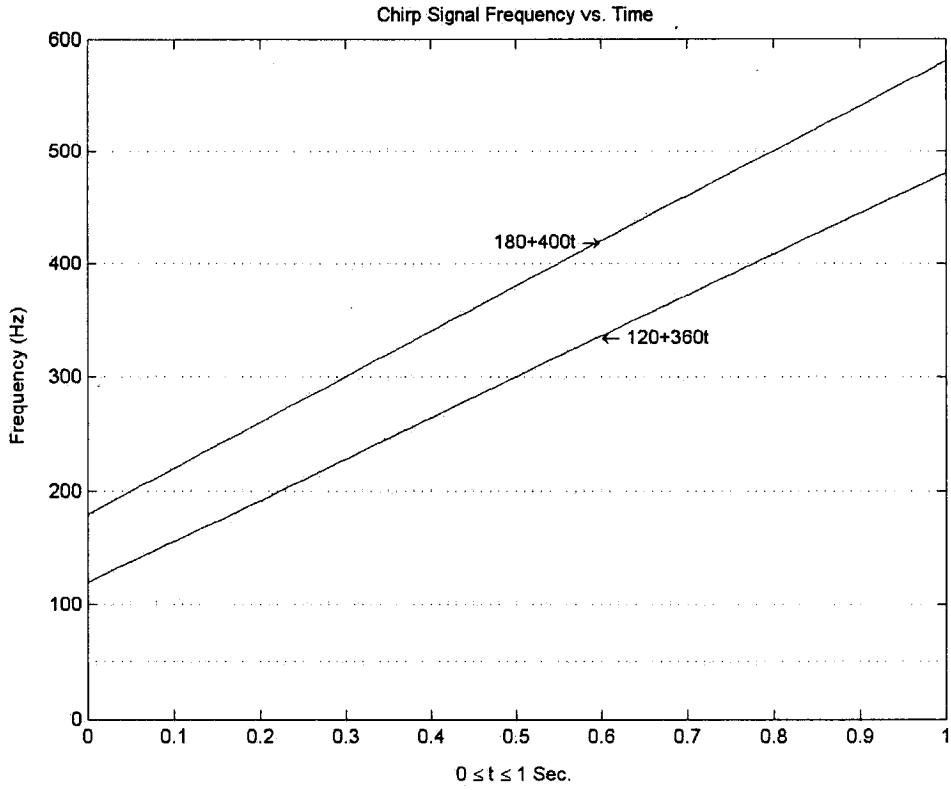

Figure 4.4 Two examples of chirp signals of frequency f(t) = b + c*t

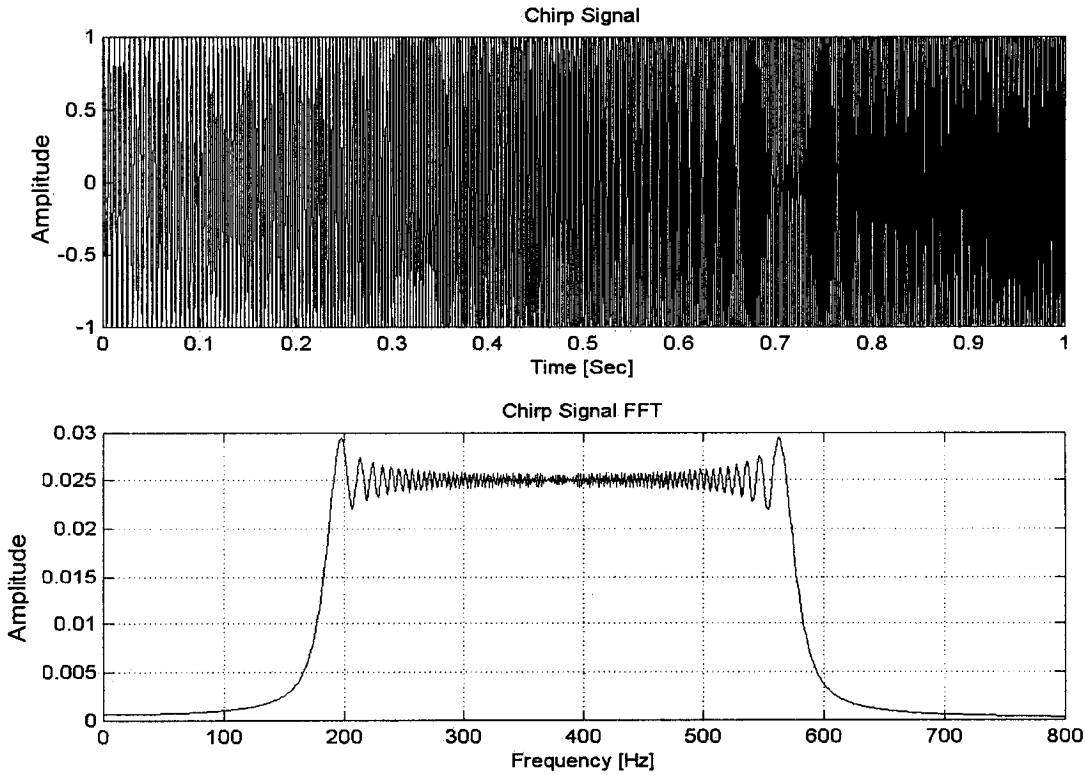

Figure 4.5 Chirp signal amplitude versus time and frequency

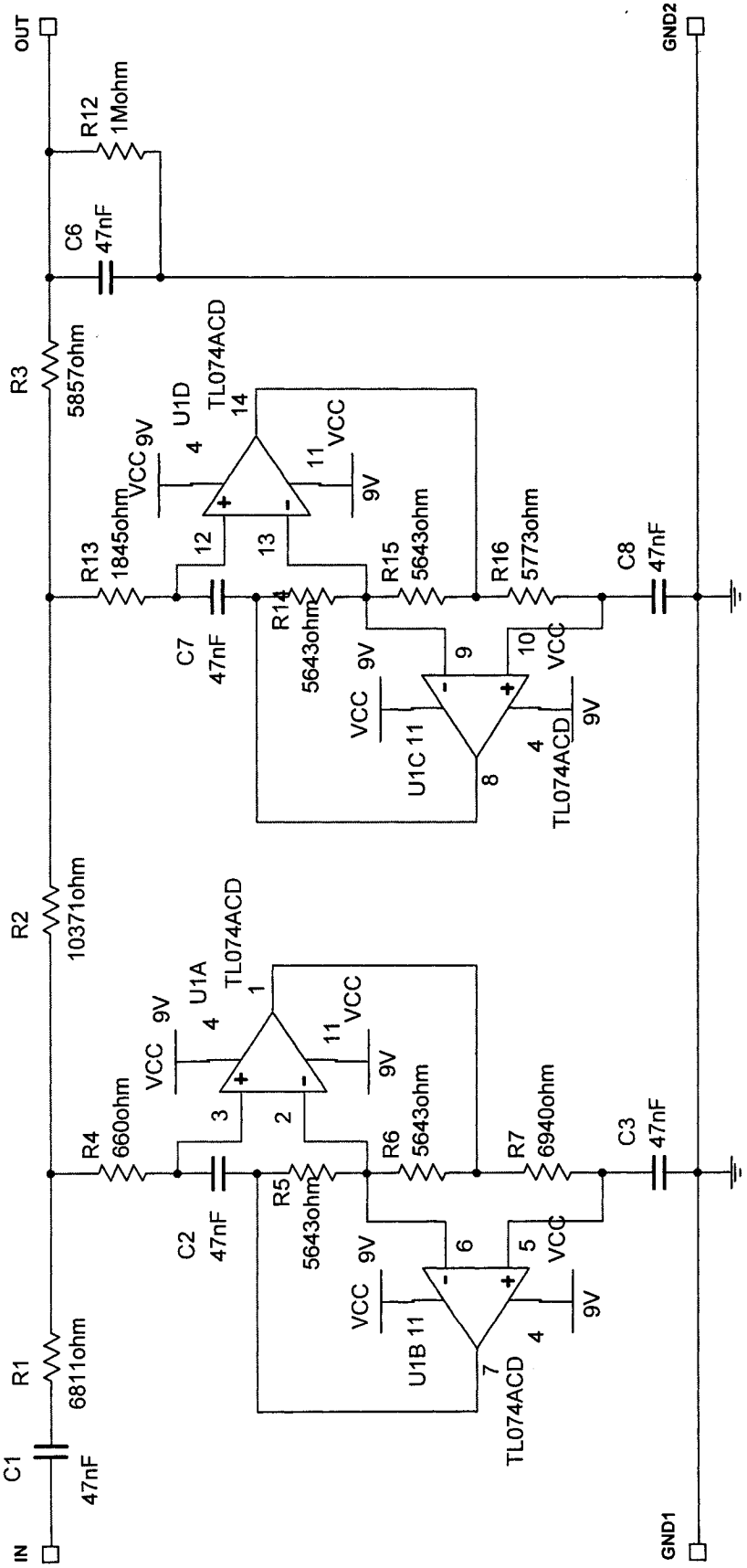

Figure 4.6 Anti-Aliasing Low-Pass Filter

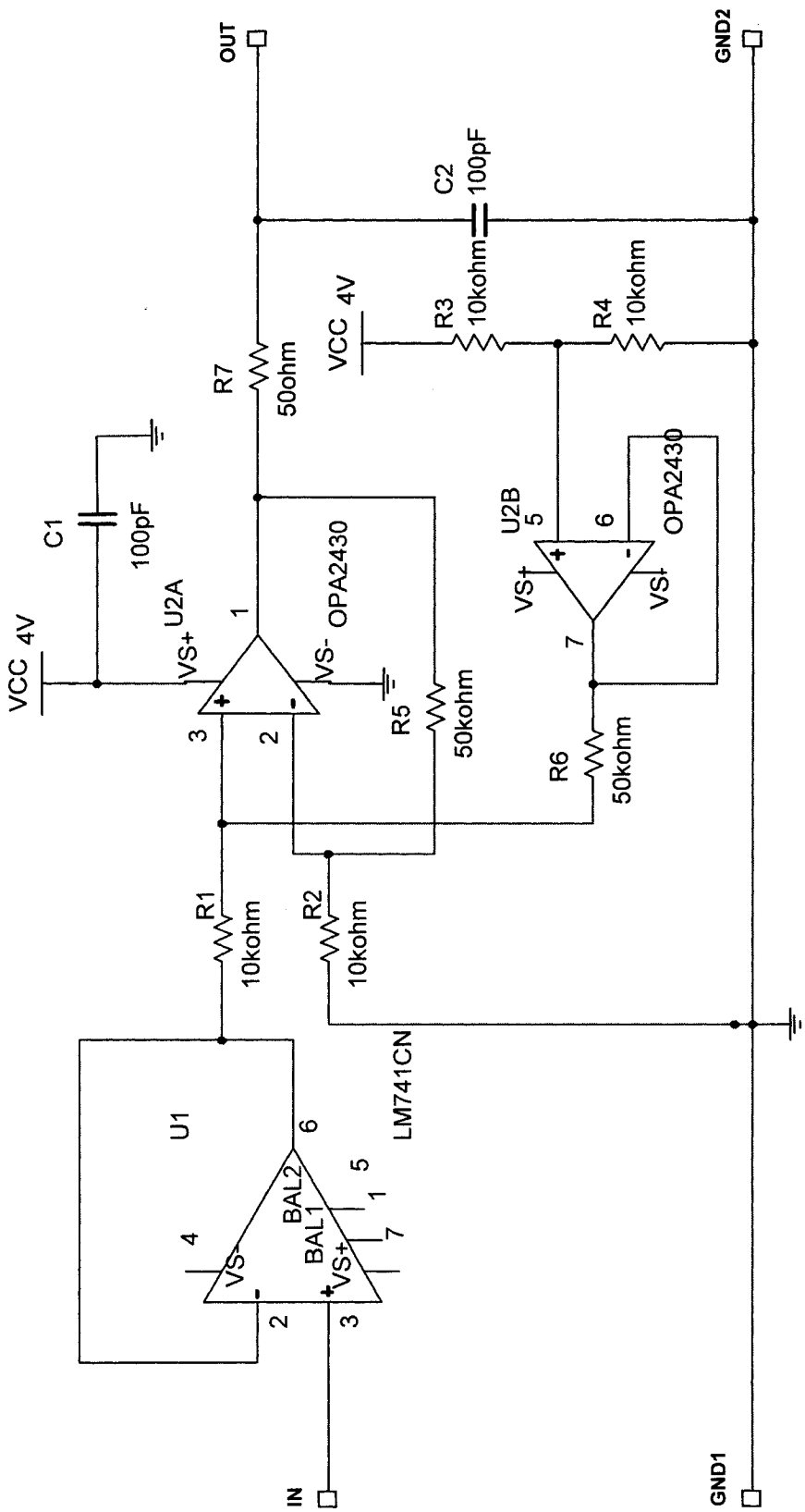

Figure 4.7 Voltage compatible circuit

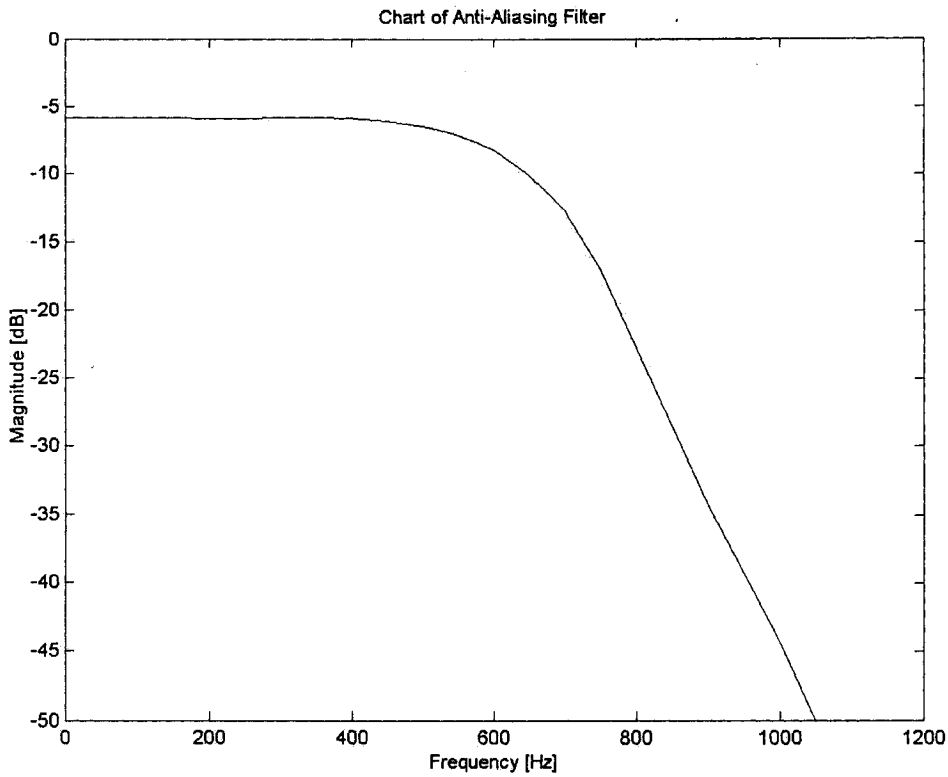

Figure 4.8 Magnitude versus Frequency after Anti-aliasing Filter

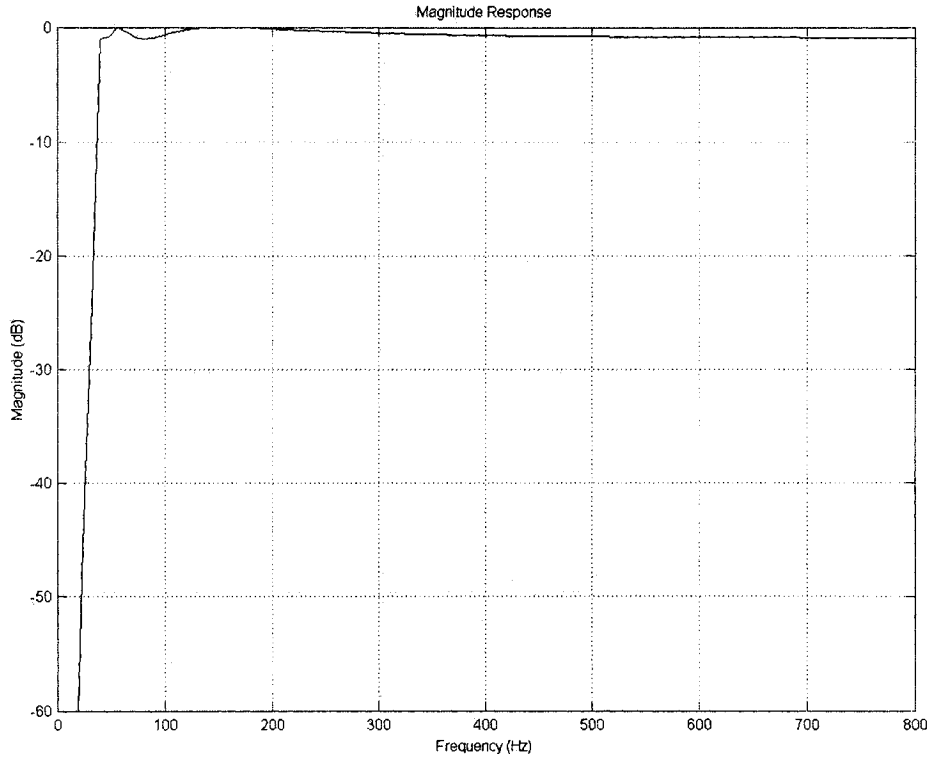

Figure 4.9 Chebyshev high-pass digital filter

Chapter 5

Frequency Response and Real-Time Detection Approach

Damage identification based upon changes in vibration characteristics is one of the few methods that monitor changes in the structure on a global basis. In this chapter, regarding frequency response methods, we will introduce for SHM. Experimental results confirm the possibility to identify the loose degree of bolt at one end of beam based on frequency response analysis. Real-time connection damage detection is also explored based on frequency response principle by introducing an embedded digital signal processor. Besides the development of a method for the evaluation of frequency response to detect bolt-loosing damage, other technical challenges are still to be addressed before its practical application for vibration-based structural health monitoring.

5.1 Background

From 1970s, the oil industry made considerable efforts to develop vibration-based damage detection methods for offshore platforms [53]. Afterwards, this damage detection approach began to extend further in civil engineering, mechanical and aerospace industries. Since then, these methods are always among the most common, principally because they are simple to implement on

any size structure. For exciting the structures, an external shaker, embedded actuators, and for measuring, embedded strain gauges or accelerometers, can be used to monitor the structural dynamic responses [54].

The model analysis is based on structural vibration, and involves a systematical research of the relationship of excitation and response in both time and frequency domain. The analysis of vibration in time domain is illustrated by the paper by H Sohn *et al* about damage diagnosis using time series analysis of vibration signals [55], and by the Master' s thesis of R D Abreu, where he tried to identify bolt loose damage by comparing the change of vibration amplitude in time domain with excitation by a transient sinusoidal signal [56]. The analysis of vibration in frequency domain is a more powerful tool for understanding structural characteristics [48], and is based on Fourier Transform. In real applications, however, the Fast Fourier Transform (FFT) is often used due to its fast algorithm when performed on digital computers. In reviewing the literature in the area of experimental modal analysis, an outline of the various techniques is helpful in categorizing the different methods that have been developed over the last thirty years. A very common approach is to group them as parametric models and non-parametric models, according to the type of models that will be used in the modal parameter estimation stage.

5.1.1 Parametric model methods

The book on modal testing by D J Ewins presented in detail general topics of the theory, practice and application [54]. The parameters that decide the character of a structure, such as natural frequency, damping ratio, impedance or admittance, mode shape and so on, could be obtained by analyzing the dynamic

response of displacement (amplitude), mobility (velocity) and accelerance (acceleration). A good report on frequency response methods can be found in the paper by B. T. Wang *et al* [57] and Y. Zou *et al* [58], which presents a review of vibration-based techniques for cantilever beam modal testing and identification for composite structure. The authors suggest that parametric model methods are capable of providing both global and local damage information, as well as a cost-effective and easily operated approach. The methods they assessed use piezoelectric sensors and actuators along with finite element analysis results to locate and estimate damage events by comparing changes in dynamic responses. The authors recommended modal analysis methods on account of their global nature, low cost, and flexibility to select measurement points, however they indicated that these methods lack the ability to localize damage and require large data storage capacity for comparisons. They claimed that frequency domain methods alone were incapable of detecting the location of damage and that when combined with time domain methods, they can detect damage events both globally and locally.

Several other papers have documented the use of a combination of the modal analysis and frequency domain methods to detect various damage types with piezoelectric actuators and sensors. Banks and Emeric [59] investigated changes in particular modes up to 1 kHz using the Galerkin method on cantilevered aluminum beams with notches, and P. A. Lovell *et al.* [60] performed an experiment to assess damage in a bolted lap joint, in which they demonstrated an approach of damping estimation from wave propagation.

5.1.2 Non-parametric model methods

Tseng et al. [61] presented in a paper their experimental results regarding non-parametric damage detection approach for a beam structure. A couple of piezoelectric ceramic (PZT) transducers were placed on the each end of the beam acting as actuator and sensor. A total of three specimens were inspected with different holes on every beam simulating the damages. The method of extracting the impedance characteristics of the PZT transducer, which is electromechanically coupled to the host structure, is adopted for damage detection. For identifying the damage, in their paper, some statistical signature pattern recognition techniques we are evaluated, and the conclusion was that the PZT transducers have a significant large sensing area for detecting even small incipient damages. Zhang *et al.* [62] investigated the use of transmittance functions for health monitoring, a technique which does not require the use of analytical models. A group of piezoelectric patches were placed on a structure, where some were used as sensors and others as actuators, and responses at certain sensor locations due to broadband actuation were recorded for the healthy structure to be later compared to a potentially damaged structure. Changes in curvature were used in this case to detect, locate and assess damage to the structure.

5.1.3 Real-time damage detection

Frequency response concerns the resonant frequency in a dynamic system, which can be seen as a parametric model method for damage detection. One of the important characters of the model-based method is to determine the

health condition by comparing current data with saved initial data. This analysis method processes a large amount of data transmitted from the sensor. In research, various spectrum analyzers are used to process the signals to frequency domain or show FR in real time. However, spectrum analyzers are expensive and cannot be embedded. For practical applications on efficient, economic, lightweight and space saving SHM system has to be found.

Although PC based data acquisition can perform signal processing, using for example LabVIEW, the operating system is not fast enough to handle large amount of data and some samples could be lost when the buffer is full. Also, such a system is not portable. Embedded computers, like micro-controllers or digital signal processors (DSP), are dedicated to real-time tasks and contain in a single integrated circuit CPU, RAM and ROM memory and interface devices for digital and analog signals [43]. These chips, especially DSP, are widely used in digital communication and image processing due to their significant capability for computation. For a practical and fully embedded connection detection system, in this thesis research a Motorola DSP56807 embedded chip with evaluation board was considered as a first solution for an embedded SHM.

DSP programming plays a critical role in damage identification, and the real-time FFT can be executed on DSP56807 so that signals can be transformed into frequency domain in real-time.

The present research investigates the feasibility of modal evaluation techniques in detecting damage for health monitoring of beam connection system. Finite element models in chapter 3 permitted to determine the band of frequencies. Subsequently, experiments were performed to validate these models

by attempting to detect the damage with dSPACE-PC based analysis and DSP56807 real-time detection.

5.2 Frequency response of a Single-Degree-of-Freedom (SDOF) system

Figure 5.1 shows basic SDOF model where $f(t)$ and $x(t)$ are general time-varying applied force and displacement response quantities. The system parameters, mass, stiffness and viscous damping, are denoted by m, k and c respectively, and the equation of motion for free vibration is

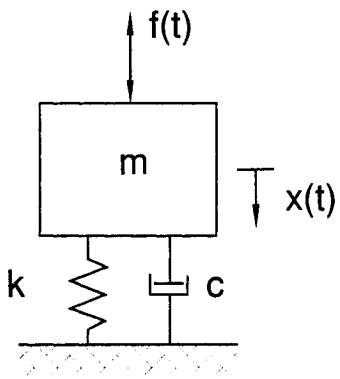

Figure 5.1 SDOF system

$$m\ddot{x} + c\dot{x} + kx = 0 \tag{5.1}$$

The general trial solution must be of the form $x(t) = Xe^{st}$ where s is complex variable. For a solution to exist, the condition $ms^2 + cs + k = 0$ must be satisfied, leading to

$$s_{1,2} = -\frac{c}{2m} \pm \frac{\sqrt{c^2 - 4km}}{2m} = -\omega_0\zeta \pm i\omega_0\sqrt{1-\zeta^2} \tag{5.2}$$

where $\omega_0^2 = (k/m)$; $\zeta = (\frac{c}{2\sqrt{km}})$.

When the force $f(t) = Fe^{i\omega_f t}$ is applied on the system, given $x(t) = Xe^{i\omega_f t}$, the equation of motion results as

$$(-\omega_f^2 m + i\omega_f c + k)Xe^{i\omega_f t} = Fe^{i\omega_f t} \tag{5.3}$$

gives complex displacement frequency response of the form

$$H(\omega_f) = \alpha(\omega_f) = \frac{1}{(k - \omega_f{}^2 m) + i(\omega_f c)} \tag{5.4}$$

We have the magnitude

$$|\alpha(\omega_f)| = \frac{|X|}{|F|} = \frac{1}{\sqrt{(k - \omega_f{}^2 m)^2 + (\omega_f c)^2}} = \frac{1/k}{\sqrt{(1 - \omega_f{}^2/\omega_0^2)^2 + 4\zeta^2(\omega_f{}^2/\omega_0^2)}} \tag{5.5}$$

In which the maximum magnitude occurs when the frequency ω_f of the excitation force equals to natural frequency ω_0. Assuming the same force with different frequencies imposed on the system, the displacement obviously get smaller when force frequency increases beyond the natural frequency, especially for light damping system ($0<\zeta<1$).

In this chapter, the frequency response of continuous systems, flexible beam, will be given by experiments for connection damage analysis.

5.3 Spectrum analysis

A Fourier transformation produces a direct frequency-domain description based on the dynamic properties of physical systems in terms of transformation of the time response of the system. The frequency response means the Fourier transform of the response or output of the system due to a given type of excitation or input to the system. For a linear system, a sinusoidal input at frequency f will produce a sinusoidal output at exactly the same frequency f, but the amplitude of the output will generally be different from the input amplitude. The energy density of the response of a system could distribute differently in the case of occurrence

of structural damages. This can be seen as the foundation of frequency response methods for damage detection.

Integral Fourier Transform is based on a continuous signal decomposition into unique set of sine or cosine waves and is mathematically expressed as [63]

$$X(f) = \int_{-\infty}^{\infty} x(t) e^{-j2\pi ft} dt \tag{5.6}$$

where $x(t)$ is time domain signal and $X(f)$ is frequency distribution from negative infinite to positive infinite. As it turns out, an infinite number of sinusoids are required to synthesize a signal. This makes it impossible to calculate the transform in a computer algorithm because digital computers can only work with information that is discrete and finite in length. So, the Discrete Fourier Transform (DFT) was developed as a solution of series signal transformation

$$X(f_k) = \Delta t \sum_{n=0}^{N-1} x(t_n) e^{-j2\pi f_k t_n} \tag{5.7}$$

where N= Blocksize (Number of samples)

Δt = Time spacing

Δf = Frequency spacing

n = 0, 1, 2,..., (N-1)

k = 0, $\pm$1, $\pm$2,..., $\pm$ (N-1)

t_n = n Δt

f_k = k Δf

The Fast Fourier Transform (FFT) is a faster version of the (DFT) while it utilizes an algorithm to provide the same final results as the DFT, but with fewer

computations on DSP based system. Hereafter, FFT will replace DFT in this thesis. The computation of FFT changes an N point input signal into two N/2+1 point output signals with frequency elements only up to N/2 Hz, if time domain signal is represented in seconds [63, 64]. Hence, the errors, such as leakage and aliasing, are brought in because the computation is done up to a limited number of discrete time signals. Leakage error is probably the most common and, therefore, the most serious digital signal processing error. This error is basically due to a violation of an assumption of the FFT, that the true signal is periodic within the sample period used to observe the sample function. In the case of FFT, however, finite time signal truncation results in frequency domain leakage errors. Another frequency domain error in this thesis experiment is aliasing due to the periodicity of the frequency domain. If the frequency spectrum is out of the range of 0 - N/2, the result is that frequency representation of the signal contains in this case alias frequencies, inexistent in the original signal. This aliasing causes two problems: frequencies aren't where they should be, and overlapping frequencies from different periods add, destroying information. The experimental reduction of these errors has been stated in Chapter 4.

5.4 Damage index

In the frequency response method for SHM, statistical techniques are helpful to develop an indicator of connection damage. The goal of this damage indicator facilitates the identification of the frequency response changes due to connection damage and to express the sensitivity by quantification. Among those techniques, Root-mean-square deviation (RMSD) between the signatures of the

two stages, which was presented first by Giurgiutiu and Rogers, is suitable as a damage index [65]. The RMSD index can be expressed as

$$RMSD(\%) = \sqrt{\frac{\sum_{i=1}^{i=N}(y_i^H - y_i^D)^2}{\sum_{i=1}^{i=N}(y_i^H)^2}} \times 100 \tag{5.8}$$

where y_i^H = The amplitude of frequency response of initial tight connection

y_i^D = The amplitude of frequency response of loose connection

Based on RMSD index, some other standard statistical methods have been purposed. In this experiment, mean absolute percentage deviation (MAPD) [61] was introduced to produce the damage indices, which consider primarily the percent difference between the magnitude of the frequency response of the healthy and damaged structures:

$$D = \frac{\Delta f}{(f_2 - f_1)} \sum_{i=1}^{N} \left| \frac{y_i^H - y_i^D}{y_i^H} \right| \tag{5.9}$$

where D = damage index

f_2 = The upper frequency of the range of interest

f_1 = The lower frequency of the range of interest

Δf = The frequency increment between measurement points

y_i^H = The amplitude of frequency response of initial tight connection

y_i^D = The amplitude of frequency response of loose connection

From the above equation it can be seen that this index presents relative differences of energy absorbed by the structure in specific frequency ranges

between the signatures of the initial condition and the damaged condition. The resonant energy is related to the stiffness of the structure, and relies on the signature of beam connection that is of interest in this thesis.

5.5 Experimental Procedure

A series of experiments designed to test the approach of frequency response, real time detection and wavelet analysis for beam connection failure detection. Other approaches, for example, wavelet analysis, will be described in Chapter 6.

5.5.1 Frequency response experiment

The experiments began from an initial condition of the connection in which the bolt has been fastened by wrench under some given force. The frequency response for the 50 - 550 Hz range was tested under this initial condition with three different chirp signals. This range of frequencies covers beam natural frequency from mode 3 to mode 15, according to FEM simulation. The reason for sweeping three different chirp signals is to keep the energy density of every frequency band at similar level so that response of every mode can be compared. These signals are $\sin(2\pi(40+180*t+240*t^2))$, $\sin(2\pi(10+50*t+200*t^2))$ and $\sin(2\pi(5*t+100*t^2))$. Figure 5.2 shows their frequency bands. To concentrate the energy and reduce zero mean noise, Hanning Window was imposed on chirp signal lasting three cycles (3 seconds) for each test (Figure 5.3). Sampling rate is 8192 Hz for both D/A and A/D. The time-voltage data from the sensor were saved,

and then their spectrums were computed by FFT function using a MATLAB toolbox.

The modal tests of loosed bolt condition were performed next using a wrench to loosen the bolt step by step (characterized by the rotation angle). All the data from initial bolt tight condition to totally loose condition were recorded and transformed to frequency domain. The function of exciting chirp signal is $\sin(2\pi(40+180*t+200*t^2))$ with 8192 Hz sampling rate, imposed by Hanning Window and lasting 5 cycles (5 seconds).

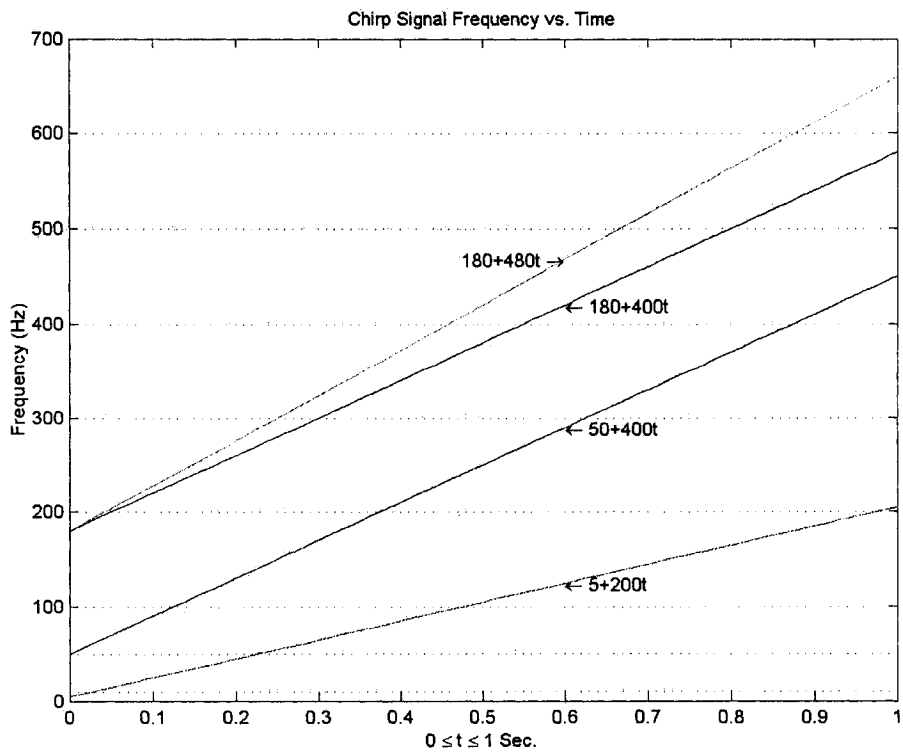

Figure 5.2 Chirp signals frequency band

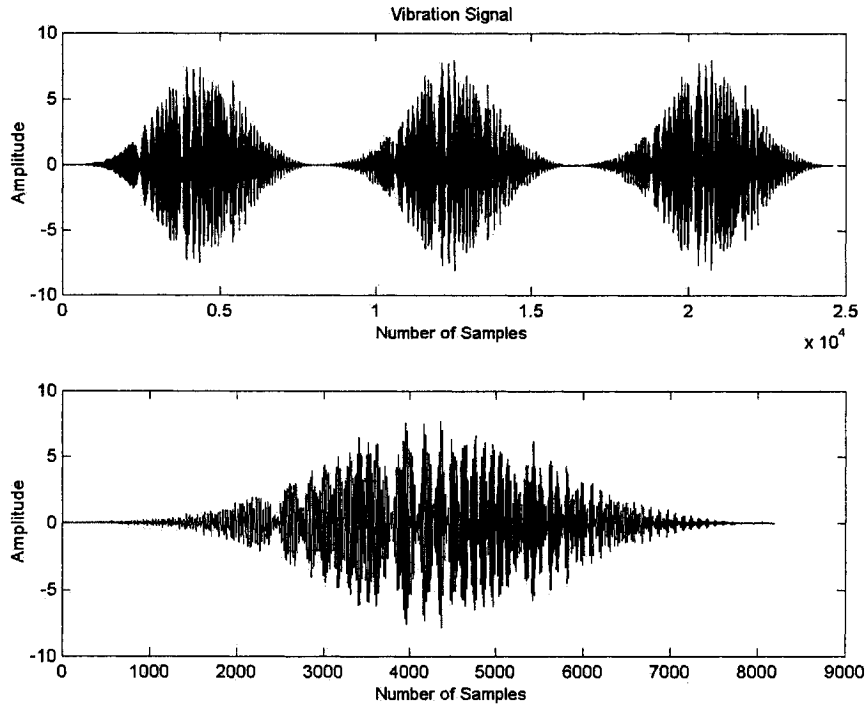

Figure 5.3 Hanning Windowed chirp signal

Top figure shows 3 cycles Hanning-Windowed time-voltage signal data. 8192 samples for one second, total 3 seconds. Bottom figure shows the average of 3 cycles. That is 8192 samples for one second.

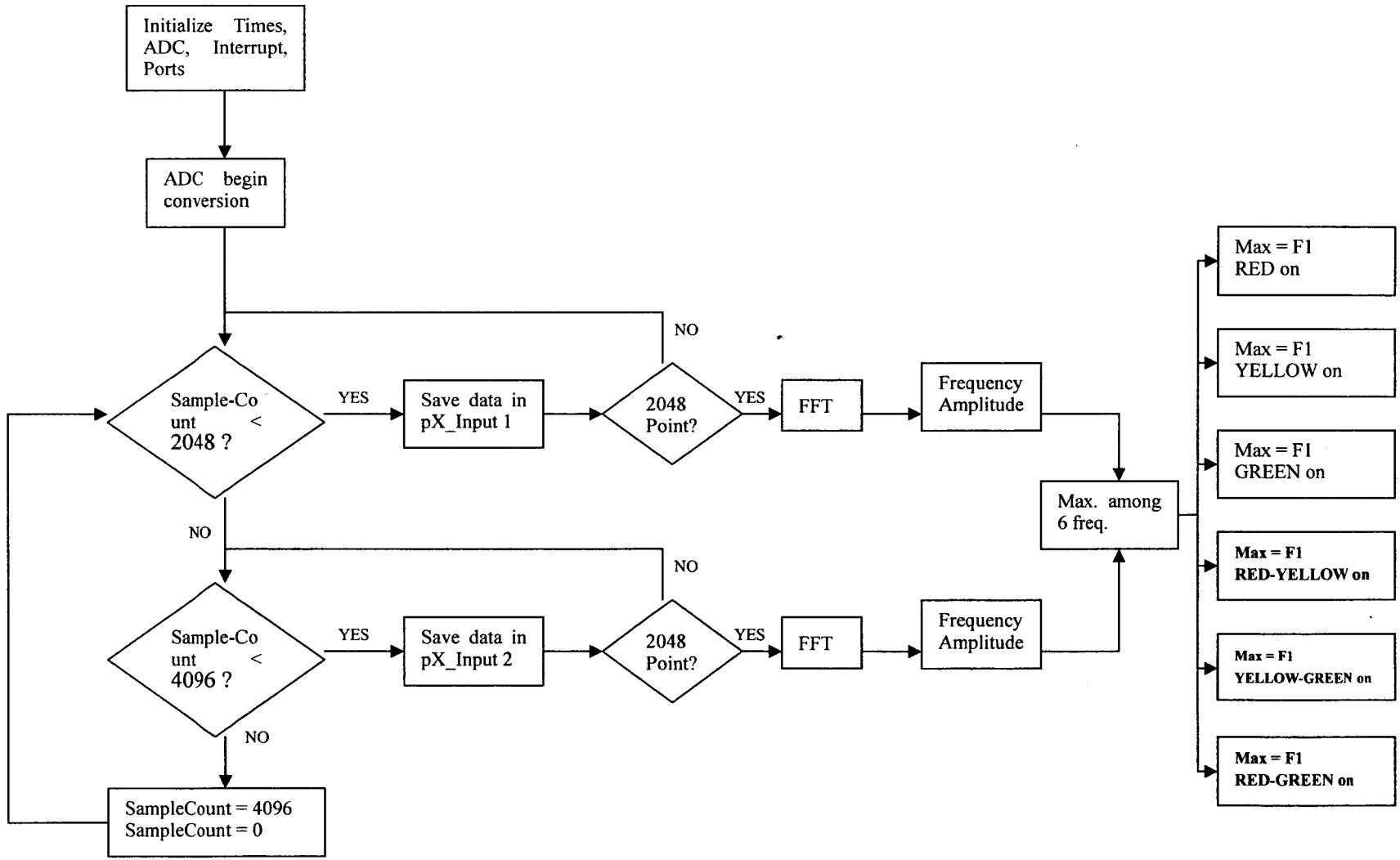

Figure 5.4 Flowchart of program on DSP56807

5.5.2 Real-time detection with embedded DSP

To be easily compared, the signals for every connection damage stage were also processed by DSP56807 for real-time detecting exploration. C language and SDK tool kits in which the FFT function is called for limit samples spectrum computation drove the DSP [66, 67]. To avoid leakage error, again, each data is multiplied by the factor of Hanning Window, which is 2048-point length, just as the ADC sampling rate. Since the samples should not be lost during the real-time FFT computation, two memory 2048-point arrays for saving samples are needed. When one memory is full, it starts FFT, and coming samples go into another memory array and this proves that there is no sample missing. The consideration of minimizing program memory is solved by an idea in terms of in-place-FFT to limit the computed data in specific size; Appendix B.5 shows the map of memory after linking.

To show the results of frequency domain, three onboard LEDs linked with port B, which can show 6 element frequencies by their combination (Red, Yellow, Green, Red-Yellow, Yellow-Green and Red-Green) - resonant frequency drifts in 6 Hz can be showed. The traced resonant frequency from initial connection condition is also 382 HZ. The flowchart of program on DSP56807 is given in Figure 5.4.

5.6 Results and Discussion

5.6.1 Frequency response detection

Under initial tight condition, chirp signal $\sin(2\pi(5*t+100*t^2))$ excited the beam for obtaining frequency response from 50 Hz to 150 Hz, $\sin(2\pi(10+50*t+200*t^2))$ for 150Hz - 350 Hz and $\sin(2\pi(40+180*t+240*t^2))$ for 300 Hz - 550 Hz. The reason why three chirp signals were used is that it is impossible to make a chirp signal maintain the same power density over a large range of frequency. Figure 5.5 shows these chirp signals and their frequency responses. Some resonant frequencies are listed in Table 5.1 and are compared with natural frequencies by FEM simulation.

Table 5.1 Computed natural frequencies vs. tested resonant frequencies

	Mode 4	Mode 5	Mode 7	Mode 9	Mode 10	Mode 11	Mode 12	Mode 13
FEM [Hz]	86.9	129.9	181.5	241.9	311	334.4	388.9	475.6
Tested [Hz]	83	123	173	234	304	342	382	468
Difference	4.7%	5.6%	4.9%	3.4%	2.3%	-2.2%	1.8%	1.6%

There above values do not include the resonant frequencies for mode 1, mode 2, mode 3, mode 6 and mode 8 because they were less detectable by the piezo-sensor. This also can be proved by mode shapes in Figure 3.5. Checking the frequency responses, most energetic resonant frequency is 382 Hz, ie. mode 12 showing that mode 12 is most sensitive to the sensor location in this experiment. Hence, tracing frequency response around 382 Hz during every loose condition can give more distinguishable results regarding connection damage. Accordingly, chirp signal $\sin(2\pi(40+180*t+200*t^2))$, whose energy

concentrate around 382 Hz, was used (Figure 5.6).

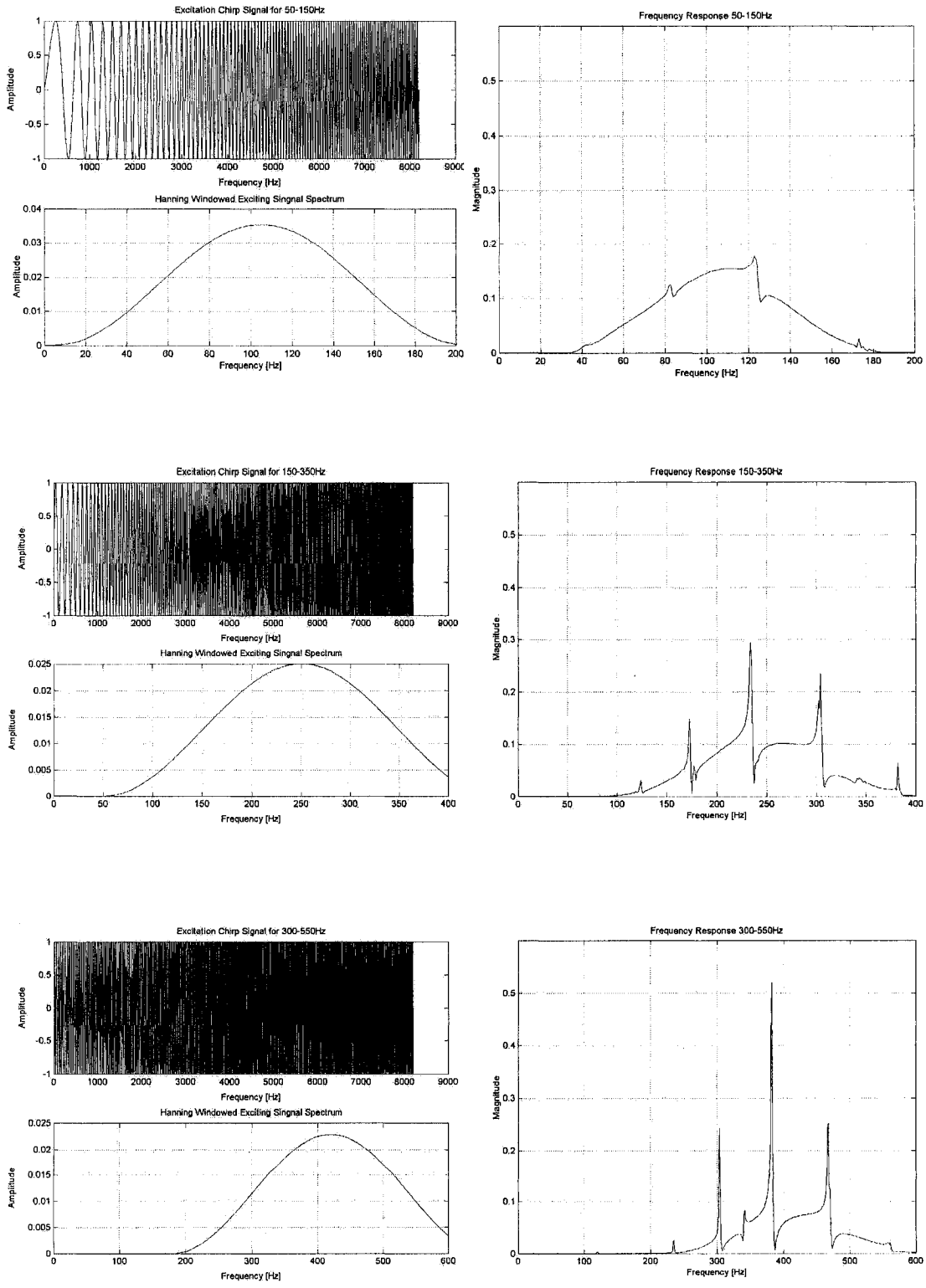

Figure 5.5 Frequency responses from 50 Hz to 550 Hz for the initial tight condition

of the connection

1. These figures are the results from three different exciting chirp signals.
2. Left figures show exciting chirp signal and spectrum distribution after Hanning-Windowed. The energies of excitation are mainly distributed in 50-150 Hz, 150-350 Hz and 300-550Hz ranges respectively. To be easy to compare the results of frequencies responses, the peak power densities are similar.
3. Right figures show frequencies responses based on different exciting frequency ranges. It is easy to see that the resonant frequency at 382 Hz is the

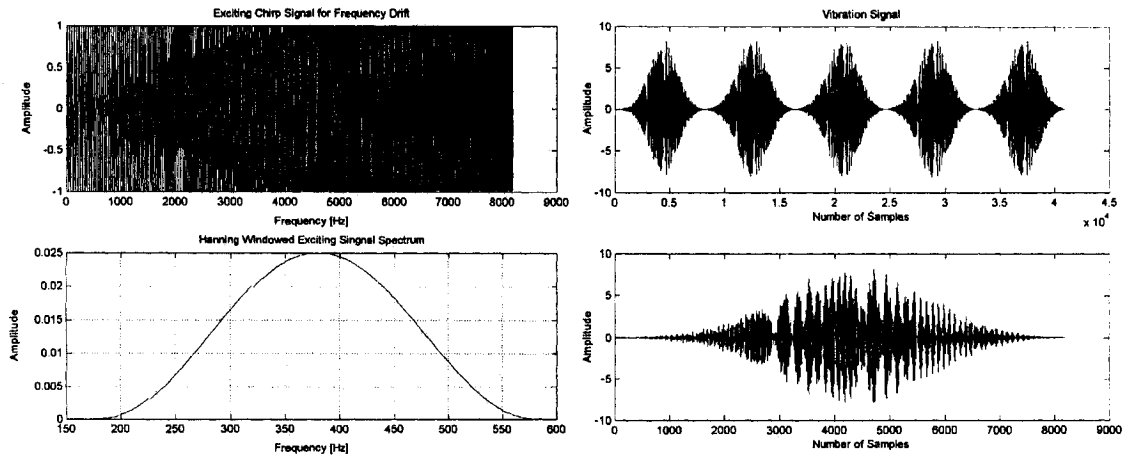

Figure 5.6 Excitation signal (left) and tight condition response signal (right)

1. Left two figures show exciting chirp signal and spectrum distribution after Hanning-Windowing. The energy of excitation is mainly distributed in 250-500 Hz.
2. Right two figures show 5 cycles Hanning-Windowed time-voltage vibration signal collected form sensor. 8192 samples for one second, total 5 seconds. Bottom figure shows the average of 5 cycles. That is 8192 samples for one second.

Since here was no need to save the excitation signal, dSPACE memory was dedicated for saving 5 cycles (40960 samples) of the response signal. Average is used to further reduce noise. Figure 5.7 shows the results of 13 different stages of bolt connection loosening. Figure 5.8 is the combination of

every frequency response, where Loose1, 2 and 4 are removed for clarity. Further analysis by extracting data of mode 12, resonant frequencies of every loose conditions related with loose rotation angle are listed in Table 5.2 and plotted in Figure 5.9.

Table 5.2 Mode 12 resonant frequencies for various rotations

	Tight	Loose1	Loose2	Loose3	Loose4	Loose5
Rotation Angle [°]	0	50	80	100	120	135
Mode 12 RF [Hz]	382	382	382	381	381	379

Loose6	Loose7	Loose8	Loose9	Loose10	Loose11	Loose12	Loose13
175	205	235	275	325	375	425	475
379	378	377	375	370	360	354	354

Damage indices were calculated for every loose stage frequency response from 200 Hz to 550 Hz. The results are listed in Table 5.3 and plotted in Figure 5.10.

Table 5.3 Damage index of loose damage

	Loose1	Loose 2	Loose 3	Loose 4	Loose 5	Loose 6
D Value	0.0770	0.0838	0.1190	0.1332	0.1982	0.2136
Loose 7	Loose 8	Loose 9	Loose 10	Loose 11	Loose 12	Loose 13
0.2725	0.3014	0.4622	0.4669	0.4529	0.6731	0.6431

The changes for every loose stage can be identified visually, primarily from frequency responses of Figure 5.7. This proves that the FR method is sensitive to connection damage of bolt loose, even incipient damage can be perceived. The problem is how to interpret these different signatures for identifying damages. Analyzing Figure 5.9, it can be seen that such a procedure can be based on the mode 12 resonant frequencies decay against connection damage level, represented by loose rotation angle. Approximately, the damage can be defined in different ranges of loose condition. From Tight to Loose2, the frequency remains 382Hz. The next sequence from Loose 2 to Loose 8 shows that the frequency drifts from 382Hz down to 377Hz and this can define a damage development zone. From Loose 8 to Loose 12, the frequency decreases rapidly from 377Hz to 354Hz. In this zone, assuming that rivet used connects the two plates, the damage starts to develop rapidly. Finally, the frequencies from Loose 12 to Loose 13 stayed at 354Hz and connection can be regarded as totally free. So far, a meaningful range of natural frequencies for safety consideration on this beam structure can be deduced upon given structural safety requirements.

Tracing specific mode frequency response signature provides roughly segmentations referring to the severity of the connection damage. In real operation, the identification of the connection damage must meet stringent safety requirements even if no apparent frequency response decay is observed. In this case, the results of damage index (Table 5.3 and Figure 5.10) based on statistical method can be used to identify minor change of connection. When the bolt was loosened nearly to fully loose, that means it could be turned with much smaller torque, some constraints at the end were weaker or even lost and caused the

boundary condition not to be stable when exciting force was applied on the beam. The system could be affected also by complex stiffness, the changing of viscous damping, slide damping, etc. However, these near end effects are lass important for SHM.

5.6.2 Real-time detection

A three LEDs combination used to display the frequency value results as Table 5.4. For each of the frequency values in the range 377-382 Hz, a different combination of LEDs on was conventionally assigned.

Table 5.4 LED results vs. frequency response

	Tight	L1	L2	L3	L4	L5	L6	L7	L8
FR (Hz)	382	382	382	381	381	379	379	378	377
DSP LED on (Hz)	R 382	R 382	R 382	Y 381	Y 381	G 380	R-Y 379	Y-G 378	R-G 377
Difference	0	0	0	0	0	1	0	0	0

1. L1 - L8 indicates Loose 1 - Loose 8.

2. R: RED LED, Y: YELLOW LED, G: GREEN.

It can be seen from above results that the real-time detection by DSP56807 identifies about the same resonant frequency signature of mode 12 as frequency response method along bolt loosing procedure. The factor affecting the accuracy of real-time analysis is a zero mean noise that can be minimized by the averaging of signals.

5.7 Conclusion

In this chapter the potential role of the frequency response of a bolt joint structure in a structural health monitoring system has been investigated. From experimental results it is evident that bolt connection failure caused detectable changes in the resonant frequencies of a simple beam. Finite element analysis proved helpful for the selection of the resonant frequency band, which was established based on computation of natural frequencies and mode shapes. The well-designed chirp signal is an effective tool for piezoelectric actuator to excite active vibration in some specific bandwidth. The damage index can numerically identify the connection damage even for minor damages in bolt tightening. Both resonant frequency decay and damage index difference can be explained theoretically by classical structural dynamics. The continuous loss of stiffness across the entire beam structure directly affects the frequency response of the structure.

Through these experiments, many advantages can be seen for frequency response methods in a SHM system; they can be implemented with minimum cost, they are easy to compute and conformal, and can provide good insight regarding the overall condition of the system.

The limitations refer to the fact that they provide little information about the local damage area unless numerous sensors are used along with accurate numerical models; the large amount of data has to be saved for comparison if numerous sensors are involved in SHM, and signal processing becomes more complicated.

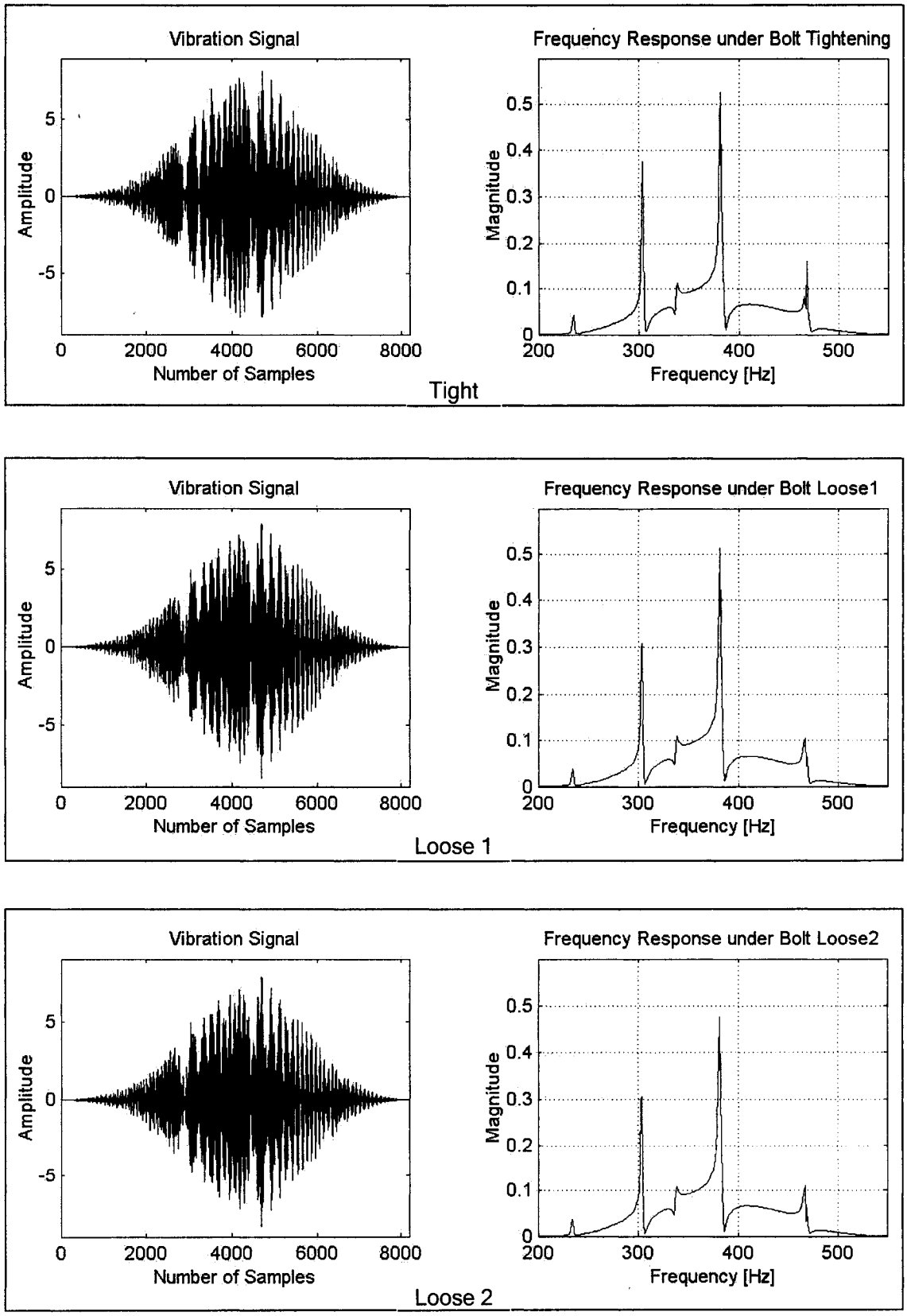

Figure 5.7 Frequency response results for 13 different loose connections

Figure 5.7 (Continued)

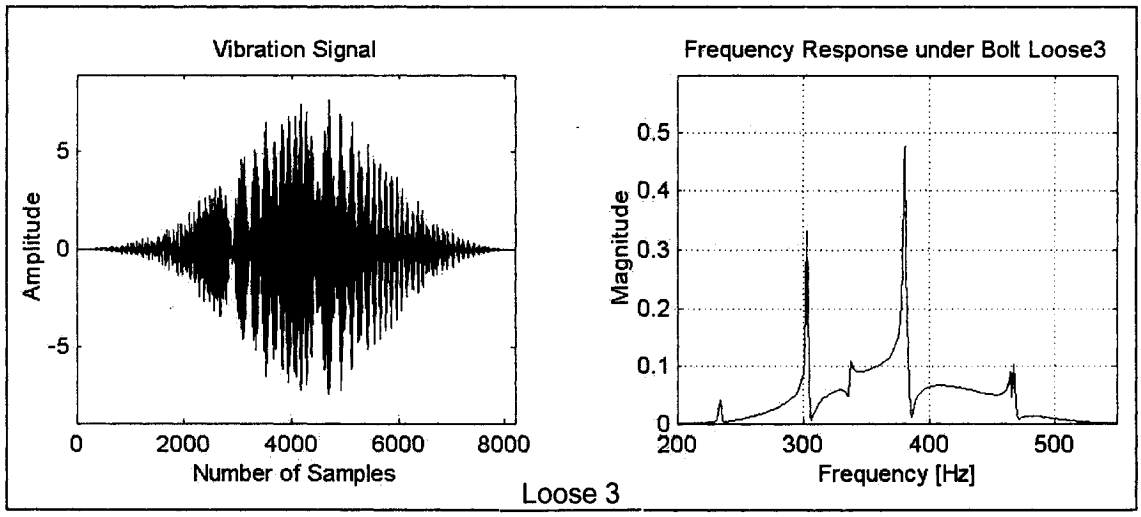

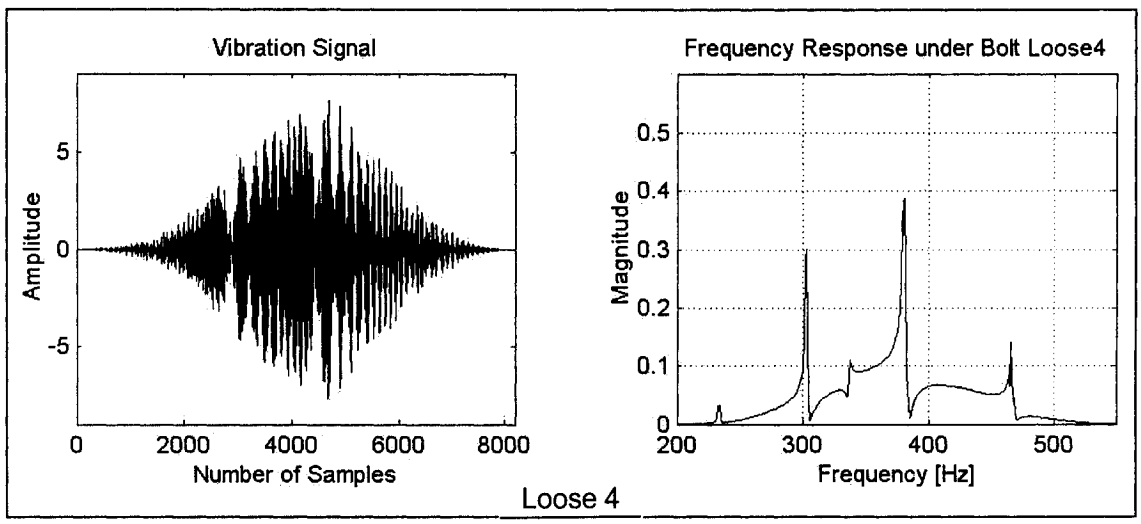

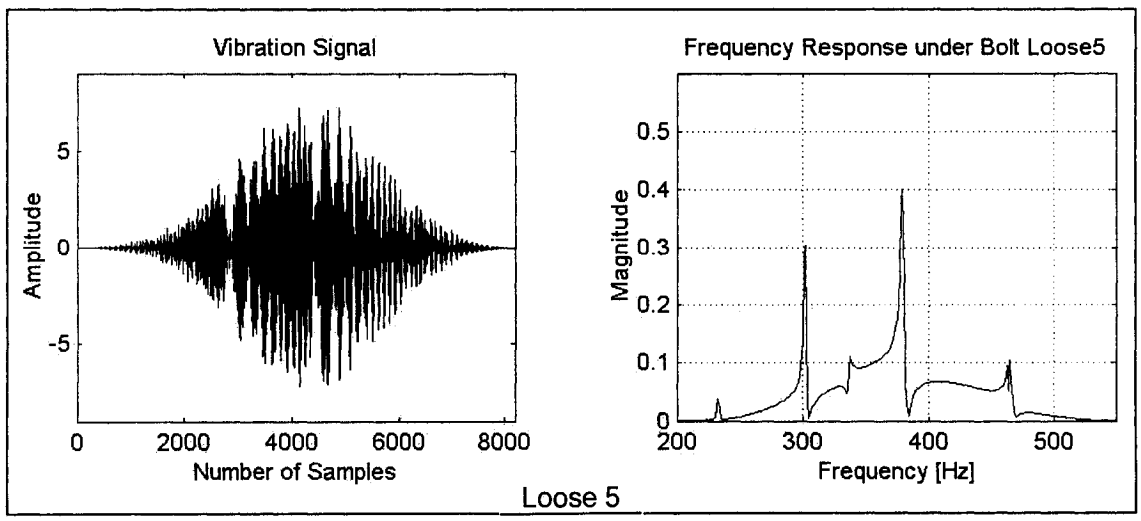

Figure 5.7 (Continued)

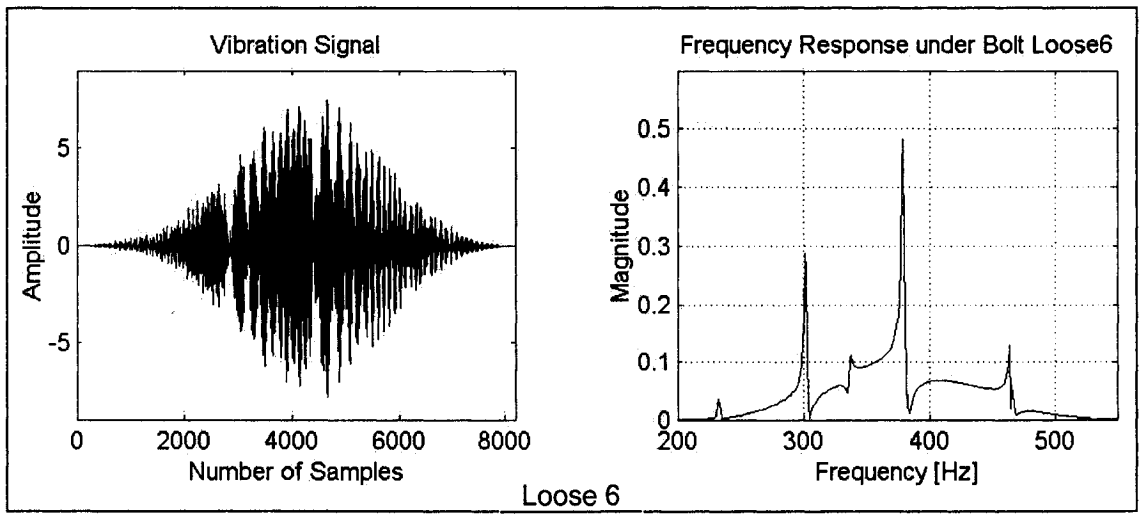

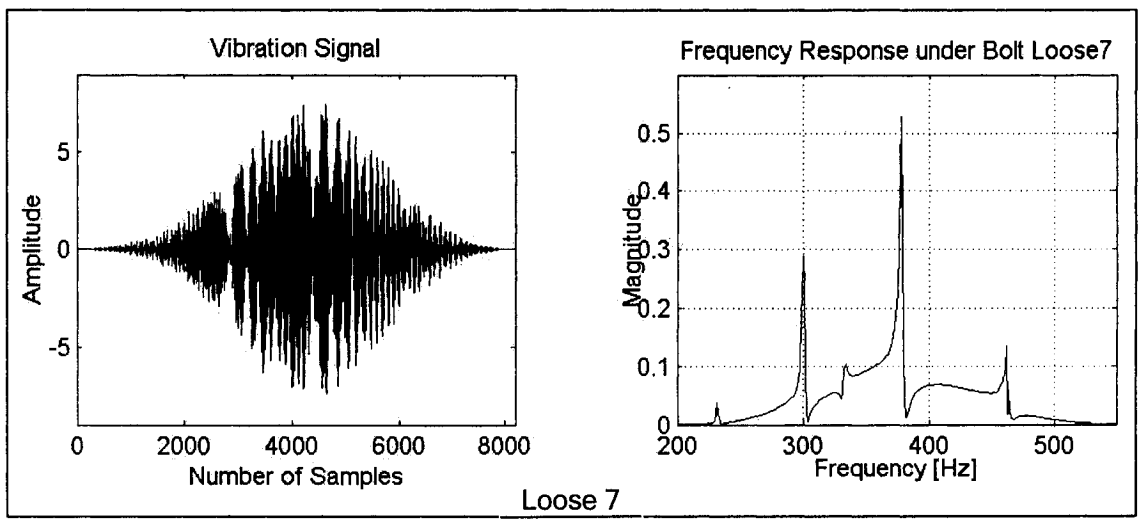

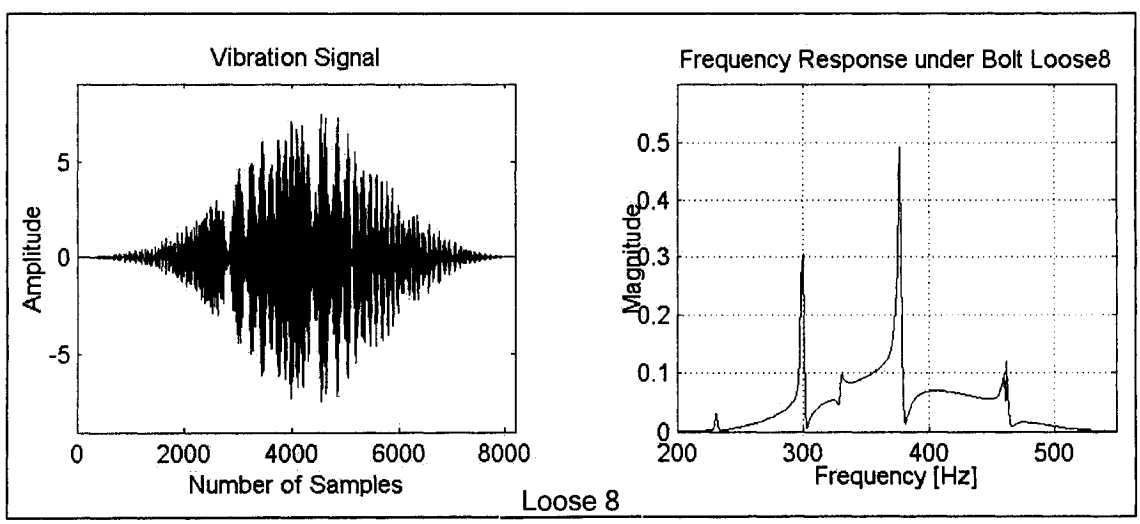

Figure 5.7 (Continued)

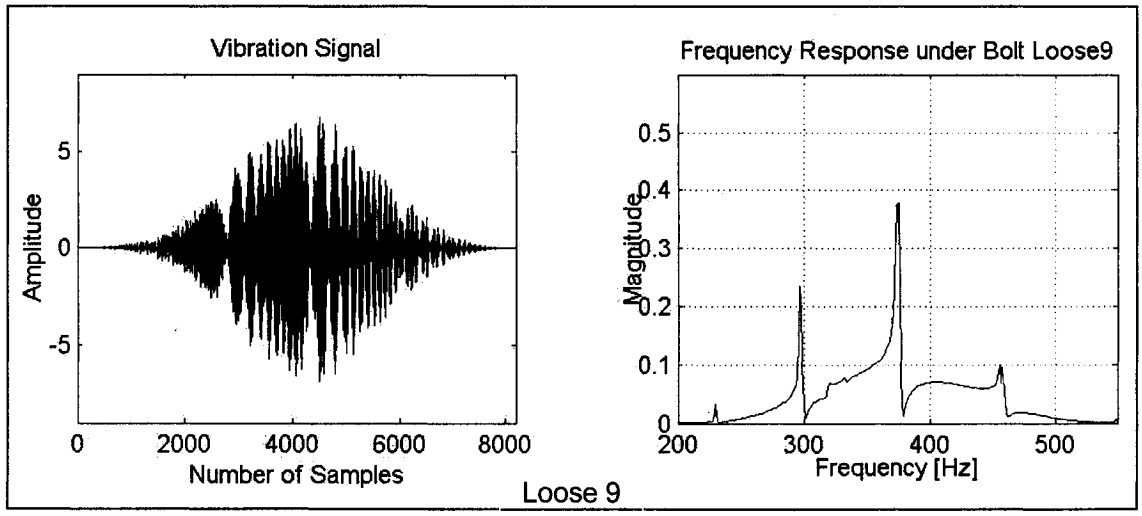

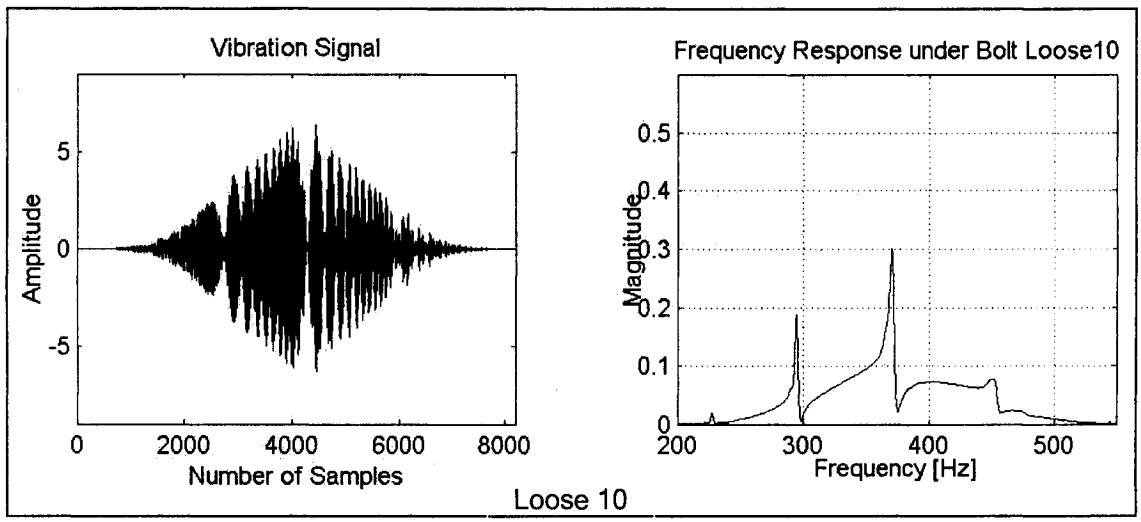

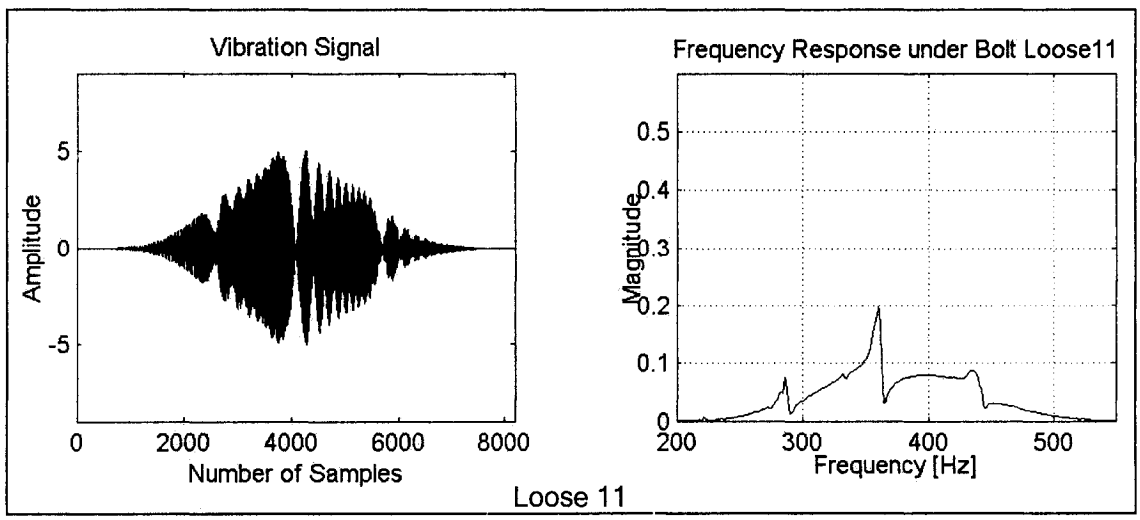

Figure 5.7 (Continued)

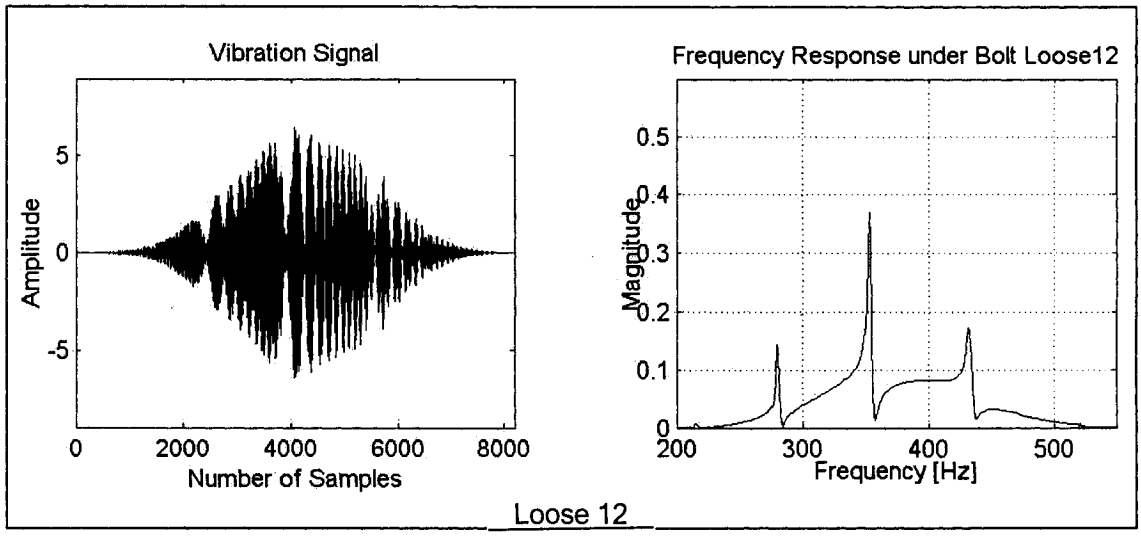

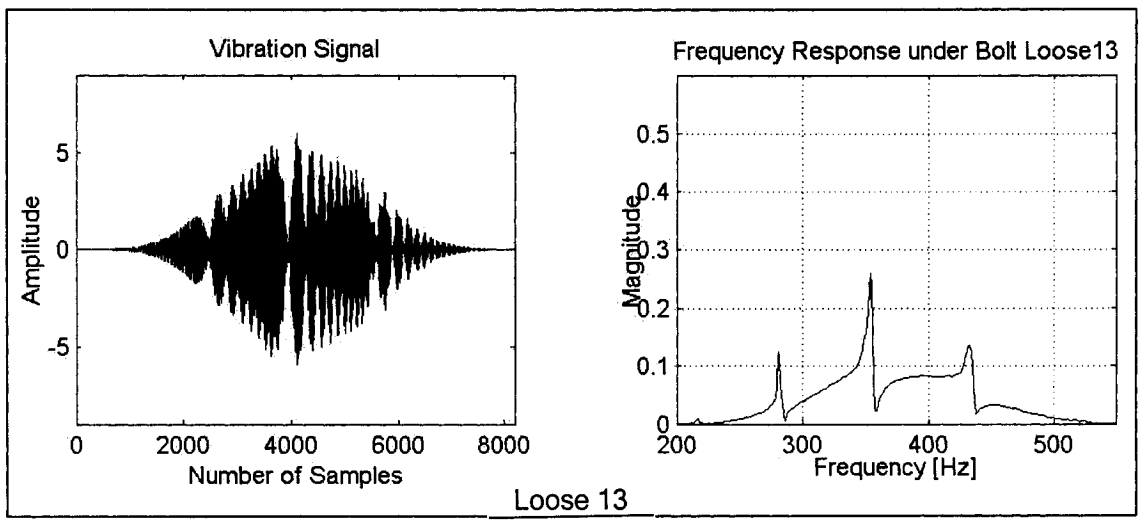

1. These results obtained from Tight to Loose 13 system frequency responses. The exciting chirp signals are all the same one: $\sin(2\pi(40+180*t+200*t2))$.
2. Left time vary signal in each stage was obtained from the average of 5 cycles (5 seconds).
3. Right frequency domain results show the various frequency responses in the range of 200-550 Hz under different connections.

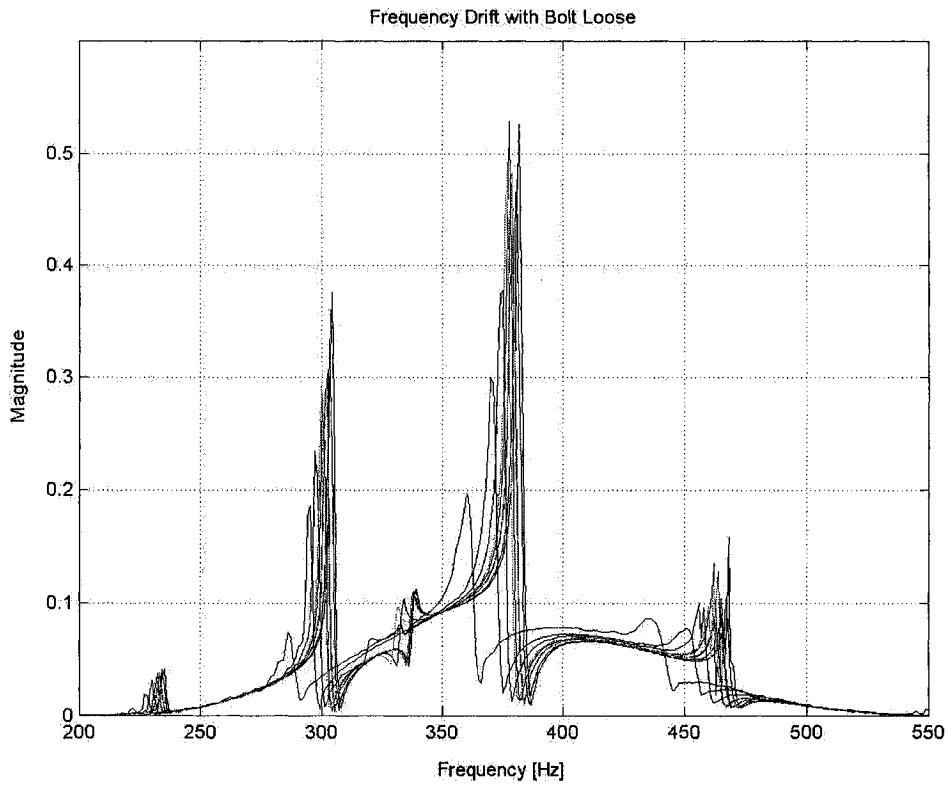

Figure 5.8 Frequency responses of loose conditions

1. This sketch shows the frequency responses from tight condition to loose conditions by combination of Figure 5.7.
2. The magnitudes of resonant frequencies were getting lower generally with bolt loose rotation angle increase, for example, Tight condition mode 12 is 0.53 while Loose 11's is 0.195; The resonant frequencies were getting smaller at the same mode shape, for example, Tight condition mode 12 is 382 Hz while Loose 11's is 360 Hz.

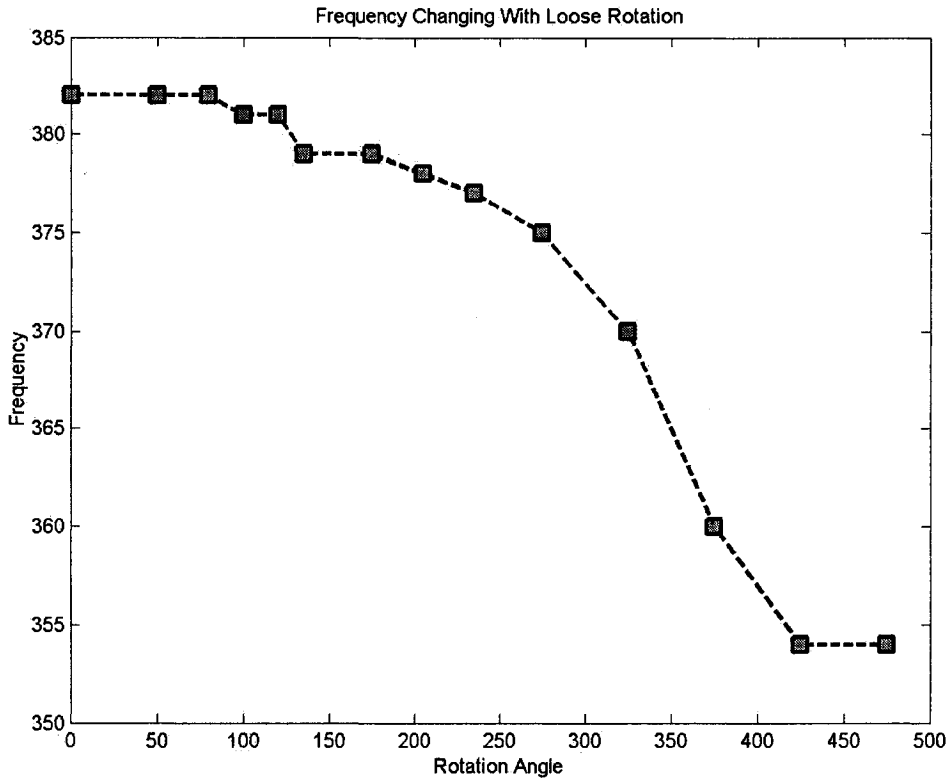

Figure 5.9 Resonant frequency of mode 12 vs. every loose condition

This sketch shows the mode 12 resonant frequencies from every bolt connection stage versus bolt loose rotation angle. With the loose increase, the resonant frequency was getting decrease.

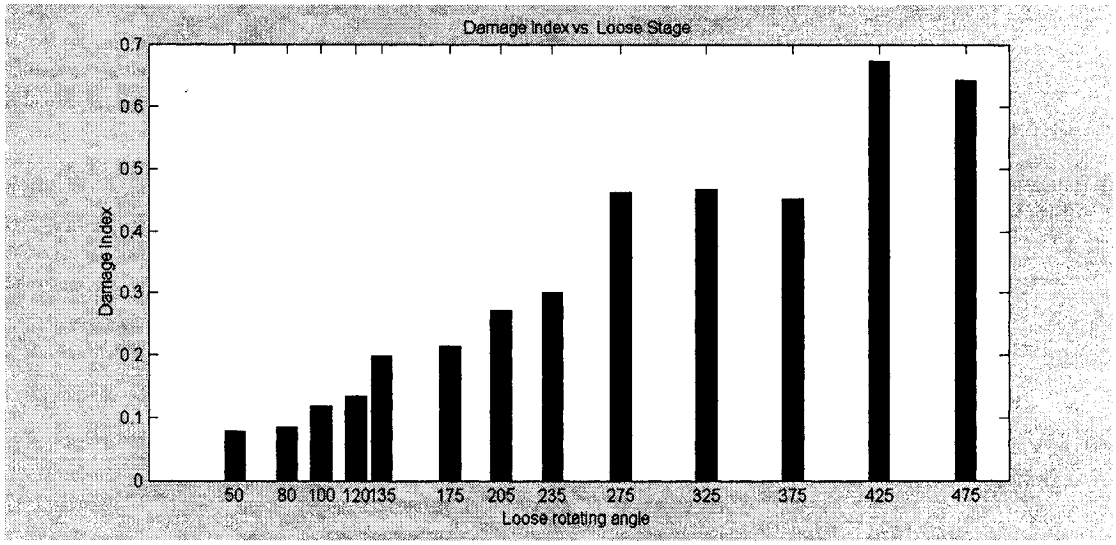

Figure 5.10 Damage Index of loose connection

1. Damage Index vs. Loose Rotation Angle (°). Refer to values listed in Table 5.3.
2. The damage index of every Loose stage is distinguishable to others and generally value goes higher when loose rotation angle increases (0° - 325°), but it is nonlinear.
3. The minor connection damage (50°, 80°) can still be perceived with damage index that shows no change by resonant frequency (382Hz).

Chapter 6

Wavelet Analysis Methods

In this chapter, the performance of connection damage detection connection by wavelet transforms is explored using piezoelectric actuators and sensors. A transient signal excites non-stationary vibrations and time-frequency analysis is carried out using continuous wavelet transformation performed with Gaussian 2 mother wavelet. The results by wavelet transforms are analyzed and compared to the results of frequency response from previous chapter.

6.1 Introduction

Wavelet-based approach for SHM, in a promising tool of damage detection and has been used for damage presence, severity, location and identification [6]. The wavelet analysis might be viewed as an extension of the traditional Fourier transform with adjustable window location and size in time. Its merits lie in the ability to examine local data with "zoom lens having an adjustable focus" to provide multi-levels of details and approximations of the original signal [68]. Hence, wavelet analysis shows an ability of revealing aspects of data that other signal analysis techniques miss. This method has been implemented in a variety of SHM published approaches.

A brief survey of applications of wavelet analysis for structural health

monitoring and damage detection had been presented by Hou *et al* [69]. In their research, a system simulated by a three degree-of-freedom spring-mass-dashpot with multiple breakable springs was employed to demonstrate a wavelet approach for damage detection and identification of damage locations. The authors showed the results of damage detection using a spike or an impulse in the plots of high resolution from wavelet decomposition of the data based on acceleration response.

One of the early applications of wavelet approach for on-line fault detection can be found in the paper by Tamaki, K. *et al* [70], who performed the inspection of rotary compressors based on decomposition of signals in time-frequency space. Stefanos, K-G *et al* [71], presented the approach for evaluating assembling quality of washing machines by analyzing the transient vibration velocity signals coming from 12 different measurement points. The faults have been classified as: missing or loose screws and other tight coupling problems; shock absorbers' and bearings' wrong assembly; misalignment of drum and motor pulley; wrong belt tension, and pattern recognition. Wavelet analysis was introduced as Euclidean, Mahalanobis, and Bayesian distance classifiers, the learned vector quantization (LVQ) classifier and the fuzzy gradient classifier for feature space.

The use of wavelet analysis for in-service damage detection refers to rotor gearbox health monitoring was reported by Wang, W. J. *et al.* [72]. They found that early damage to a gear tooth causes a short time variation in the associated vibration signal so that wavelet transform could be used to detect incipient damage of gearbox. The type of damages includes pitting corrosion on

one tooth initially where time variation is less than one tooth-meshing period; later, the duration of the abnormal variation becomes longer. Other distributed faults, like eccentricity and wears, can cover the most part or the whole revolution of the gear. In experiments, The Gaussian wavelet was employed for time-frequency analysis, and the authors collected time domain averages from a helicopter main rotor gearbox undergoing fatigue testing in a full-scale back-to-back gearbox test facility. They found a fatigue crack first at the root of one tooth by comparing the wavelet transforms results with initial condition, and then two fatigue cracks detected on different tooth due to the propagation of fatigue cracks. Luo, G-Y [73] performed similar research on helicopter gearbox health monitoring, and other works on this damage detection region are also available from some papers [74,75].

Currently, researchers explore the application on wavelet methods for structural health monitoring. The piezoelectric sensor and actuator bonded on beams or plates are applied to detect damage also discussed in some literatures. A detailed report regarding beam structural damage can be found in a published paper by Okafor *et al.* [76], in which a generic experiment was designed for identifying the presence of damage, the location of the damage and the amplitude of the damage peak. The author indicates that wavelet transform is capable to identify damage severity and location as well as limitation due to the characteristics of beam vibration. All of the methods they assessed use piezoelectric actuator and laser vibrometer for mode shape scanning. A notch is machined deliberately on beam to simulate the damage with increasing depth to define different levels of severity. Some lower vibration mode shape signals were

recorded as time domain signals while continuous wavelet transform is used to process time domain signal into the time-frequency domain after decomposition of original signal. The results regarding the damage are obtained by observing 3-D coefficient plot with a higher and higher amplitude appearing on the area of damage. As a result, the author claims that the damage and the location can be observed as well as damage severity expressed by the amplitude of coefficients. In spite of the fact that the laser vibrometer is not cost-effective and can't be embedded, the methods of continuous wavelet transform remain of interest as reference for other applications.

Another important approach involving wavelet transform is the analysis of wave propagation along an elastic material since the propagating wave can bring useful information about structural health that merges in the wave signal. By signal decomposition using wavelet transform, the meaningful signal is extracted out of the original signal. This approach needs to choose the propagating wave carefully by considering the dispersion of wave energy on the way to the sensor. Since the wave frequency usually falls into sounds frequency range, the wave sometimes called acousto-ultrasonic signal, also called lamb wave. Some results about wavelet analysis regarding wave propagation have been published in literature [77-80]. A good report was presented by Kessler *et al.* [81], in which a couple of embedded piezoelectric actuator and sensor are described but separately located on both ends of the testing beam. In this paper, the author claims that the results permit damage identification and localization. The goal of author is to detect delamination on resin beam and the approach of finding damage based on wavelet transform is referenced.

In this thesis, only connection damage and damage severity are the goals and damage location is left for future work.

6.2 Wavelet transforms

Wavelet transform is related to Short Time Fourier Transform (STFT), which performs FFT in a relative short time window. An important physical phenomenon - the Heisenberg uncertainty principle, stating that it is impossible to find both time and frequency on only one point in a signal has to be taken into account. It results in the fact that narrow windows give good time resolution, but poor frequency resolution, while wide windows give good frequency resolution, but poor time resolution. This is a dilemma to STFT, that its poor frequency accuracy accompanies precise time location. The continuous wavelet transform was developed as an alternative approach to the Short Time Fourier Transform to overcome the resolution problem. Similarly, the wavelet transform is done in a window, in the sense that the signal is multiplied with a function, called wavelet, and the transform is computed separately for different segments of the time-domain signal. However, the width of the window is changed as the transform is computed for every single spectral component and negative frequencies are not computed [82-84].

A continuous wavelet transform of a function $x(t)$ is defined as follows

$$CWT(\tau,s)=\frac{1}{\sqrt{|s|}}\int x(t)\psi^{*}(\frac{t-\tau}{s})dt \qquad (6.1)$$

Where $x(t)$ = a function (time domain signal) to be transformed

τ = The translation parameter

s = The scale parameter

ψ^* = Mother wavelet

$CWT(\tau, s)$ = Calculated wavelet coefficients

The mother wavelet represents the window functions with different region of support that are used in the transformation process and are derived from one main function. In other words, the mother wavelet is a prototype for generating the other window functions by a series of scales. The calculated wavelet coefficients refer to the closeness of the signal to the wavelet at the current scale.

There are two criteria that must be satisfied when a ψ^* function is accepted as a mother wavelet [82,83]:

- Regularity criteria: it should be well localized in both physical and Fourier space;
- Admissibility criteria

$$C_\psi = 2\pi \int |\hat{\psi}(k)|^2 \frac{dk}{k} < \infty$$

$$\Rightarrow \int_{-\infty}^{\infty} \psi(x) dx = 0 \qquad (6.2)$$

Where C_ψ = Constant dependent on the type of mother wavelet used.

$\hat{\psi}(k)$ = Fourier transform of $\psi(x)$.

This condition guarantees the existence of an inverse transform to recover the signal $x(t)$.

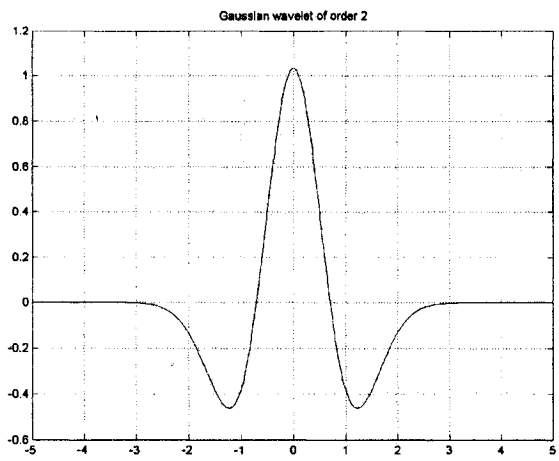

Figure 6.1 Gaussian 2 Wavelet

The mother wavelet used for the analysis in this thesis research is the Gaussian (gausN) wavelet since it possesses the optimal time-frequency localization property [76]. The function is

$$Gaus(x,n) = C_p e^{-x^2} \qquad (6.3)$$

where C_p is such that the 2-norm of the P-th derivative of $Gaus(x,n)$ is equal to 1. Figure 6.1 shows the plot of Gaussian 2 wavelet.

The term **translation** in transform function is related to the location of the window, as the window is shifted through the signal. In other words, this term corresponds to time information in the transform domain. A **scale** parameter, however, is defined as "1/frequency" in place of frequency parameter. High scales mean low frequencies which correspond to global information of a signal usually spanning the entire signal, whereas low scales mean high frequencies which correspond to detailed information of a hidden pattern in the signal, usually lasting a relatively short time. For all practical purposes, the signals are bandlimited, and therefore, computation of the transform for a limited interval of scales is usually adequate.

In this thesis, signal processing is done by using a MATLAB toolbox regarding continuous wavelet function in which the procedure starts from scale s=1 and continues for the increasing values of s. The analysis will start from

high frequencies and proceed towards low frequencies. The first value of s corresponds to the most compressed wavelet. As the value of s is increased, the wavelet will dilate.

In the sense of time, the transform starts at $t = 0$, with respect to the wavelet, placing it at the beginning of the signal. The wavelet, at same scale, is then shifted by τ to the location $t = \tau$, and the above equation is computed to get the transform value at $t = \tau$, $s = 1$ in the time-frequency plane. This procedure is repeated until the wavelet reaches the end of the signal, and then the same procedure is repeated with increased scale until the transform finish at all scales. In MATLAB, both parameters are increased by a step size defined by the program.

6.3 Wavelet transform analysis for beam connection damage detection

Resonance is a dynamic response phenomenon when excitation frequency matches one of the structural natural frequencies. It can be seen that the amplitude becomes higher and higher if the structure has no damping or only light damping. From energy viewpoint, the resonance is a phenomenon in which the accumulated energy increases in time. If the frequencies mismatch, the energy and the amplitude of vibration are smaller than in the case of resonance.

In the previous discussion of modal analysis, it was shown that the natural frequency of a structure changes for different boundary conditions. When a transient excitation signal is applied to a beam, by analyzing the energy

distribution of response vibration in time-frequency domain, the entire information about structure can be brought out. This can motivate to apply wavelet transform to detect connection damage in a beam structure.

6.4 Experimental procedure

The resonant frequency 382 Hz at mode 12 is again used as main exciting signal due to its high sensitivity versus excitation. A deterministic sinusoidal signal with 382 Hz lasted 30 cycles for time duration of 0.08 seconds, and then stopped. The 30 cycles excitation is considered to provide enough amplitude of vibration (at about ± 8 volts signals) under initial conditions, and during the relaxation, the signal can be kept within a limit time to meet the size of dSAPCE memory. The active response and the relaxing signal are combined to be the transient signal that would be processed by wavelet transform. The beam kept vibration due to the release of the accumulating energy while the vibration signals were recorded for 1.316 seconds for later wavelet analysis.

This series of experiments ended with a frequency response test at the same time using the procedure shown before in Figure 4.2. dSPACE, driven by a C program, produced multi-cycle sinusoidal signals, outputted an analog exciting signal with amplitude ± 10 volts through D/A port on DS2101 board to supply the piezoelectric actuator that produced the excitation for beam vibration. The piezoelectric sensor sends transient signals produced by beam vibration to an anti-aliasing low-pass filter. The data were collected by ADC on DS2001 board and saved in dSPACE system.

A digital 250-550 Hz bandpass filter made in MATLAB toolbox filtered data. A MATLAB program calls cwt (Continuous Wavelet Transform) function with

the Gaussian 2 wavelet to convert time domain signal into time-frequency domain. The results were presented in a 2-D top view and in a 3-D plot on time-frequency plane.

6.5 Experimental results

Figure 6.2 shows the transient vibration signal for a beam, starting from the stage of Tight to Loose 10. The time variation of exciting response and relaxation are on the upper left side of every boundary condition; 3D plots of Translation-Scale-Coefficient are on the right hand side. The vertical abscissa gives the value of coefficient of CWT marked by Amplitude, while the two abscissas show the sample number on Translation, which corresponds to time in samples, where for 25000 samples the time is 25000/19100 = 1.309 seconds, and reciprocal of the frequency of vibration signals on Scale. The contour and 3D view represent the distribution of energy versus time (translation) and frequency (scale). A ripple separates the shape into two distinct parts: the region representing response to the excitation for the first 0.08s and then relaxation from 0.08 to 1.309s, along time (translation) abscissa. For the Scale abscissa, Table 6.1 gives the conversion of scale units from 0 - 64 into frequencies from 6880.7 to 107.5 Hz. 2-D top views show contour of coefficient on the lower left side, which the amplitude of coefficient on 3-D plots are displayed by the various intensities of black shades

To evaluate the connection damage, the maximum coefficient that is the peak value of the 3-D plot under every loose condition has been computed and results are shown in Table 6.2 and Figure 6.3. From the initial Tight connection stage to Loose 7 stage, the maximum coefficient decreases steadily. Maximum

coefficients remain at 382 Hz on Frequencies (Scale) with resolution ± 4 Hz and on corresponding time (Translation) coordinate the change from excitation to relaxation is observable at 0.08s. The decrease of maximum coefficient from Loose8 to Loose 10 stage before 0.08s can be explained from Figure 5.7 which the 382 Hz is about the ditch of frequency response. Due to further damage (Loose 9-10), the difference between forced frequency (382 Hz) and resonant frequency (before 377 Hz) getting much larger, and the displacement response is smaller and smaller, in accordance to the analysis obtained from chapter 5.2. In this case, the maximum coefficient does not occur after the excitation ends and moves to the beginning of excitation. However, for structural health monitoring, our attention needs to focus only on first several stages of connection damage and very loose connection states are of low significance.

6.6 Discussion

There are generally three sequential goals for connection damage detection, each of which is achieved with increasing difficulty and complexity. The first is the identification of the occurrence of connection damage. The second is the estimation of the extent of severity of the damage. The third is the determination of the damage location. The scope of this research focuses on the first two goals only.

From Table 6.2 and Figure 6.3, the difference of maximum coefficient of every loosen stage is shown clearly, even at incipient connection damage. Maximum coefficient values occur at the end of the excitation (0.08s) for Tight to Loose 2 conditions, at the beginning of relaxation (0.09s) for Loose 3 to 8 and at

the beginning of the excitation (0.006s) for Loose 9 and 10. The explanation for the case of Loose 9 and 10 was given in the previous section based of a significant reduction of mode 12 frequency to less than 377 Hz, significantly different from the 382 Hz excitation frequency. Evaluating the wavelet analysis with the frequency response, the results from Table 6.1 and Figure 6.3 show the decrease of maximum coefficients before Loose 7 is significant, and the ratio of Loose1 to Loose7 is 993.15, while the ratio of Loose7 to Loose1 by damage index is only 3.54. Although both show the non-linearity relationship between damage severity (Damage Index in frequency response and Max. Coef. in wavelet analysis) and damage stage, the wavelet analysis is more sensitive than frequency response at the beginning of connection damage because of the significant decay of maximum coefficient up to Loose 7 stage.

6.7 Conclusions and proposals for future work

6.7.1 Conclusions of wavelet analysis

This chapter has explored the application of wavelet analysis approach to connection damage detection on beam bolt connection structure. An optimized frequency parameter derived from frequency response was applied for transient excitation. The non-stationary structural response due to sinusoidal transient excitation brought the information of beam connection out, and the differences could be distinguished in the results of wavelet transform at any connection stage. The 3-D plots of Translation-Scale-Coefficient display different shapes that are owned by every unique connection stage. The maximum coefficients of every stage are extracted to be the characteristic of various connection conditions. By a

series of experiments, the feasibility of detecting connection damage and discrimination of the severity level of early damage were demonstrated by the comparison between maximum coefficients.

As discussed above, the wavelet analysis provided higher and more distinct ratio between the coefficients at the relatively early connection damage. This means that wavelet analysis could identify early connection damage more clearly than frequency response methods. That could be an outstanding advantage to use this technique in SHM. However, similar to frequency response methods, large amounts of data have to be saved processed. Another disadvantage of wavelet analysis is that the results are more complicated and more difficult to interpret than the case of other techniques.

6.7.2 Frequency response vs. wavelet analysis and future works

In actual frequency response methods have been practiced on structural damage detection and many satisfied results proving these methods are effective in specific area. However, the application on SHM for frequency response is still subject to further development. In chapter 5 the effective role of frequency response for connection damage has been discussed. However, their care on only global parameters of structure constrained their usage on finding and warning damages but no extensive usage on damage identification, number or location.

The implementation of wavelet analysis on damage detection can however be the most powerful and effective for the in-situ determination of the presence, severity and localization of the structural damage. In this thesis

research we provide just the ability of damage detection by wavelet analysis, but this technique can still be competent on the detection of damage identification and location. This is also proved by some researches mentioned before. For obtaining damaged bolt location, discrete wavelet transform could be used to extract useful data. Future research can reallocate actuator and sensor separately on both sides of lap joint of two flexible beams so that the vibration wave can propagate through lap joint, and bring the bolt clamping information out for analysis. Acoustic emission (AE), which has proved having less propagating dispersion, could be used for signal transmission on solid structures. Finally, a DSP embedded chip can play an important role for on-line data processing in real-time wavelet analysis.

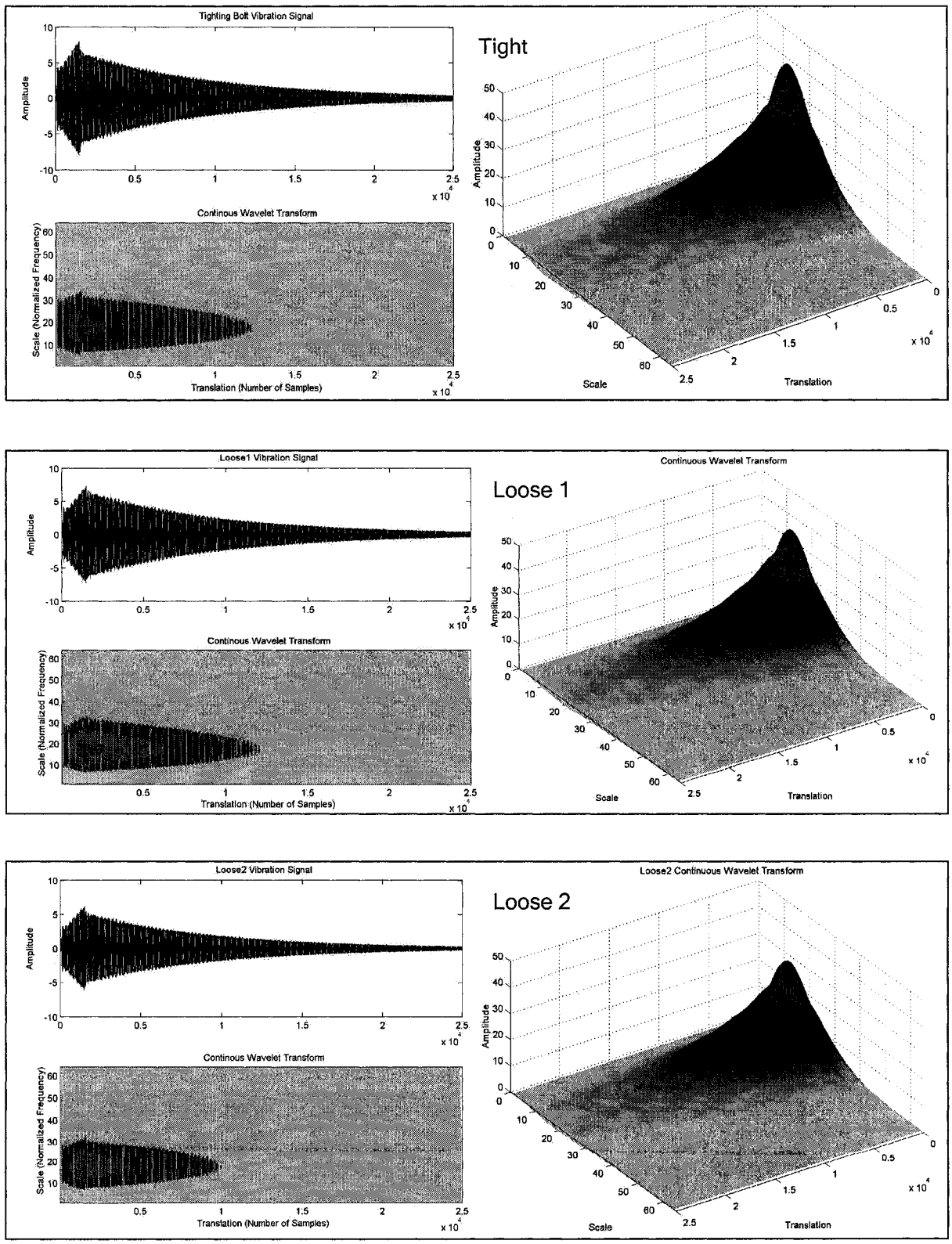

Figure 6.2 Transient vibration signals and 3D, 2D contour plots of wavelet analysis

Figure 6.2 (Continued)

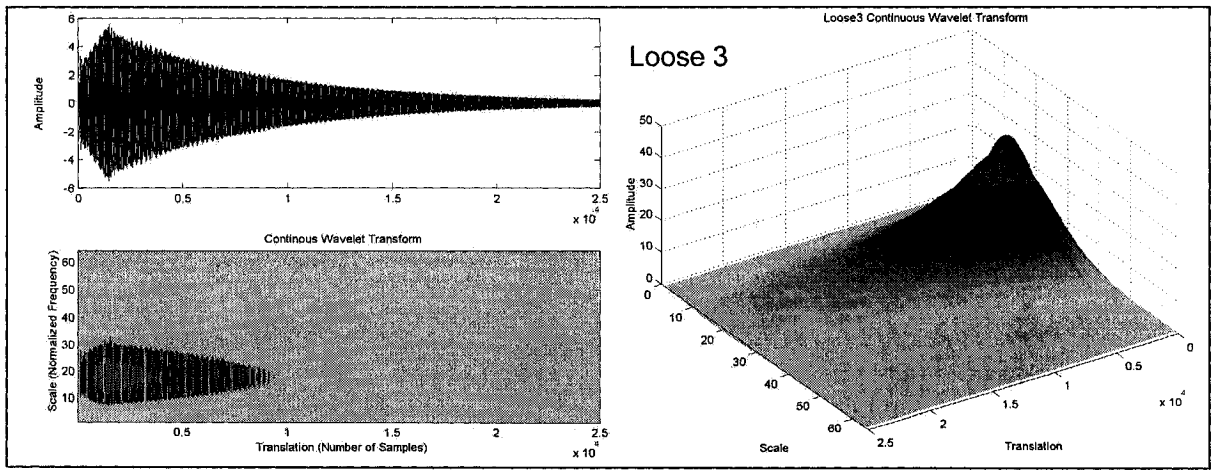

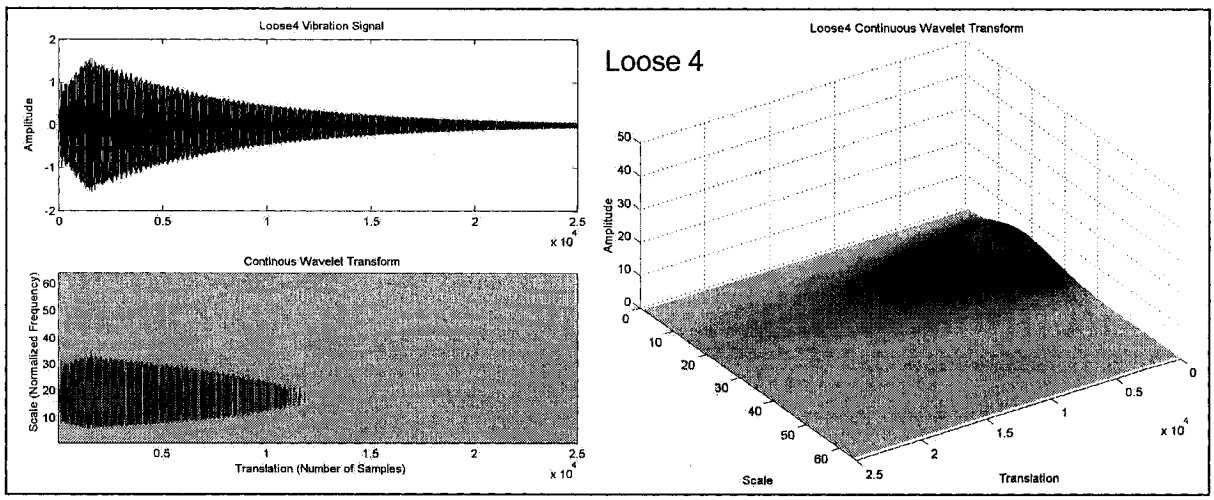

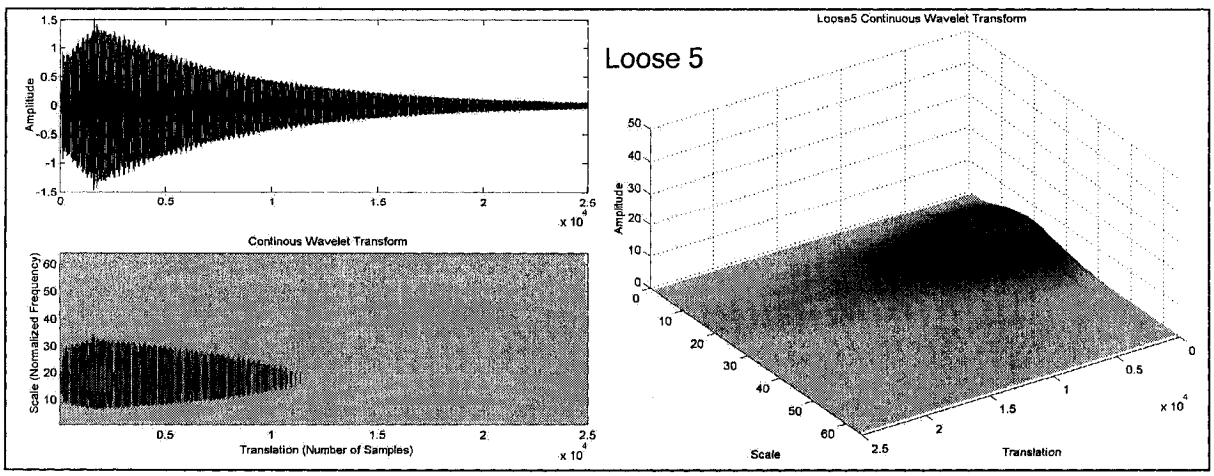

Figure 6.2 (Continued)

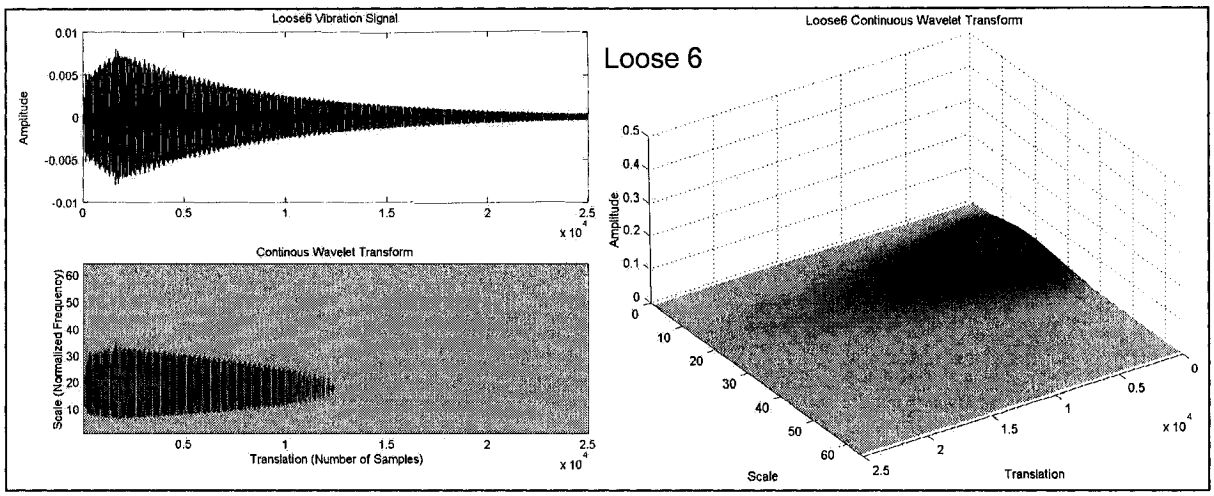

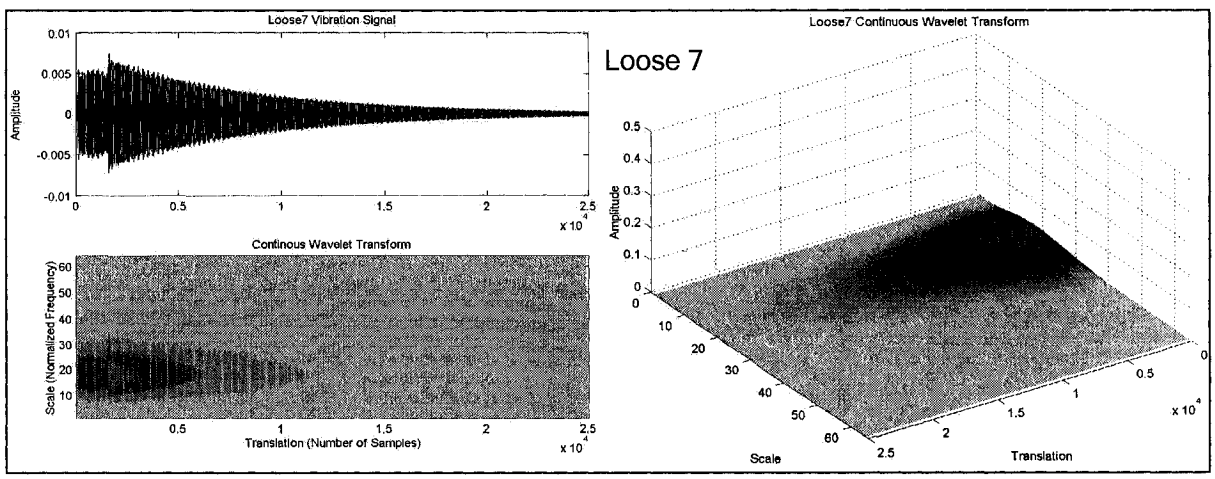

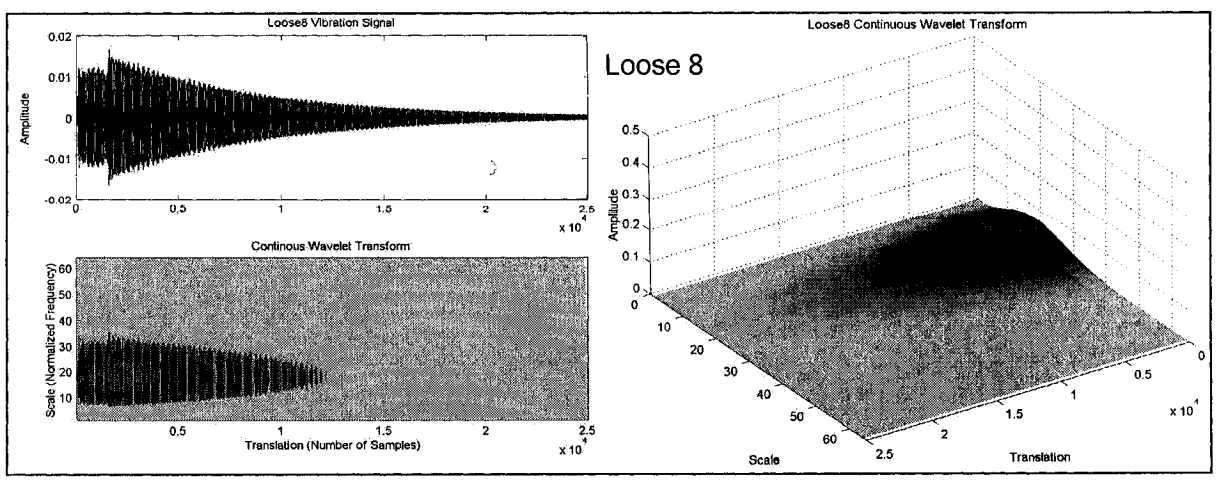

Figure 6.2 (Continued)

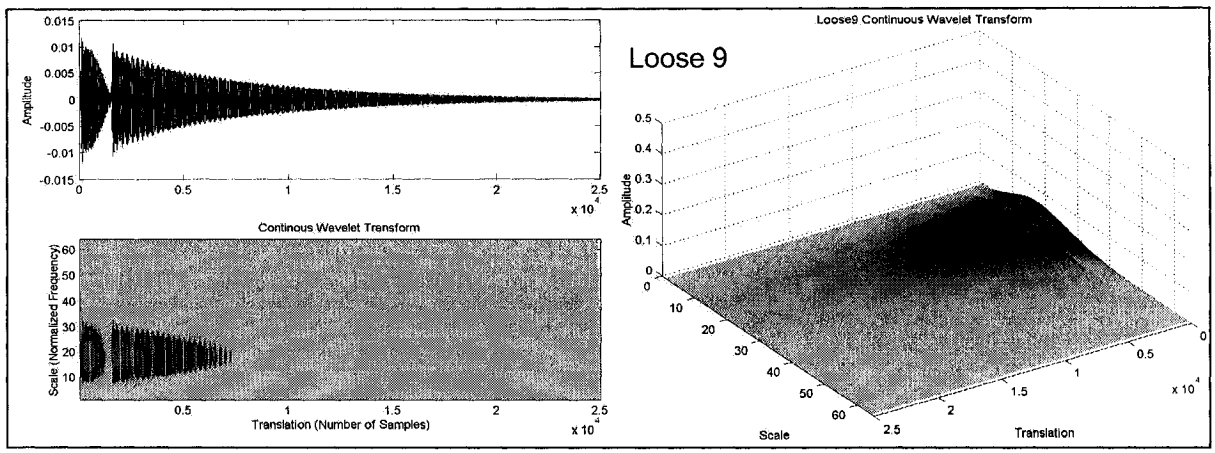

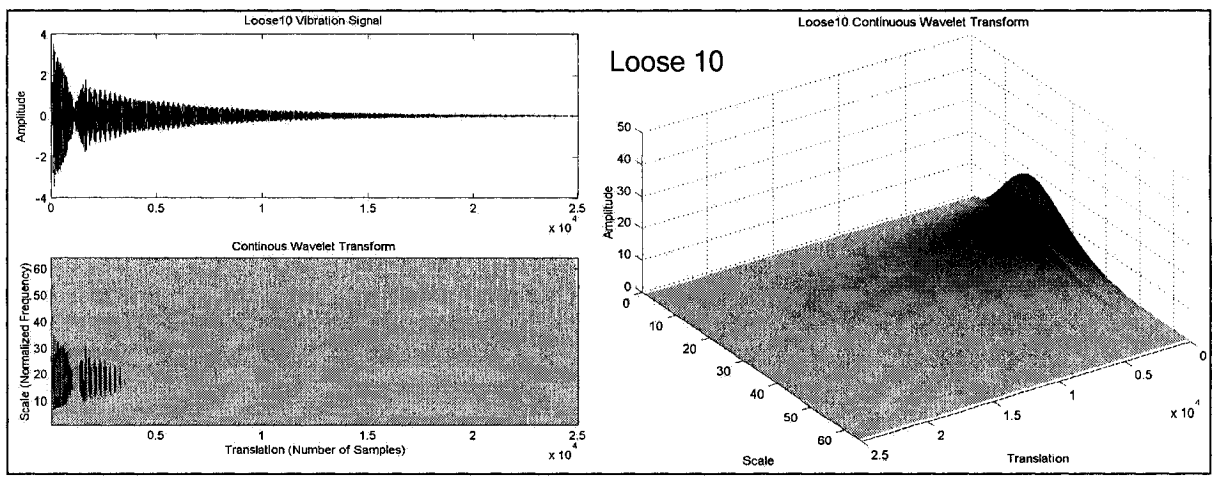

Table 6.1 Scale VS. Frequency (Hz)

Scale	Frequency	Scale	Frequency	Scale	Frequency	Scale	Frequency
1	*6880.7*	17	*404.7*	33	*208.5*	49	*140.4*
2	*3440.4*	18	*382.3*	34	*202.4*	50	*137.6*
3	*2293.6*	19	*362.1*	35	*196.6*	51	*134.9*
4	*1720.2*	20	*344.0*	36	*191.1*	52	*132.3*
5	*1376.1*	21	*327.7*	37	*186.0*	53	*129.8*
6	*1146.8*	22	*312.8*	38	*181.1*	54	*127.4*
7	*983.0*	23	*299.2*	39	*176.4*	55	*125.1*
8	*860.1*	24	*286.7*	40	*172.0*	56	*122.9*
9	*764.5*	25	*275.2*	41	*167.8*	57	*120.7*
10	*688.1*	26	*264.6*	42	*163.8*	58	*118.6*
11	*625.5*	27	*254.8*	43	*160.0*	59	*116.6*
12	*573.4*	28	*245.7*	44	*156.4*	60	*114.7*

13	*529.3*	29	*237.3*	45	*152.9*	61	*112.8*
14	*491.5*	30	*229.4*	46	*149.6*	62	*111.0*
15	*458.7*	31	*222.0*	47	*146.4*	63	*109.2*
16	*430.0*	32	*215.0*	48	*143.3*	64	*107.5*

1. Translation to Time: 19000 samples/second.
2. These results obtained from Tight to Loose 10 system responses.
3. Left top sketches show time domain signals and bottom show
4. Right sketches show 3D plots of wavelet analysis.

Table 6.2 Maximum coefficients under damaged conditions (from Tight to Loose10) and the corresponding time of occurrence

	Tight	Loose1	Loose2	Loose3	Loose4
Max. Coef.	43.715	39.726	33.253	30.429	8.519
Scale (Hz)	382.3	382.3	382.3	382.3	382.3
Translation	0.08s	0.08s	0.08s	0.09s	0.09s
Loose5	Loose6	Loose7	Loose8	Loose9	Loose10
8.068	0.044	0.040	0.092	0.062	18.403
382.3	382.3	382.3	382.3	382.3	382.3
0.09s	0.09s	0.09s	0.09s	0.006s	0.006s

* The results in this table contain Max. Coef. that always at Scale 18, i.e. a frequency around 382 ± 4 Hz, for Tight - Loose 10 conditions.

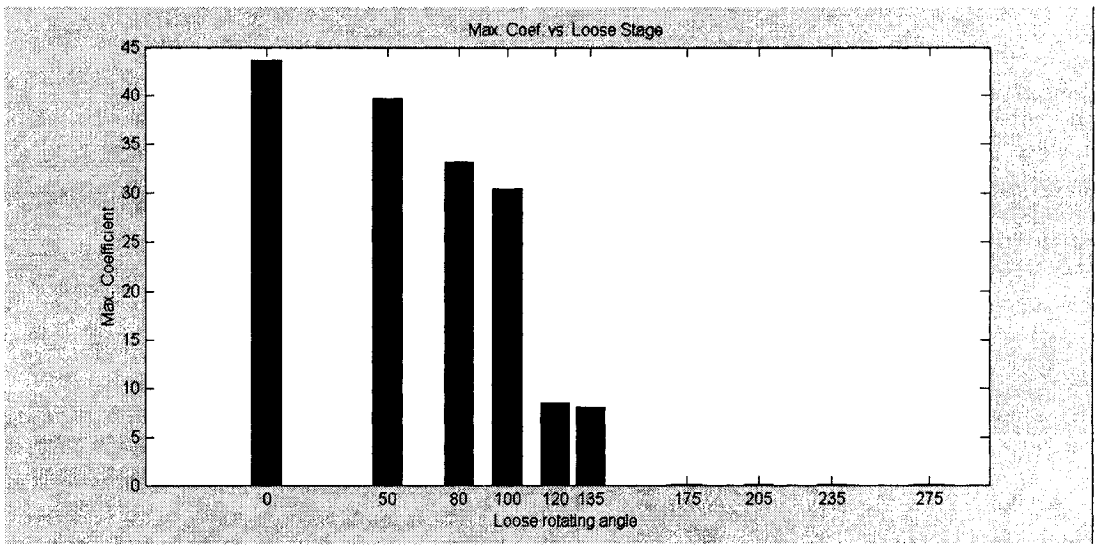

Figure 6.3 Max. coefficient of loose connection

1. Maximum Coefficients vs. Loose Rotation Angle (°). Refer to values listed in Table 6.1.
2. The Maximum Coefficients of every Loose stage is distinguishable to others and generally value goes lower when loose rotation angle increases (0° - 205°), but it is nonlinear.
3. The minor connection damage (50°, 80°) can still be perceived with Maximum Coefficients that shows no change by resonant frequency (382Hz).

References

1. Chang, F-K. **Structural Health Monitoring: A summary report on the first Stanford workshop on structural health monitoring.** Stanford University, Stanford, September 1997.

2. Sohn, H. and Farrar, C. R. **Damage diagnosis using time series analysis of vibration signals.** *Smart materials and Structures*, V.10, 2001, 446-451.

3. Hall S. R. and Conquest, T. J. **The total data integrity initiative - structural health monitoring, the next generation.** *Proceeding of the USAF Aircraft Structural Integrity Program (ASIP)*, 1999, 2nd ed.

4. Iong, K-V. **Smart structure integrity monitoring using transient response.** MS. Thesis. University of Ottawa. 1997.

5. De Abreu. **Real-time damage detection for flexible structures using transient vibrational response.** MS. Thesis. University of Ottawa. 1999.

6. Dandine, M-F and Necsulescu, D. **Real-Time failure detection in smart structures using wavelet analysis.** *Proc. 5th Conf. Dynamics and Control of Structures in Space, Combridge,* 14-18 July 2002.

7. Salgado, N. **Boundary element methods for damage tolerance design of aircraft structures.** Southampton, UK ; Boston, USA : Computational Mechanics Publications, 1998.

8. Nagar A. **Damage tolerance concept for aerospace structures.** *Durability and Damage Tolerance, AD-Vol. 43, ASME* 1994, 1-18.

9. Edited by Harris C. E. **FAA/NASA international symposium on advanced structural integrity methods for airframe durability and damage tolerance.** NASA conference publication, no. 3274, 1994.

10. deKoning A. U. and Henriksen, T. K. **Damage tolerance analysis of bolt/nut assemblies.** NTR Technical Publication, 1996.

11. **Review of damage tolerance for composite sandwich airframe structures.** Final report, DOT/FAA/AR-99/49, 1999.

12. **Damage tolerance for composite sandwich airframe structures.** Final report, DOT/FAA/AR-99/91, 2000.

13. Ugo Mariani **Flaw tolerance/damage tolerance agusta experience on metal parts.** *Damage tolerance in helicopters - situation today, session A.* University of Cranfield, UK. 2001.

14. Krasnowski, B. R. **Application of damage tolerance to increase safety of helicopters in service.** *Application of damage tolerance principles for improved airworthiness of rotorcraft*, RTO MP-24, 1999.

15. Lincoln, J. W. **Role of nondestructive inspections in airworthiness assurance.** *Application of damage tolerance principles for improved airworthiness of rotorcraft*, RTO MP-10, 1998.

16. Smith, R. A. **Non-destructive evaluation for corrosion in ageing aircraft: part 1.** *Insight* Vol. 37, 1995.

17. Smith, R. A. **Non-destructive evaluation for corrosion in ageing aircraft: part 2.** *Insight* Vol. 37, 1995.

18. Necsulescu, D. S. **Mechatronics.** Prentice-Hall, Inc. 2002.

19. Matrat, J., Levin, K. and Jarlas, R. **Effect of debonding on strain measurement of embedded Bragg grating sensors.** *Proceedings of the 2nd international workshop on Structural Health Monitoring,* 1999,651-659.

20. Patsias, S. and Staszewski, W. J. **Damage detection using optical measurements and wavelets.** *Structural Health Monitoring*, V.1(1), 2002, 5-21.

21. Chang, F-K. **A summary report of the 2nd workshop on structural health monitoring.** Stanford University, Stanford, September 2000.

22. Boller, C. **Ways and options for aircraft structural health management.** *Smart Materials and Structures,* V.10, 2001, 432-440.

23. Giurgiutiu, V. and Rogers, C. A. **Recent advancements in the electro-mechanical (E/M) impedance method for structural health monitoring and NDE.** *Part of the SPIE Conference on Smart Etructures and Integrated Systems*, SPIE Vol.3329, 1998, 536-547.

24. Chang, F-K. **Structural Health Monitoring: A summary report on the first**

Stanford workshop on structural health monitoring. Stanford University, Stanford, September 1997.

25. Dickson, J. C., Martin, W. and Collingwood, G. **Operational evaluation of a Health and Usage Monitoring System (HUMS)**. NASA/CR-1998-207409, April 1998.

26. Neumair, M. **Requirements on future structural health monitoring systems.** *Proceedings of the 7th RTO Meetings*, May 1998.

27. Caron, Y. and Richard, Y. **CF-18 Fatigue life management program**, NATO publication RTO-MP-7, AC/323 (AVT) TP/4, Paper 4.

28. Van, C. B., Kudva, J. N., Schoess, J. N., Zeigler, M. L. and Aiper, J. M. **Aircraft structural health monitoring system development - overview of the air force/navy smart metallic structures program.** *SPIE* Vol. 2443, 1995, 277-285.

29. Kudva, J. N., Grage, M. J. and Roberts, M. M. **Aircraft structural health monitoring and other smart structures technologies - perspectives on development of future smart aircraft.** *Smart structures and materials*, 1995, 107-117.

30. Ikegami, R. **Structural health monitoring: Assessment of aircraft customer needs.** *Proceedings of the 2nd International Workshop on Structural Health Monitoring*, 2000, 13-23.

31. Cowan, R. S. and Winer, W. O. **Research developments in integrated diagnostics and prognostics.** *Proceedings of the 2nd International Workshop on Structural Health Monitoring*, 2000, 237-246.

31. Lovell, P. A. and Pines, D. J. **Damage assessment in a bolted lap joint.** *Proceeding of the 5th Annual SPIE Smart Materials and Structure Symposium: Smart Buildings, Bridges and Highways*, Vol.3325, 1998, 112-126.

32. Chang, F. K. **Strength of bolted joints in laminated composites.** Publisher: Ann Arbor, University of Michigan. 1983.

33. Necsulescu, D. S., DeAbreu and F. Bakhtiari-Nejad. **Smart structure monitoring using transient response.** *Proceedings of the first international conference on computational methods for smart structures and materials*, 1998.141-150.

34. Rao, S. S. **Mechanical vibrations, 2nd ed.** 375-408. Addison-Wesley publishing company. 1990.
35. James, M. L., Smith, G.M., Wolford, J. C. and Whaley, P. W. **Vibration of mechanical and structural systems, 2nd ed.** HarperCollins College Publishers, New York, NY. 1994.

36. **Theory and Modeling Guide.** Volume I: ADINA, Report ARD 02-7 September 2002. ADINA R& D, Inc.

37. William weaver, Jr. and Johnston, P. R. **Finite elements for structural analysis.** Prentice-Hall, Inc. 1984. 51-141, 279-311.

38. Reddy J. N. **An introduction to the finite element method.** 2nd ed. McGraw-Hill, Inc. 1993. 143-198.

39. 黄德武 (Huang, Dewu)《实用有限元法》兵器工业出版社 1992，46-71。

40. Inman, D. J. **Engineering vibration.** Prentice-Hall, Inc. 1994. 400-426.

41. Krishnamoorthy, C. S. **Finite element analysis theory and programming,** 2nd ed. Tata McGraw-Hill publishing company Ltd, New Delhi. 1994. 402-437.

42. Necsulescu, D. S. **Mechatronics.** Prentice-Hall, Inc. 2002.

43. 邵贝贝 (Shao, Beibei)，龚光华(Gong, Guanghua)，薛涛(Xue, Tao)，刘永毅(Liu, Yongyi) 《**Motorola DSP 型 16 位单片机原理与实践**》北京航空航天大学出版社 2003。

44. **DSP56F801/803/805/807 16-Bit Digital Signal Processor User's Manual** http://motorola.com/semiconductors/, MOTOROLA INC, 2001.

45. **DSP56F807 Evaluation Module Hardware User's Manual** http://motorola.com/semiconductors/, MOTOROLA INC, 2001.

46. Allemang, R. J. **Vibration: experimental modal analysis.** University of Cincinnati, UC-SDRL-CN-20-263-663/664, 1999.

47. Steve Goldman **Vibration spectrum analysis - a practical approach,** 2nd ed. Industrial press Inc. 1999. 26-45.
48. Grover, D. & Deller, J. R. **Digital signal processing and the microcontroller.** Prentice-Hall, Inc. 1999. 333-379.

49. Williams, A. B. **Electronic filter design handbook: LC, active, and digital filters.** 2nd ed. McGraw-Hill publishing company 1988.

50. Antoniou, Andreas **Digital filters: analysis, design and applications.** 2nd ed. McGraw-Hill, Inc. 1993.

51. MatLab 6.1 **Signal processing toolbox.** The MathWorks, Inc. 1984-2001.

52. Farrar, C. R., Doebling, S. W. **Vibration-Based damage detection.** Tech. Rept. LA-UR-99-1237, Los Alamos National Laboratory. 1999.

53. Ewins, D. J. **Modal testing: theory, practice and application,** 2nd ed. Research studies Press Ltd. 2000.

54. Sohn, H. and Farrar, C. R. **Damage diagnosis using time series analysis of vibration signals.** *Smart Materials and structures*, v.10, 2001, 446-451.

55. De Abreu. **Real-time damage detection for flexible structures using transient vibrational response.** MS. Thesis. University of Ottawa. 1999.

56. Wang, B. T. and Wang, C. C. **Feasibility analysis of using piezoceramic transducers for cantilever beam modal testing.** *Smart Materials and structures*, v.6, 1997, 106-116.

57. Zou, Y., Tong, L. and Steven, G. P. **Vibration-Based model-dependant damage (delamination) identification and health monitoring for composite structures - A review.** *Journal of Sound and Vibration*, v.2, 2000, 357-378.

58. Banks, H. T. and Emeric, P. R. **Detection of non-symmetrical damage in smart plate-like structures.** *Journal of Intelligent Material Systems and Structures*, v.9, 1998, 818-828.

59. Lovell, P. A. and Pines, D. J. **Damage assessment in a bolted lap joint.** *Proceedings of 5th Annual SPIE Smart Materials and Structure Symposium: Smart Bulidings, bridges and Highways*, V.3325, 1998, 112-126.

60. Tseng, K. K-H and Naidu, A. S-K **Non-parametric damage detection and characterization using smart piezoceramic material.** *Smart Materials and structures*, v.11, 2002, 317-329.

61. Zhang, H., Schulz, M. J. and Ferguson, F. **Structural health monitoring using**

transmittance functions. *Mechanical Systems and Signal Processing*, v.13(5), 1999, 765-787.

62. Proakis, J. G. and Manolakis, D. G. **Digital signal processing principles, algorithms, and applications**, 3rd ed. Prentice-Hall, Inc. 1996.

63. Taylor, F. J. **Principles of signals and systems.** McGraw-Hill, Inc. 1994.

64. Giurgiutiu, V. and Rogers, C. A. **Recent advancements in the electro-mechanical (E/M) impedance method for structural health monitoring and NDE.** SPIE V.3329.

65. **Embedded SDK (Software Development Kit) programmer's guide.** http://motorola.com/semiconductors/, MOTOROLA INC, 2002.

66. **Embedded SDK (Software Development Kit) targeting Motorola DSP56F80x platform.** http://motorola.com/semiconductors/, MOTOROLA INC, 2001.

67. Corbin, M., Hera, A. and Hou, Z. **Locating damage regions using wavelet approach.** *Proceedings of the 14th ASCE Engineering Mechanics Conference*, Austin, Texas, May 21-24, 2000.

68. Hou, Z. K. and Noori, M. **Application of wavelet analysis for structural health monitoring.** *Proceedings of the 2nd International Workshop on Structural Health Monitoring*, Stanford university, Stanford, CA, Sept. 8-10, 1999, 946-955.

69. Tamaki, K., Matsuoka, Y., Uno, M. and Kawana, T. **Wavelet transform based signal waveform identification: inspection of rotary compressor.** *IECON '94: 20th International Conference on Industrial Electronics, Control, and Instrumentation,* 1994, 1931-1936.

70. Goumas, S. K., Zervakis, M. E. and Stavrakakis, G. S. **Classification of washing machines vibration signals using discrete wavelet analysis for feature extraction.** *IEEE Transactions on Instrumentation and Measurement*, V.51, No.3, 2002, 497-508.

71. Wand, W. J. and Mcfadden, P. D. **Application of wavelets in non-stationary vibration signal analysis for early gear damage diagnosis.** *Proceedings of the international conference on vibration engineering.* ICVE'94 Beijing, 1994, 615-620.

72. Luo, G-Y. **Vibration Signal Analysis with Wavelet Algorithms.** *ACE-UK Proceeding.* Vol. 3, No. 2, Autumn Edition, 2000, 11-19.

73. Giurgiutiu, V. Cuc, A. and Goodman, P. **Review of vibration-based helicopters health and usage monitoring methods.** *55th Meeting of the Society for Machinery Failure Prevention Technology*, 2001.

74. Kim, J. and Ewins, D. J. **Monitoring transient vibrations in rotating machinery using wavelet analysis.** *Proceedings of the 2nd International Workshop on Structural Health Monitoring*, Stanford university, Stanford, CA, Sept. 8-10, 1999, 287-297.

75. Okafor, A. C. and Dutta, A. **Structural damage detection in beams by wavelet transforms.** *Smart materials and structures.* V.9, 2000, 906-917.

76. Lemistre, M. and balageas. **Structural health monitoring system based on diffracted lamb wave analysis by multi-resolution processing.** *Smart materials and structures.* V.10, 2001, 504-511.

77. Veidt, M. Liu, T. and Kitipornchai, S. **Flexural waves transmitted by rectangular piezoceramic transducers.** *Smart materials and structures.* V.10, 2001, 681-688.

78. Lin, X. and Yuan, F. G. **Diagnostic lamb waves in an integrated piezoelectric sensor/actuator plate: analytical and experimental studies.** *Smart materials and structures.* V.10, 2001, 907-913.

79. Quek. S. T., Wang, Q., Zhang, L. and Ong, K. H. **Practical issues in the detection of damage in beams using wavelets.** *Smart materials and structures.* V.10, 2001, 1009-1017.

80. Kessler, S. S., Spearing, S. M. and Soutis, C. **Damage detection in composite materials using lamb wave methods.** *Smart materials and structures.* V.11, 2002, 269-278.

81. Chan, Y. T. **Wavelet basics.** *Kluwer Academic Publishes.* 1995, 24-52.

82. Chui, C. K. **An introduction to wavelets.** *Academic Press Inc.* 1992.

83. Benedetto, John. J. and Frazier, Michael W. **Wavelets: mathematics and applications.** *CRC Press.* 1994, 23-203.

Appendix A

C Language Program On dSPACE

A.1 Chirp Signal Excitation and Beam Response Collection

```
/*************************************************************************
*
*    Description: The program runs on dSPACE and outputs analog signal by D/A board
*                 to drive piezo-actuator on beam, then piezo-sensor sends vibrational
*                 signal back to A/D board in dSPACE.
*    Excitation sampling frequency: 8192 Hz
*    ADC sampling frequency: 8192 Hz
*    EXcitation duration: 5 seconds and 5 cycles
*
*************************************************************************/

/*****************************************/
/*      declaration of input / output functions          */
/*****************************************/

float ds2002(long base, long channel);
void  ds2101(long base, long channel, float value);

#include <c:\c30tools\math.h>
#include <c:\c30tools\stdio.h>

/*******************************/
/*       declaration of variables        */
/*******************************/

const int cycles = 5;      /* Number of excitation cycles  */
const float mag10 = 1.;   /* Magnitude of excitation divided by 10 */

float ht;                  /* Sampling time */
```

```
long  int i = 0;
long  int j = 0;
float excite;                /* Forcing function */
float gain1,gain2;           /* Gain adjustments */
float mes_sgn_nf=0.;         /* measured variables from A/D converter (DS2002) */
float tdelay;
int   samples_per_cycle;
float ych;
float yh;

/*********************************/
/*              interrupt loop               */
/*********************************/

c_int10()
{

/*  Using Trace program to read desired program variables  */

 ht=1./(8192);
 tdelay=10.*(1/ht);          /*  10 sec delay  */
 samples_per_cycle=1/(ht);

 if (j>tdelay)
 {
   asm("       trapu    27"); /* call TRACE30 */
 }

/*************************************************************************/
/**                          D/A signal to Actuator   (delay for 10 sec)                          **/
/*************************************************************************/

 if (j>tdelay)
 {
     float tt=i*ht;

     ych=sin(2*3.1416*(40+180*tt+200*tt*tt));  /* chirp signal function */
     yh=0.5*(1-cos(2*3.1416*tt));              /* hanning windowed function */
     excite=mag10*ych*yh;

     if (i==samples_per_cycle-1) i=-1;
```

```
   if(j>(tdelay+cycles*samples_per_cycle)) excite=0.;
    ds2101(0x00000090,0x00000004,excite);

     i=i+1;

/*************************************/
/**            A/D for sensor reading          **/
/*************************************/

    gain1=38.849;    /* gain adjustment so trace30 beam response */
    gain2=.6977;     /* gain adjustment (measured with oscilloscope) */

     mes_sgn_nf = gain1*gain2*yh*ds2002(0x00000020, 0x0000000b);

/* y axis 50X agrees with beam response on oscilloscope */

  }
  j=j+1;

}

/*****************************************************/
/*                 the main part of program (loop)                 */
/*****************************************************/

void init();
void timer1(float time);

main()

{
 init();
 timer1(1./(8192));  /* timer configuration */

 for (;;)
   ;
}
```

A.2 Limit Cycles Sinusoidal Excitation and Response For Wavelet Analysis

```
/*************************************************************************
*
*    Description: The program runs on dSPACE and outputs analog signal by D/A board
*                 to drive piezo-actuator on beam, then piezo-sensor sends vibrational
*                 signal back to A/D board in dSPACE.
*    Excitation sampling frequency: 19100 Hz
*    ADC sampling frequency: 19100 Hz
*    Excitation duration: 0.08 seconds and 50 cycles
*
*************************************************************************/

/*****************************************/
/*      declaration of input / output functions        */
/*****************************************/

float ds2002(long base, long channel);
void  ds2101(long base, long channel, float value);

#include <c:\c30tools\math.h>
#include <c:\c30tools\stdio.h>

/*******************************/
/*       declaration of variables       */
/*******************************/

const float f = 382        /* Total cycles in a second */
const int cycles = 30;     /* Number of excitation cycles  */
const float mag10 = 1.;  /* Magnitude of excitation divided by 10 */

float ht;                  /* Sampling time */
long  int i = 0;
long  int j = 0;
float excite;              /* Forcing function */
float gain1,gain2;         /* Gain adjustments */
float mes_sgn_nf=0.;     /* measured variables from A/D converter (DS2002) */
float tdelay;
```

```
int  samples_per_cycle;


/*********************************/
/*              interrupt loop              */
/*********************************/

c_int10()
{

/* Using Trace program to read desired program variables */

 ht=1./(19100);
 tdelay=10.*(1/ht);          /*  10 sec delay  */
 samples_per_cycle=1/(ht*f);

 if (j>tdelay)
 {
   asm("      trapu   27"); /* call TRACE30 */
 }

/*************************************************************************/
/**                          D/A signal to Actuator  (delay for 10 sec)                          **/
/*************************************************************************/

 if (j>tdelay)
 {
     excite = mag10*sin(2*3.1416*f*ht*i); /* Sinusoidal singal */

   if(j>(tdelay+cycles*samples_per_cycle)) excite=0.;
    ds2101(0x00000090,0x00000004,excite);

     i=i+1;

/*************************************/
/**             A/D for sensor reading          **/
/*************************************/

    gain1=38.849;    /* gain adjustment so trace30 beam response */
    gain2=.6977;     /* gain adjustment (measured with oscilloscope) */
```

```
      mes_sgn_nf = gain1*gain2*yh*ds2002(0x00000020, 0x0000000b);

/* y axis 50X agrees with beam response on oscilloscope */

   }
   j=j+1;

}

/*****************************************************/
/*                  the main part of program (loop)                  */
/*****************************************************/

void init();
void timer1(float time);

main()

{
  init();
  timer1(1./(19100));   /* timer configuration */

  for (;;)
    ;
}
```

Appendix B

C Language and Assembly Language Programs On DSP56F807

B.1 Real Time FFT Main Program

```
/*************************************************************************
*
*    Description: This program was made for real time FFT or time frequency analysis.
*                 ADCA AN1 & GND are configured to snapshot analog signal in
*                 single end mode. PIN3 & 9 are connected. The sampling rate is 2048
*                 samples/second. Samples are saved in two dynamic allocated memories
*                 so that sample can also be saved after another memory is full and
*                 begin to call FFT function. It prove that no any signal is missed while
*                 the process is going. 2048 Hz is the maximum frequency of signal
*                 can be measured. Three LEDs are used to demonstrate specific frequency
*                 elements.
*
*************************************************************************/

#include "port.h"
#include "arch.h"
#include "prototype.h"
#include "dfr16.h"
#include "dfr16priv.h"
#include "stdio.h"
#include <stdlib.h>
#include "assert.h"
#include "input_rfft.h"
#include "mem.h"
#include "mfr16.h"
#include "afr16.h"
#include "adc.h"
```

```
#include "quadraturetimer.h"
#include "io.h"
#include "fcntl.h"
#include "bsp.h"
#include "led.h"
#include "56807.h"


#define length 2048

typedef  unsigned short WORD;
EXPORT   Result dfr16RFFTC (dfr16_tRFFTStruct *, Frac16 *, dfr16_sInplaceCRFFT *);
EXPORT       pcmasterdrvRecorder();

/*************************************************************************/
/*   Function prototypes declarations                                    */
/*************************************************************************/

void InitDevices (void);
void CC_Callback(adc_eCallbackType type, adc_tSampleMask causedSampleMask);
static void timer100ms(qt_eCallbackType CallbackType, void* pParam);
void Freq_Led();

/*************************************************************************/
/*   LED Function prototypes                                             */
/*************************************************************************/

void      RedOn(void);
void      YellowOn(void);
void      GreenOn(void);
void Red_YellowOn(void);
void Yellow_GreenOn(void);
void Red_GreenOn(void);

/*************************************************************************/
/*   Define variables                                                    */
/*************************************************************************/

static    UInt16        TimerC2FD, TimerC0FD;
static    UInt16        Adc0FD;
static    UInt16        LedFD;
```

```
static    int  ipushpos=0;
static    int  SampleCount=0;

/*****************************************************************************/
/*   Device Configuration                                                    */
/*****************************************************************************/

const qt_sState quadParam = {
/* Configured for specific ADC sample rate (see below) at 80MHz */
  /* Mode = */                  qtCount,
  /* InputSource = */           qtPrescalerDiv8, /* See Below */
  /* InputPolarity = */         qtNormal,
  /* SecondaryInputSource = */  0,

  /* CountFrequency = */        qtRepeatedly,
  /* CountLength = */           qtUntilCompare,
  /* CountDirection = */        qtDown,

  /* OutputMode = */            qtToggleOnCompare, /*toggle output*/
  /* OutputPolarity = */        qtNormal,
  /* OutputDisabled = */        0,

  /* Master = */                0,
  /* OutputOnMaster = */        0,
  /* CoChannelInitialize = */   0,
  /* AssertWhenForced = */      0,

  /* CaptureMode = */           qtDisabled,

  /* CompareValue1 = */         0,
  /* CompareValue2 = */         0,
  /* InitialLoadValue = */      1221, /* See Below */

  /* CallbackOnCompare = */     { 0, 0 },
  /* CallbackOnOverflow = */    { 0, 0 },
  /* CallbackOnInputEdge = */   { 0, 0 },

};

/*
    Quad Timer toggles output, so output goes high every other clock period.
```

```
    Input clock is IPBus clock = 1/2 of system clock.

    For sample rate: 2048 Hz
    Prescaler:      8
    Clock Frequency: (80 Mhz/2)/32 = 40 Mhz/8 = 5.0 MHz
    Clock Ticks in one period = 5,000,000 Hz /(2 * 2048) = 1221
*/

const qt_sState quadParam0 = {
/* Configured for specific ADC sample rate (see below) at 80MHz */
  /* Mode = */                    qtCount,
  /* InputSource = */             qtPrescalerDiv128, /* See Below */
  /* InputPolarity = */           qtNormal,
  /* SecondaryInputSource = */    0,

  /* CountFrequency = */          qtRepeatedly,
  /* CountLength = */             qtUntilCompare,
  /* CountDirection = */          qtDown,

  /* OutputMode = */              qtToggleOnCompare, /*toggle output*/
  /* OutputPolarity = */          qtNormal,
  /* OutputDisabled = */          0,

  /* Master = */                  0,
  /* OutputOnMaster = */          0,
  /* CoChannelInitialize = */     0,
  /* AssertWhenForced = */        0,

  /* CaptureMode = */             qtDisabled,

  /* CompareValue1 = */           0,
  /* CompareValue2 = */           0,
  /* InitialLoadValue = */        31250u, /* See Below */

  /* CallbackOnCompare = */       { timer100ms, 0 },
  /* CallbackOnOverflow = */      { 0, 0 },
  /* CallbackOnInputEdge = */     { 0, 0 },

};

/*
```

```
    Quad Timer toggles output, so output goes high every other clock period.
    Input clock is IPBus clock = 1/2 of system clock.

    For sample period: 100ms = 10hz
    Prescaler:      128
    Clock Frequency: (80 Mhz/2)/128 = 40 Mhz/128 = 0.3125 MHz
    Clock Ticks in one period = 312500 Hz /10 = 31250
*/

/*
    Quad Timer toggles output, so output goes high every other clock period.
    Input clock is IPBus clock = 1/2 of system clock.

    For sample period: 1s = 1hz
    Prescaler:      128
    Clock Frequency: (80 Mhz/2)/128 = 40 Mhz/128 = 0.3125 MHz
    Clock Ticks in one period = 312500 Hz /1 = 312500
*/

static const adc_sState sadc0 = {
 /* AnalogChannel      = */ ADC_CHANNEL_1,
 /* SampleMask         = */ 0x02,

 /* OffsetRegister     = */ FRAC16(0.0),
 /* LowLimitRegister   = */ 0,
 /* HighLimitRegister  = */ 0,
 /* ZeroCrossing       = */ 0,
};

/*****************************************************************************/
/*   Other global variables                                                  */
/*****************************************************************************/

static    Frac16   Sample0;
UInt16    n = 2048;
Frac16   *pX2048;
static    Frac16   *mag; // magnitude.
static    Frac16   *pX;
Frac16    pX_input1[length];
Frac16    pX_input2[length];
```

```
int main(void)
{
  dfr16_sInplaceCRFFT *pZ;
  Result res;
  UInt16 options = FFT_SCALE_RESULTS_BY_N;
  Frac16 *han2048;
  const CFrac16 *Actual_op;
  dfr16_tRFFTStruct *pRFFT;
  Int16 i, j;

  Frac16Freq[6];
  Frac16MaxValue;
  UInt16      MaxIndex;

  han2048=(Frac16 *)han_vector; // Copy Hanning Window vectors.

  InitDevices(); // Initialize all ports.

  pX=(Frac16 *) memMallocEM(n*sizeof(Frac16)); // define memory size for pX.
  pZ=(dfr16_sInplaceCRFFT *) memMallocEM(sizeof(dfr16_sInplaceCRFFT) +
    sizeof(CFrac16)*(n/2-2)); //define memory size for pZ.
  mag=(Frac16 *) memMallocEM((n/2+1)*sizeof(Frac16));
    // define memory size for magnitude.

      /* check available memory is enough or not. */

            if (pX == NULL)
      {
        assert(!"Cannot allocate memory");
      }

      if (pZ == NULL)
      {
        assert(!"Cannot allocate memory");
      }

    /* collect signal and calculate frequency in FFT algorithm */

  while(1)
  {
        if(SampleCount==2048)
```

```
{

    pX2048 = (Frac16 *)pX_input1;


      for (i=0; i < n; i++)
        {pX[i] = mult(pX2048[i],han2048[i]);}

      Actual_op = &Actual_op_2048[0];

      /* Call FFT Create function */
      pRFFT = dfr16RFFTCreate (2048, options);

     if(!pRFFT)
     {
        break;
     }

res = dfr16RFFTC (pRFFT, &pX[0], pZ);

        /* obtain magnitude array from frequncy elements. */

mag[0] = mult((*pZ).z0, (*pZ).z0);
mag[n/2] = mult((*pZ).zNDiv2, (*pZ).zNDiv2);

 for (i = 0; i<(n/2-1); i++)
  {mag[i+1] = add(mult(pZ->cz[i].real, pZ->cz[i].real),
          mult(pZ->cz[i].imag, pZ->cz[i].imag));
  }

        /* obtain the expecting band of 6 frequncies. */

for (i=0; i<6; i++)
        Freq[i]=mag[i+382];

/* Calculate the maximum value in specific frequency band */

      MaxValue = afr16Max(Freq, sizeof(Freq)/sizeof(Freq[0]), &MaxIndex);


        /* Turn LEDs off by clearing all bits in Port B data register */
```

```
        *((WORD *)GPIO_B_DR) = 0x0000;

      if(Freq[5]== MaxValue)
          RedOn();            /* toggle Red LED */
        if(Freq[4]== MaxValue)
        YellowOn();                 /* toggle Yellow LED */
        if(Freq[3]== MaxValue)
        GreenOn();            /* toggle Green LED */
      if(Freq[2]== MaxValue)
        Red_YellowOn();           /* toggle Red & Yeliow LED */
      if(Freq[1]== MaxValue)
          Yellow_GreenOn();     /* toggle Yellow & Green LED */
      if(Freq[0]== MaxValue)
       Red_GreenOn();       /* toggle Red & Green LED */
      if(MaxValue==0)
        *((WORD *)GPIO_B_DR)     = 0x0000;      // Clear data register


/* RFFT destroy */
dfr16RFFTDestroy (pRFFT);
}

if(SampleCount==4096)
{

      pX2048 = (Frac16 *)pX_input2;


        for (i=0; i < n; i++)
          {pX[i] = mult(pX2048[i],han2048[i]);} .

        Actual_op = &Actual_op_2048[0];

        /* Call FFT Create function */
        pRFFT = dfr16RFFTCreate (2048, options);

if(pRFFT == NULL)
{
      break;
}
```

```
res = dfr16RFFTC (pRFFT, &pX[0], pZ);

        /* obtain another magnitude array from frequncy elements. */

mag[0] = mult((*pZ).z0, (*pZ).z0);
mag[n/2] = mult((*pZ).zNDiv2, (*pZ).zNDiv2);

for (i = 0; i<(n/2-1); i++)
  {mag[i+1] = add(mult(pZ->cz[i].real, pZ->cz[i].real),
            mult(pZ->cz[i].imag, pZ->cz[i].imag));
  }

        /* obtain the expecting band of 6 frequncies. */

        for (i=0; i<6; i++)
        Freq[i]=mag[i+187];

/* Calculate the maximum value in specific frequency band */

      MaxValue = afr16Max(Freq, sizeof(Freq)/sizeof(Freq[0]), &MaxIndex);


        /* Turn LEDs off by clearing all bits in Port B data register */

        *((WORD *)GPIO_B_DR) = 0x0000;

    if(Freq[5]== MaxValue)
        RedOn();            /* toggle Red LED */
      if(Freq[4]== MaxValue)
      YellowOn();               /* toggle Yellow LED */
      if(Freq[3]== MaxValue)
      GreenOn();            /* toggle Green LED */
    if(Freq[2]== MaxValue)
      Red_YellowOn();           /* toggle Red & Yeliow LED */
    if(Freq[1]== MaxValue)
        Yellow_GreenOn();   /* toggle Yellow & Green LED */
    if(Freq[0]== MaxValue)
     Red_GreenOn();       /* toggle Red & Green LED */
    if(MaxValue==0)
      *((WORD *)GPIO_B_DR)    = 0x0000;     // Clear data register
```

```
            /* RFFT destroy */
            dfr16RFFTDestroy (pRFFT);
            }
        }
        return;
}

void InitDevices (void)
{
    // open timer C2
    TimerC2FD = open(BSP_DEVICE_NAME_QUAD_TIMER_C_2, 0, &quadParam );

    // open ADC port 0
    Adc0FD = open(BSP_DEVICE_NAME_ADC_0, 0, &sadc0);

    // open timer C0
    TimerC0FD = open(BSP_DEVICE_NAME_QUAD_TIMER_C_0, 0, &quadParam0 );

    // Disable all interrupt features on Port B
    *((WORD *)GPIO_B_IAR)  = 0x0000;
    *((WORD *)GPIO_B_IENR) = 0x0000;
    *((WORD *)GPIO_B_IPOLR)= 0x0000;
    *((WORD *)GPIO_B_IESR) = 0x0000;

    // Configure the Port B lines
    *((WORD *)GPIO_B_DR) = 0x0000;     // Clear data register
    *((WORD *)GPIO_B_PER)     = 0x0000;     // Lines are dedicated GPIO
    *((WORD *)GPIO_B_DDR)     = 0x0007;     // Set bits 0, 2, 4 as outputs to drive LEDs

  LedFD = open(BSP_DEVICE_NAME_LED_0, 0);  // open LED driver

} //end InitDevices

void CC_Callback(adc_eCallbackType type, adc_tSampleMask causedSampleMask)
{
    /*
      read samples and put them into first array when number is less than 2048, but
      into anothe array when equal or larger than 2048 but snaller than 4096. If the
      number reach 4096, let it be 0 and save in the first array.
    */
```

```
    read( Adc0FD, &Sample0, 1 );

    if(SampleCount==4096) {
        ipushpos=0;
        SampleCount=0;
    }
    if(SampleCount<2048)
        pX_input1[ipushpos++] = Sample0;
    else
        pX_input2[(ipushpos++)-2048] = Sample0;

    SampleCount++;

} // end CC_Callback


static void timer100ms(qt_eCallbackType CallbackType, void* pParam)
{
    pcmasterdrvRecorder();
}

void RedOn(void)
{
    *((WORD *)GPIO_B_DR) = 0x0001;
    asm(rts);
}

void YellowOn(void)
{
    *((WORD *)GPIO_B_DR) = 0x0002;
    asm(rts);
}

void GreenOn(void)
{
    *((WORD *)GPIO_B_DR) = 0x0004;
    asm(rts);
}

void Red_YellowOn(void)
```

```
{
    *((WORD *)GPIO_B_DR) = 0x0003;
    asm(rts);
}

void Yellow_GreenOn(void)
{
    *((WORD *)GPIO_B_DR) = 0x0006;
    asm(rts);
}

void Red_GreenOn(void)
{
    *((WORD *)GPIO_B_DR) = 0x0005;
    asm(rts);
}
```

B.2 Assembly Language Program for LEDs

```
/*************************************************************************
*
*    Description: This assambly language program configure GPIO for LEDs on/off,
*                 which would be called by main program
*
*************************************************************************/

; DSP56807 Port B bits and address
RED             equ $0001
YELLOW          equ $0002
GREEN           equ $0004
RED_YELLOW      equ $0003
YELLOW_GREEN    equ $0006
RED_GREEN       equ $0005
GPIO_B_DR       equ $13c1


    SECTION user
```

```
    ORG P:
;;;;;;;;;;;;;;;;;;;;;;;;;;;;;;;;;;;;;;;;;;;;;;;;;;;;;;;
    ;GLOBAL FRedOn                      ; Turn on red LED
;;;;;;;;;;;;;;;;;;;;;;;;;;;;;;;;;;;;;;;;;;;;;;;;;;;;;;;
FRedOn:
    bfset   #RED,x:GPIO_B_DR            ; Write bit to GPIO
    rts
;;;;;;;;;;;;;;;;;;;;;;;;;;;;;;;;;;;;;;;;;;;;;;;;;;;;;;;
    ;GLOBAL FYellowOn                   ; Turn on yellow LED
;;;;;;;;;;;;;;;;;;;;;;;;;;;;;;;;;;;;;;;;;;;;;;;;;;;;;;;
FYellowOn:
    bfset   #YELLOW,x:GPIO_B_DR         ; Write bit to GPIO
    rts
;;;;;;;;;;;;;;;;;;;;;;;;;;;;;;;;;;;;;;;;;;;;;;;;;;;;;;;
    ;GLOBAL FGreenOn                    ; Turn on green LED
;;;;;;;;;;;;;;;;;;;;;;;;;;;;;;;;;;;;;;;;;;;;;;;;;;;;;;;
FGreenOn:
    bfset   #GREEN,x:GPIO_B_DR          ; Write bit to GPIO
    rts
;;;;;;;;;;;;;;;;;;;;;;;;;;;;;;;;;;;;;;;;;;;;;;;;;;;;;;;
    ;GLOBAL FRed_YellowOn               ; Turn on red LED
;;;;;;;;;;;;;;;;;;;;;;;;;;;;;;;;;;;;;;;;;;;;;;;;;;;;;;;
FRed_YellowOn:
    bfset   #RED_YELLOW,x:GPIO_B_DR ; Write bit to GPIO
    rts
;;;;;;;;;;;;;;;;;;;;;;;;;;;;;;;;;;;;;;;;;;;;;;;;;;;;;;;
    ;GLOBAL FYellow_GreenOn             ; Turn on yellow LED
;;;;;;;;;;;;;;;;;;;;;;;;;;;;;;;;;;;;;;;;;;;;;;;;;;;;;;;
FYellow_GreenOn:
    bfset   #YELLOW_GREEN,x:GPIO_B_DR   ; Write bit to GPIO
    rts
;;;;;;;;;;;;;;;;;;;;;;;;;;;;;;;;;;;;;;;;;;;;;;;;;;;;;;;
    ;GLOBAL FRed_GreenOn                ; Turn on green LED
;;;;;;;;;;;;;;;;;;;;;;;;;;;;;;;;;;;;;;;;;;;;;;;;;;;;;;;
FRed_GreenOn:
    bfset   #RED_GREEN,x:GPIO_B_DR      ; Write bit to GPIO
    rts


    ENDSEC
    END
```

B.3 Application Header File

```
/*************************************************************************
*
*    Description:  Refer to config/config.h for complete list of all components and
*                  component default initialization
*
*************************************************************************/

#ifndef __APPCONFIG_H
#define __APPCONFIG_H


/*************************************************************************
*
* Include needed SDK components
*
*************************************************************************/

#define INCLUDE_BSP                 /* BSP support */
#define INCLUDE_DSPFUNC             /* DSP Function Library */

#define INCLUDE_STACK_CHECK   /* Check for stack overflow */


#define INCLUDE_ADC                 /* ADC support */
#define INCLUDE_FILEIO              /* File I/O support */
#define INCLUDE_GPIO                /* General Purpose I/O support */
#define INCLUDE_IO                  /* I/O support */
#define INCLUDE_LED                 /* LED support for target board */
#define INCLUDE_QUAD_TIMER    /* Quadrature timer support */
#define INCLUDE_SCI                 /* SCI support */
#define INCLUDE_MEMORY              /* memory support */
#define INCLUDE_PCMASTER            /* PC Master support */


// Define GPR = 1 for interrupts 3-6,8,9 to trap unhandled
// interrupts in archUnhandledInterrupts. Check N for interrupt #.

#define GPR_INT_PRIORITY_3 1    // Illegal Instruction
```

```
#define GPR_INT_PRIORITY_4 1   // Software Interrupt
#define GPR_INT_PRIORITY_5 1   // HW Stack Overflow
#define GPR_INT_PRIORITY_6 1   // OnCE Trap
#define GPR_INT_PRIORITY_8 1   // IRQA
#define GPR_INT_PRIORITY_9 1   // IRBB

/************************************************************************
*
*    Overwrite default component initializations from config/config.h
*    using #defines here
*
************************************************************************/

/* PLL configuration */
#define PLL_MUL  20        // for 80 MHz clock

/* Quad Timer configuration */
#define INCLUDE_USER_TIMER_C_2  0     // used to drive ADC A SYNC input
#define INCLUDE_USER_TIMER_C_0  0     // used for timer to trigger recorder

/* ADC Configuration */
#define ADC_SCANMODE                ADC_SEQUENTIAL_TRIGGERED
#define ADCA_INITIATE_SCAN          ADC_INITIATE_SCAN_ON_SYNC
#define ADCA_CLOCK_DIVISOR          3
#define ADCA_RAW_CONVERSION_COMPLETE_CALLBACK CC_Callback

#define GPR_INT_PRIORITY_57 4
#define GPR_INT_PRIORITY_55 4


/* Include one sample */
#define INCLUDE_ADCA_SAMPLE_1

//#define ADCA_QUEUE_DEPTH (2048*16)

#if 1
/* this line makes room to store samples on the EVM */
#define PC_MASTER_REC_BUFF_LEN 1542

/* this line sets the time base for the recorder. */
#define PC_MASTER_RECORDER_TIME_BASE  0x4064
```

```
#define SCI_USER_BAUD_RATE_1 SCI_GET_SBR(115200u) // Baud rate 19200

#endif
```

B.4 Memory Map and Size File

```
# Memory map:
  v_addr   p_addr   size     name
  00000000 00000000 00000086 .pInterruptVector
  00000086 00000086 00002BBD .pExtRAM
  00000000 00000000 00000030 .xAvailable
  00000030 00000030 00000010 .xCWRegisters
  00000040 00000040 00000FC0 .xIntRAM_DynamicMem
  00001000 00001000 00000800 .xPeripherals
  00001800 00001800 00000800 .xReserved
  00002000 00002000 00002000 .xFlash
  00004000 00004000 00001D24 .xExtRAM
  0000E000 0000E000 00001000 .xExtRAM_DynamicMem
  0000F000 0000F000 00000F80 .xStack
  0000FF80 0000FF80 00000080 .xCoreRegisters

# Link start time: Mon Apr 14 22:22:21 2003
# Link end time: Mon Apr 14 22:22:22 2003
```

Appendix C

MatLab M-File Program

```
%%%%%%%%%%%%%%%%%%%%%%%%%%%%%%%%%%%%%%%%%%%%%%%
%
%        Chirp signal and frequency distribution
%
%%%%%%%%%%%%%%%%%%%%%%%%%%%%%%%%%%%%%%%%%%%%%%%

dt=1/8192;
dur=1;
n = 8192;
r = 8192;
t = n/r;
tt=0:dt:dur;
psi=2*pi*(40+180*tt+200*tt.*tt);
A=sin(psi);
yy = fft(A);
m = abs(yy);
mm = m/n;
N = length(yy)-1;
fHz = (0:1/t:N/t);
subplot(2,1,1); plot(tt,A);
title('Chirp Signal');
ylabel('Amplitude'); xlabel('Time [Sec]');
subplot(2,1,2);
plot(fHz,mm); grid;
title('Chirp Signal FFT');
ylabel('Magnitude'); xlabel('Frequency [Hz]');
```

```
%%%%%%%%%%%%%%%%%%%%%%%%%%%%%%%%%%%%%%%%%%%%%%%%%%%%%%%%%%%%
%
%       Hanning Windowed Chirp signal and frequency distribution
%
%%%%%%%%%%%%%%%%%%%%%%%%%%%%%%%%%%%%%%%%%%%%%%%%%%%%%%%%%%%%
dt=1/8192;
dur=1;
tt=0:dt:dur;
psi=2*pi*(40+180*tt+200*tt.*tt);
A=sin(psi);
n = 8192;
r = 8192;
yh = 0.5*(1-cos(2*pi*(0:n)/n));
y = yh.*A;
%t = n/r;
yy = fft(y);
m = abs(yy);
mm = m/n;
N = length(yy)-1;
f = (0:N);
df = r/n;
fHz = f*df;
subplot(2,1,1); plot(A)
title('Exciting Chirp Signal for Frequency Drift');
ylabel('Amplitude'); xlabel('Frequency [Hz]');
subplot(2,1,2); plot(fHz,mm); grid;
title('Hanning Windowed Exciting Singnal Spectrum');
ylabel('Amplitude'); xlabel('Frequency [Hz]');



%%%%%%%%%%%%%%%%%%%%%%%%%%%%%%%%%%%%%%%%%%%%%%%%%%%%%%%%%%%%
%
%       Frequency band analysis of chirp signal
%
%%%%%%%%%%%%%%%%%%%%%%%%%%%%%%%%%%%%%%%%%%%%%%%%%%%%%%%%%%%%

x=0:.01:1;
y1=50;
y2=100;
y3=200;
```

```
y4=300;
y5=400;
y6=500;
y7=600;
z1=120+360*x;
z2=180+400*x;
plot(x,y1,x,y2,x,y3,x,y4,x,y5,x,y6,x,y7,x,z1,x,z2)
xlabel('0 \leq t \leq 1 Sec.')
ylabel('Frequency (Hz)')
title('Chirp Signal Frequency vs. Time')
text(0.6,336,'\leftarrow 120+360t',...
   'HorizontalAlignment','left')
text(0.6,420,'180+400t \rightarrow',...
   'HorizontalAlignment','right')


%%%%%%%%%%%%%%%%%%%%%%%%%%%%%%%%%%%%%%%%%%%%%%
%
%        Wavelet Analysis and results showed by 3-D plot
%
%%%%%%%%%%%%%%%%%%%%%%%%%%%%%%%%%%%%%%%%%%%%%%

B1=B1(1:8192);
ccfs = cwt(B1,1:32,'gaus2');
surf(ccfs)
colormap hsv
axis([0 8192 0 32 0 30])
shading interp
xlabel('Translation')
ylabel('Scale')
zlabel('Amplitude')
title(' Tighting bolt Continuous Wavelet Transform for Chirp Signal')
view([10,15,20])
```

```
%%%%%%%%%%%%%%%%%%%%%%%%%%%%%%%%%%%%%%%%%%%%%%%%%%%%%%%%
%
%        Wavelet Analysis and results showed by 2-D contour plot.
%
%%%%%%%%%%%%%%%%%%%%%%%%%%%%%%%%%%%%%%%%%%%%%%%%%%%%%%%%

ccfs = cwt(B12,1:64,'gaus2');
subplot(2,1,1); plot(B12);
ylabel('Amplitude')
title('Loose12 Vibration Signal')
subplot(2,1,2); contour(ccfs);
colormap hsv
xlabel('Translation (Number of Samples)')
ylabel('Scale (Normalized Frequency)')
title('Continous Wavelet Transform')
```

Appendix D

RTFFT Diagram on LabView